Professur für Hydrologie
Albert-Ludwigs-Universität Freiburg

Assessing the impact of water balance dynamics on peatland CO_2-emissions using thermal satellite imagery

Carolina Carrión Klier

Referent: Dr. Tobias Schütz

Korreferent: Prof. Dr. Barbara Koch

Eingereicht zur Erfüllung der Anforderungen
für den Grad des Master of Science

Freiburg in Breisgau, Dezember 2015

Abstract

This study introduces a method which attempts to examine groundwater level changes in peatland areas, based on temperature contrasts between water saturated and non-saturated zones, using Satellite Thermal Infrared imagery. With an adequate estimation of groundwater levels, soil volume exposed to anaerobic conditions in the peatland could be approximated and CO_2 emissions estimated. For the study region, located in Baden-Württemberg, Germany, temperature contrasts between groundwater temperature and soil temperature are given during the summer and winter. Water saturation conditions are characteristic of peatland areas, for this reason, the peatland cadastre of Baden-Württemberg was used to identify the zones which were expected to carry the temperature signature of groundwater, while the peatland surrounding zone represented non-saturated conditions. This study made use of temperature measurements derived from Satellite Thermal Infrared imagery taken under the Landsat program, which has been acquiring this type of imagery since 1984. Landsat imagery was selected because of its potential to offer a long-time cost-effective analysis tool. Temperature contrast measurements between peatland and surrounding areas with grassland cover were computed. Grassland was selected as the preferred land cover for this comparison because of its predominance in the study area and its relative proximity to the ground. With the resulting temperature contrast approximations, this method attempted to detect: 1) If there is a yearly pattern to temperature contrast measures. 2) If the yearly pattern has changed over the years of available Landsat imagery. 3) If temperature contrast had a significant correlation to groundwater levels. The method tested in this study could not detect a conclusive pattern under any of these three aspects. It is likely that temperature contrast measurements taken during the summer were dominated by the vegetation cover, without transmitting any information about the water saturation conditions on the underlying ground. As for the winter, because the imagery for the study region was mostly clouded during that time of the year, the dataset was reduced to a point were no conclusive analysis could be carried through.

Keywords: Groundwater level; Satellite Thermal Infrared imagery; Peatland; Baden-Württemberg; Long-term analysis; CO_2 emission

Zusammenfassung

In dieser Studie wird eine Methode vorgestellt, welche Änderungen im Grundwasserspiegel von Moorgebieten aus Temperaturunterschieden zwischen wassergesättigten und ungesättigten Zonen von thermischen Infrarot Bildern ableitet. Durch eine korrekte Abschätzung des Grundwasserlevels kann auch das unter anaeroben Bedingungen stehende Bodenvolumen von Moorgebieten ermittelt werden, was wiederum eine Einschätzung von möglichen CO_2 Emissionen erlaubt. Im Studiengebiet in Baden-Württemberg in Deutschland sind während Sommer und Winter deutliche Temperaturunterschiede zwischen Grundwasser- und Bodentemperatur vorhanden. Dies lässt sich auf jährliche saisonale Zyklen zurückführen, welche die Bodentemperatur, nicht aber das Grundwasser betreffen. Eine Eigenschaft von Moorgebieten ist die Wassersättigung, daher wurde der Moorkataster von Baden-Württemberg verwendet um Zonen ausfindig zu machen, in welchen eine Temperatursignatur des Grundwassers zu erwarten wäre. Die an Moorflächen angrenzenden Bereiche wurden als ungesättigt klassifiziert. Die in vorliegender Studie verwendeten thermischen Infrarot Bilder wurden dem Landsat-Programm entnommen, welches diese Daten seit 1984 aufzeichnet. Die Landsat-Bilder wurden aufgrund ihres Potentials zur kostengünstigen Langzeitanalyse ausgewählt. Temperaturkontraste zwischen Moor- und Umgebungsflächen wurden mithilfe von Grasbedeckung ermittelt. Grasland eignet sich hierfür aufgrund seines Vorkommens im Forschungsgebiet sowie seiner relativen Nähe zum Boden. Die abgeschätzten Temperaturkontraste wurden für folgende Fragestellungen verwendet: 1) Abschätzung von jährlichen Mustern im Temperaturkontrast. 2) Mögliche Änderungen dieser Muster über die Zeit. 3) Gibt es eine signifikante Korrelation zwischen Temperaturkontrast und Grundwasserlevel? Keiner dieser drei Aspekte konnte mit der hier vorgestellten Methode hinreichend erklärt werden. Es ist anzunehmen, dass Kontrastwerte im Sommer stark vegetationsbeeinflusst sind, wodurch Informationen über die Sättigungsbedingungen im Untergrund überlagert werden. Im Winter war der Datensatz durch starke Bewölkung auf ein Minimum zusammengeschrumpft, wodurch eine umfassende Analyse unmöglich wurde.

Schlüsselwörter: Grundwasserspiegel; Thermal-Infrarot Satellitenbilder; Moor; Baden-Württemberg; Langzeitanalyse; CO_2 Emissionen

"Dr. Sayer: *I was to extract one decagram of myelin from 4 tons of earthworms. I was the only one who believed in it. Everybody said it couldn't be done.*

Dr. Tayler: *It can't.*

Dr. Sayer: *I know. I proved it.*"

— Dr. Oliver Sacks, *Awakenings*

Contents

Abstract i

Zusammenfassung i

List of Tables ix

List of Figures xiii

List of Abbreviations xv

List of Symbols xvii

1 Introduction 1

1.1 State of the Art 2

2 Hypothesis 9

3 Material and Methods 11

3.1 Data 11

3.1.1 Primary data sources 11

3.1.2 Secondary data sources 12

3.2 Study region 14

3.3 Groundwater and soil surface temperature difference 16

3.4 Landsat Satellite imagery 17

3.5 Land use definition and zonification 21

3.6 Satellite thermal imagery data extraction and transformation process 23

3.7 Difference between temperature means and z-score 25

3.8 Groundwater level and its correlation to temperature difference or z-score . . 27

4 Results **29**

4.1 Groundwater, soil and air temperature 29

4.2 Land use zonification 33

4.3 Landsat Thermal Infrared imagery 36

4.4 Temperature difference between means and z-score 39

4.5 Groundwater level 45

4.6 Relationship between temperature contrasts and groundwater level 48

5 Discussion **53**

5.1 Groundwater, soil and air temperature 53

5.2 Zonification process and Landsat imagery availability 55

5.3 Landsat Thermal Infrared imagery 57

5.4 Temperature difference between means and z-score 58

5.5 Groundwater level and its correlation to temperature contrast 59

6 Conclusion **63**

Bibliography **65**

Appendix **71**

A Boxplots for Pfrunger-Ried peatland grassland temperatures **73**

B Additional figures **81**

List of Tables

3.1 Peatland details overview. 16

3.2 Landsat mission dates. 17

3.3 Proxy groundwater stations and comparison zones in Pfrunger-Ried 23

3.4 Peatland details overview 27

4.1 Pfrunger-Ried unavailable Landsat imagery due to cloud or snow coverage in selected areas. 36

4.2 Simple linear regression results for correlations between $\Delta_{\overline{T}}$ or z-score and GWL' 52

List of Figures

3.1 Study Area. 14

3.2 Overview of Landsat available data. 19

3.3 Example of a striped damaged Landsat image. 20

3.4 Hypothetical temperature contrast wave in a year's cycle 27

3.5 Sketch of the hypothetical relationship between temperature contrast and interpolated groundwater level. 28

4.1 Yearly groundwater temperature cycle. 29

4.2 Yearly air and soil temperature measurements in the study site. 30

4.3 Yearly groundwater to soil (or air) temperature difference. 31

4.4 Relationship between air and soil temperature. 32

4.5 Relationship between soil (or air) temperature and groundwater temperature. 32

4.6 Peatland and surrounding buffer zones for Pfrunger-Ried. 33

4.7 Pfrunger-Ried grassland zone definition. 34

4.8 Grassland peatland and surrounding zonification for Pfrunger-Ried. 34

4.9 Grassland peatland and surrounding zonification for a) Fetzach-Taufach, b) Arrisrieder, c) Reicher, d) SW of Goettlishofen, e) Isnyer, f) bei Rengers, g) Christazhofen, h) Oberweihermoor, i) Roemerkastell. 35

4.10 Yearly cycle of at-sensor mean temperatures and standard deviations for Pfrunger-Ried peatland and surrounding zones. 37

4.11 Relationship between daily mean air (or soil) temperature and at-sensor temperature for DWD station #3927. 38

4.12 Pfrunger-Ried temperature contrast between peatland and surrounding expressed as $\Delta_{\overline{T}}$ and z-score. 40

4.13 Pfrunger-Ried temperature contrast between raised bog and peatland expressed as $\Delta_{\overline{T}}$ and z-score. 40

4.14 Pfrunger-Ried temperature contrast between GW2025pr and EastCZ expressed as $\Delta_{\overline{T}}$ and z-score. 41

4.15 Pfrunger-Ried temperature contrast between GW2013pr and WestCZ expressed as $\Delta_{\overline{T}}$ and z-score. 42

4.16 $\Delta_{\overline{T}}$ (Peatland $\overline{T}$ - Surrounding $\overline{T}$) for peatland areas: a) Arriesdieder, b) Fetzach-Taufach, c) Reicher, d) SW of Göttlishofen 43

4.17 $\Delta_{\overline{T}}$ (Peatland $\overline{T}$ - Surrounding $\overline{T}$) for peatland areas: a) Isnyer, b) bei Rengers, c) Christazhofen, d) Oberweihermoor, e) Roemerkastell 44

4.18 Yearly groundwater level cycle for station GW2025. 46

4.19 Yearly interpolated groundwater level for station GW2025. 46

4.20 Yearly groundwater level cycle for station GW2013. 46

4.21 Yearly interpolated groundwater level for station GW2013. 46

4.22 Mean annual groundwater level for station GW2025. 47

4.23 Relationship between $\Delta_{\overline{T}}$ (Peatland $\overline{T}$ - Surrounding $\overline{T}$) and interpolated groundwater level at stations GW2025 and GW2013. 49

4.24 Relationship between z-sore (Peatland vs. Peatland & Surrounding) and interpolated groundwater level at stations GW2025 and GW2013. 49

4.25 Relationship between $\Delta_{\overline{T}}$ (Raised Bog $\overline{T}$ - Peatland $\overline{T}$) and interpolated groundwater level at stations GW2025 and GW2013. 50

4.26 Relationship between $\Delta_{\overline{T}}$ [(GW2025pr $\overline{T}$ - EastCZ $\overline{T}$) or (GW2013 $\overline{T}$ - WestCZ $\overline{T}$)] and interpolated groundwater level at stations GW2025 or GW2013. 51

4.27 Relationship between $\Delta_{\overline{T}}$ and interpolated groundwater level at station GW2025 excluding measurements taken in transition months (March, April, September and October). 51

A.1 Boxplots for Pfrunger-Ried peatland grassland temperatures in 1984 73

A.2 Boxplot for Pfrunger-Ried peatland grassland temperatures in 1985 73

A.3 Boxplots for Pfrunger-Ried peatland grassland temperatures in 1986 74

A.4 Boxplots for Pfrunger-Ried peatland grassland temperatures in 1987 74

A.5 Boxplots for Pfrunger-Ried peatland grassland temperatures in 1988 74

A.6 Boxplots for Pfrunger-Ried peatland grassland temperatures in 1989 74

A.7 Boxplots for Pfrunger-Ried peatland grassland temperatures in 1990 75

A.8 Boxplots for Pfrunger-Ried peatland grassland temperatures in 1991 75

A.9 Boxplots for Pfrunger-Ried peatland grassland temperatures in 1992 75

A.10 Boxplots for Pfrunger-Ried peatland grassland temperatures in 1993 75

A.11 Boxplots for Pfrunger-Ried peatland grassland temperatures in 1994 76

A.12 Boxplots for Pfrunger-Ried peatland grassland temperatures in 1995 76

A.13 Boxplots for Pfrunger-Ried peatland grassland temperatures in 1996 76

A.14 Boxplots for Pfrunger-Ried peatland grassland temperatures in 1997 76
A.15 Boxplots for Pfrunger-Ried peatland grassland temperatures in 1998 77
A.16 Boxplots for Pfrunger-Ried peatland grassland temperatures in 2000 77
A.17 Boxplots for Pfrunger-Ried peatland grassland temperatures in 2001 77
A.18 Boxplots for Pfrunger-Ried peatland grassland temperatures in 2003 77
A.19 Boxplots for Pfrunger-Ried peatland grassland temperatures in 2004 78
A.20 Boxplots for Pfrunger-Ried peatland grassland temperatures in 2005 78
A.21 Boxplots for Pfrunger-Ried peatland grassland temperatures in 2006 78
A.22 Boxplots for Pfrunger-Ried peatland grassland temperatures in 2009 78
A.23 Boxplots for Pfrunger-Ried peatland grassland temperatures in 2010 79
A.24 Boxplots for Pfrunger-Ried peatland grassland temperatures in 2011 79

B.1 Additional plots representing the yearly cycle of at-sensor mean temperatures and standard deviation on small peatland areas. 81
B.2 Additional plots representing yearly cycle of z-score values (Peatland vs. Peatland & Surrounding) on small peatland areas. 82
B.3 Additional plots representing the groundwater level on other groundwater station in the Pfrunger-Ried. 83
B.4 Additional plots representing the relationship between z-score to interpolated groundwater level. 84

List of Abbreviations

a.g.s.l. Above ground surface level

a.s.l. Above sea level

b.g.s.l. Below ground surface level

cfmask cloud-masking data

DEM Digital Elevation Model

EastCZ East comparison zone

EOLi Earth Observation Link

ESA European Space Agency

ETM+ Enhanced Thematic Mapper Plus

GDAL Geospatial Data Abstraction Library

GHG Greenhouse Gas

GMT Greenwich Mean Time

GW Groundwater

GW2013 Groundwater station 2013/570-8

GW2013pr Proxy zone for groundwater station 2013/570-8

GW2025 Groundwater station 2025/570-5

GW2025pr Proxy zone for groundwater station 2025/570-5

GWL Groundwater Level

GWL' Groundwater Level modeled with interpolation method

LGRB Landesamt für Geologie Rohstoffe und Bergbau (State Office for Geology Raw Materials and Mining)

LT Local Time

LUBW Landesanstalt für Umwelt Messungen und Naturschutz Baden-Württemberg (Institute for Environment Measurements and Nature Conservation)

NIR Near Infared

SD Standard Deviation

TIR Thermal Infared

TM Thematic Mapper

USGS United States Geological Survey

WaBoA Wasser- und Bodenatlas Baden-Württemberg (Water and Soil Atlas for Baden-Württemberg)

WestCZ West comparison zone

List of Symbols

R^2 Coefficient of determination

T Temperature

$\overline{T}$ Mean temperature

T_{GW} Groundwater temperature

T_G Soil temperature

$\overline{T_P}$ Mean temperature inside the peatland

$\overline{T_S}$ Mean temperature in the peatland surrounding area

Δ_T Temperature difference

$\Delta_{\overline{T}}$ Difference between mean temperatures

L_{cal} Calibrated radiance

K_1 Calibration constant 1

K_2 Calibration constant 2

σ Standard Deviation

μ Population mean

z z-Score (Standard Score)

1 Introduction

Water saturation conditions in peatland areas are the driving factor in the emission of greenhouse gases (GHG) (Weinzierl & Waldmann 2014). Thus, an identification of long-term saturation dynamics in known peatland areas would enable a quantification of carbon storage and carbon emissions from these ecosystems. This study makes an incursion into available tools to determine water saturation conditions and presents an alternative using long-term remotely sensed data.

Peatland ecosystems are characterized by the ability to accumulate and store dead organic matter under conditions of almost permanent water saturation (Joosten & Clarke 2002). When the water saturation conditions in a peatland are lowered, this leads to a continuous loss in the saturated thickness of the peatland, resulting from a mineralization of the peat (Weinzierl & Waldmann 2014). The groundwater level (GWL), which is the relative distance of the groundwater table to the to ground surface, expressed in meters below ground surface level (b.g.s.l.), is frequently used as proxy for air-filled porosity (Bechtold et al. 2014). The product of this distance times the area over which it extends, represents the peat volume exposed to aerobic conditions. With an approximation of this volume, climate relevant CO_2 emissions can be estimated.

The groundwater table can be modeled by spatial interpolation between in situ GWL measurements, yet such approximation is highly dependent on the distribution of the measuring points network. GWL measurements might not always be available on the spatial or temporal resolution necessary to answer certain research questions. For this reason many studies have explored alternatives to infer GWLs based on large scale cost-effective tools. One approach has been to use the temperature difference between groundwater and ground surface in temperate regions, to locate areas where the groundwater table reaches the ground surface level. Groundwater is less susceptible to seasonal temperature fluctuations that affect ground surface, such as: ambient temperature, solar radiation and wind (Breman 2002), therefore, it maintains a relatively constant temperature all year round, offering cooling in the summer and warming in the winter (Younger 2009). This phenomenon can be used in the summer or winter in temperate regions as an indicator of drained and water saturated conditions in peatland areas.

To achieve a large scale spatial pattern of temperature differences, several studies have used Thermal Infrared imagery (TIR) (Schuetz & Weiler 2011, Pfister et al. 2010, Mutiti et al. 2010). A large scale, freely accessible tool which has received a lot of attention over the last years is remotely sensed Landsat TIR imagery (Sass et al. 2014, Lalot et al. 2015). The archive of Landsat TIR imagery compiles records on a 16 days cycle since 1984. The present study seeks to use this archive to reconstruct the water saturation conditions in the peatland areas of Baden-Württemberg, Germany, over the last three decades. If water saturation conditions can be reconstructed using this tool, GHG emissions from this areas could be estimated.

1.1 State of the Art

Peatland ecosystems

Peatland ecosystems are the most common wetland form in the world. They cover over four million km^2 or 3 % of the land and freshwater surface of the planet, an area which represents 50 to 70 % of the global wetlands (Joosten & Clarke 2002). Wetlands are characterized by the presence of water at or near the land surface, conditions which are propitious for soils with low oxygen content and a specialized flora adapted to grow in these environments. The key feature of peatlands is the presence of peat, a fresh material which is composed of a living plant layer and thick accumulations of preserved plant detritus from previous years' growth. The near surface layer is relatively oxygen-rich, while the deeper layer is oxygen-poor. The low oxygen content is primarily given by water logging conditions, which are required for the active formation and accumulation of peat (Charman 2002, p.4-5). Peatlands include moors, mires, fens, bogs, swamp forests and marshes. The specific definition of these peatland forms often variate in the English-language literature. Generally speaking, the terms 'moors' and 'mire' are used synonymously with the term 'peatland'. The term 'fen' usually refers to a peatland which is "influenced by water from outside its own limits", while the term 'bog' or 'raised bog' refers to "a peatland which receives water solely from rain and/or snow falling on to its surface". A swamp is a loose term often referring to a fen with forest cover while a marsh usually implies a fen with tall herbatious vegetation (Charman 2002, p.4). In this study, the term peatland is used to define an ecosystem where a layer of at least 30-40 cm of peat has formed and which is in contact with water from outside its own limits. In these ecosystems the GWL is frequently at ground surface level or between 5 to 30 cm b.g.s.l. (Schweikle 2001).

Peatlands are carbon-rich ecosystems, on a global scale, they store between 400 and 500 Gt carbon (Roulet 2000), which represents approximately one third of the world's soil organic carbon (Joosten & Clarke 2002). Peatland ecosystems, with a GWL near the ground surface, serve a CO_2 sequestering function. Said function is threatened by drainage and land use change which leads to organic matter oxidation and increased emission of organic carbon. As carbon evaporates into the atmosphere in the form of a GHG, it has an impact on the climate (Jaenicke et al. 2008). Drained peatlands are estimated to be the source of 6 % of total anthropogenic CO_2-emissions, and the hotspots for those emissions are primarily located in Southeast Asia, Central and Eastern Europe, parts of the United States and Northeast China (Tanneberger & Wichtmann 2011). In order to create protocols for the stabilization of GHG concentrations in the atmosphere, a quantification of these losses is required (Roulet 2000).

Approaches to quantify GHG emissions from peatland areas

Jaenicke et al. (2008) presented a method for the determination of the amount of carbon stored in Indonesian peatlands. In that study, a 3D modeling based on a combination of remote sensing data and ground peat thickness measurements was tested. Landsat Enhanced Thematic Mapper Plus (ETM+) and a Digital Elevation Model (DEM) generated from satellite radar data were used to delineate peat domes. Peat thickness data for 542 locations, obtained using manually operated peat corers, was spatially interpolated for the previously delineated area and used to calculate peat volume and estimate carbon storage. Because large tropical peatland areas have a characteristic dome shape which can be easily identified in a DEM, this method was qualified as suitable for large-scale investigations of tropical peatlands, yet likely unsuitable for small peatland areas in mountainous regions as it is the case in Europe.

Weinzierl & Waldmann (2014) reported the longtime CO_2 emissions from peatland areas in upper Swabia (Baden-Württemberg, Germany) based on historical and current peat thickness measurements. Historical data relied upon an archive of 17,190 peatland profiles measured between 1949 and 1974 by Prof. Karlhans Göttlich. 11,541 of those profiles included peatland thickness and peatland elevation in m a.s.l. and were remeasured between 2012 and 2013. The loss in saturated peat thickness was measured over the span of time between recordings as a cumulative value, resulting in a median annual thickness loss between 2.9 and 8.8 mm depending on the peatland area and land use. The loss in saturated thickness of peatlands, the bulk density and the organic Carbon concentration in peat allowed for the calculation of CO_2

emissions from these areas. Weinzierl & Waldmann (2014) calculated 626,626 tons of annual CO_2 emissions for all peatland areas in Baden-Württemberg and a total organic carbon store of 34,1 million tons, which equates 125 million tons of CO_2. Despite the exceptionally large amount of peatland profiles, these measurements correspond to an area which represents only 15 % of the total peatland area in Baden-Württemberg.

Kopp et al. (2013) investigated the impact of long-term drainage on summer groundwater flow patterns in the Mer Bleue peatland, Ontario, Canada. Said study compared the groundwater flow patterns in a drained area which was later a forested area, and a non drained bog area. Groundwater flow patterns were found to alternate between "mostly downward flow and occasionally upward flow in the bog area and mostly upward-orientated in the forested area" (p.3485). This shift in the flow pattern was confirmed by one to three orders of magnitude lower hydraulic conductivity in the upper layer of peat in the forested area as compared to the bog area. Findings in that study suggest that the flow pattern in the forested area have changed to an upward direction due to increased evapotranspiration and interception in the summer by the tree cover. Jarasius et al. (2014) investigated the drainage impact on plant cover and hydrology of a raised bog area in western Lithuania. Degraded drained raised bog areas and recently burnt areas showed the largest anthropogenic impact as the proportion of plant species atypical to ombrotrophic raised bogs was the highest. The GWL in active raised bogs was significantly higher and water electrical conductivity significantly lower compared to degraded raised bog habitats. The optimum GWL for most of the typical bog plant species was found to lie in a range of -20 to -32 cm.

The response of GHG emissions to GWL has been examined in several laboratory and field experimental studies (Zhou et al. 2014, Furukawa et al. 2005, Bechtold et al. 2014, Berglund & Berglund 2011, Hahn-Schöfl et al. 2011, Moore & Roulet 1993). While results of the exact degree of GHG emission response to GWL, vary among studies, all studies show that GWL is negatively related to CO_2 emissions but positively related to CH_4 emissions (Zhou et al. 2014). High GWL might sustain the carbon stock of peatlands by preventing aerobic respiration of root biomass and underground soil, whilst drainage might greatly increase the CO_2 emissions from peatland to the atmosphere (Couwenberg et al. 2010, Zhou et al. 2014). GHG CO_2 and N_2O are produced on soils under aerobic conditions (Regina et al. 1996) while CH_4 emissions occur under anaerobic conditions (Levy et al. 2012). Bechtold et al. (2014) state that over various studies there is a general trend where there is "a strong increase of CH_4 emissions for annual mean GWL $>$ -0.1 m and an increase of CO_2 emissions for GWL $<$ -0.1 m with a trend similar to a saturation function that levels out approximately between -0.4 and -0.8 m" (p.3320). This relationship was represented by a hypothetical transfer function, relating the normalized GHG budget (i.e., the sum of the CO_2-equivalents of the three main greenhouse gases) to the GWL. In order to calculate GHG emissions, GWL measurements are required. The upscaling of punctual GWL measurements is the topic of further investigation. Bechtold et al. (2014) evaluated a statistical modeling method for a large-scale regionalization of GWL in peatland areas. The model was based on predictor variables which contained information about land use, ditch network, protected areas, topography, peatland characteristics and climatic boundary conditions for a data set with 1094 GWL measuring stations in 53 peatland areas in Germany. The model explained 45 % of the GWL variance conditions and a large fraction of the GWL variance could not be explained by the available predictor variables. The study suggests that in order to improve the predictive performance of this model, predictors with stronger GWL indication, relying for example on detailed water management maps or remote sensing products, are required.

Identification of groundwater presence by temperature contrast

Using heat to identify the presence of groundwater in an environment of contrasting temperature is an idea introduced in a series of studies published in the 1960s (Anderson 2005). The premise is based on the observation that groundwater temperature is relatively constant throughout the year. In temperate regions, where there is a yearly seasonality, a contrasting heat signature between water coming from the ground and surface water (or surface soil) can be detected during the summer or during the winter (Anderson 2005, Pfister et al. 2010, Schuetz & Weiler 2011). The application of this idea re-gained interest with the arrival of TIR. One of its earliest applications was introduced by Huntley (1978), where TIR was used to detect shallow aquifers. Schuetz & Weiler (2011) presented an effective application of ground-based TIR to quantify localized groundwater inflow in small streams during the summer and winter seasons. The method also enabled a determination of the length required for complete mixing between surface and groundwater. Pfister et al. (2010) apply the same tool for the mapping of saturated area connectivity and dynamics. The study found that by an analysis of ground-based TIR, the spatial connectivity between the hillslope - riparian - stream system could be identified. Ground-based TIR as these, are particularly useful in areas that cannot be easily monitored from airborne sensor platforms (e.g. forested catchments).

Faced with questions which require a large scale assessment, research has turned its attention to remote-sensing techniques using Landsat imagery. Landsat satellites have been collecting imagery of the Earth's surface since 1972. Eight Landsat missions have been launched so far and seven thereof have achieved orbit and collected data. The ground sampling interval (i.e. the area on the ground surface represented in one pixel) for visible and near-infrared (NIR) bands ranges from 57 x 79 m on the earliest mission to 30 x 30 m on the latest mission. The ground sampling interval for the thermal band ranges from 120 x 120 m on the earliest Landsat mission with a thermal band to 30 x 30 m on the latest mission. The spatial resolution of Landsat images is poor compared to airborne TIR imagery, however, Landsat images have the advantage of covering large ground areas and of being freely available at different dates (Lalot et al. 2015).

An example for the use of Landsat images for the identification of near surface groundwater presence is a study by Mutiti et al. (2010). The study used satellite spectral band combinations to find areas for potential ground water development in Kenya. First, areas presenting linear features were identified. In the research area these features are indicative of either shallow ground water or areas of increased subsurface hydraulic conductivity, as ground water there is structurally controlled by faults and fractures (Sander et al. 1996). Then, this information was combined with features derived from ground and remotely sensed data, such as surface moisture and vegetation. This combination was used to indicate areas with the highest potential for ground water development. While the study successfully used satellite imagery to detect groundwater, it is not directly related to the temperature conditions described previously. Perhaps a better example is a study by Bobba et al. (1992), where near-infrared energy data from the first Landsat mission was used to detect potential groundwater flow systems. A digital processing technique using bands 7 and 5 was tested and results were found to be directly comparable with thermal data collected by aircraft overflights of the watersheds. Results indicated, that recharge and discharge areas could be identified by changes in near-surface temperature. Later Landsat missions (Landsat 4 and up) include a TIR band, so combinations of near-infrared band were no longer needed, and a single Landsat band could be used for TIR imagery. This is shown in a study by Becker (2006), where ground available data and TIR data was used to infer ground water behavior in a terrestrial ecosystem.

The use of satellite TIR imagery in the identification of discharge zones has been probably more common in freshwater and marine aquatic ecosystems. A common application is the identification of groundwater discharge zones in the sea (Breman 2002, Wilson & Rocha 2012), lakes (Tcherepanov et al. 2005) or large rivers (Lalot et al. 2015, Handcock et al. 2006, Wawrzyniak et al. 2012). An example of this application can be described through a study by Lalot et al. (2015), where the contribution of the Beauce's groundwater watershed to the Loire river discharge is quantified using satellite TIR imagery. The study used seven satellite images from the Landsat 7 ETM+, five images taken during the warm season and two during the cold season. Using the radiance values extracted from the TIR band, temperature values for the Loire river were calculated. Additionally, in situ temperature observations, recorded on an hourly basis, were available for two sites in the river. Results showed that, on average, the TIR images tend to overestimate the river's water temperature in winter (+0.3 °C) and to underestimate it in summer (-1 °C). During low flow, or when water temperature is high this difference can reach -2 °C. However, overall, 75 % of the temperature differences, between in situ observations and temperatures derived from the satellite TIR imagery, remained within the ± 1 °C interval. Thus, the study found that river temperature may be studied from satellite TIR images. Using these TIR images, the evolution of the temperature along a section of the Loire river which overlapped the Beauce's groundwater watershed, was characterized. Finally, the groundwater discharge's contribution into the Loire river was estimated using a heat budget model. Although the study found several sources of uncertainty in the groundwater discharge estimation using this method, the estimated result stayed in the order of magnitude of the groundwater discharge calculated with the groundwater budget. Despite possible deviations from the real magnitude of groundwater discharge, the study proved that groundwater discharge into the Loire's river could be identified using temperature gradients as registered by satellite TIR imagery, on summer and winter days.

This Master's thesis is primarily based on a study by Sass et al. (2014), which presents an adaptation of the approach described previously to terrestrial conditions. The study makes use of the temperature contrast between groundwater and soil surface to map discharge water, i.e. to identify zones where the groundwater flows up towards the land surface or where the water table intersects the land surface. The study's methodology is based on the assumption that in terrestrial environments, just as in aquatic systems, groundwater discharge zones have a distinct thermal signature, being cooler than non-discharge zones in the summer and warmer in the winter (Cartwright 1974). The study region was centered in the Cooking Lake moraine located in the central region of Canada. The land cover is primarily perennial crops and pasture lands, as well as annual croplands mingled with mixed-wood boreal forest. The natural forest vegetation is composed mainly of deciduous tree species. Urban areas and open water areas were masked out from the temperature comparison due to the fact that these areas present temperatures which do not reflect the underlying soil temperature. The method was applied using three Landsat-5 TIR images taken during the winter months. The images selected had no clouds or haze across the study region, presented no anomalies, and had a snow pack not greater than 5 cm depth. This is mainly because snow can act as an insulating layer where the surface temperatures do not necessarily reflect the temperature of the soil. The snow depth and hourly air temperature were recorded on ground stations in the study region. The radiance values extracted from the satellite TIR imagery were converted to temperature values, these values were then averaged and compared to the average air temperature measured on ground stations within the study region at the time of Landsat image acquisition. The study found a near one-to-one relationship between at-sensor and ground measured temperature values. The three images were combined into one thermal map by computing an average at-sensor temperature, standard deviation and coefficient of variation for each pixel. The averaged thermal map was then used to analyze the spatial pattern of surface temperature by classifying zones as discharge and non discharge zones based on abrupt temperature differences. The mapping results were validated using the locations of known water springs and the GWL depth measured in shallow wells. 85 % of the groundwater springs were located within the discharge zones as predicted by the thermal map. Discharge zones were about 1.5 °C warmer than non-discharge zones. Shallow GWLs were slightly closer to the ground level within the discharge areas ($p < 0.1$). Total dissolved solids, sodium and electrical conductivity, which are commonly used as tracers of groundwater flow, showed higher averages in shallow wells located within the discharge zones than in the non-discharge zones ($p < 0.05$). In conclusion, Sass et al. (2014) showed that discharge zones could be identified using cloud free, winter Landsat TIR imagery with a snow cover < 5 cm.

Research gap

Heat has been widely used as a groundwater tracer in several studies (Anderson 2005). The application of this method has been successfully tested using TIR imagery (Schuetz & Weiler 2011, Pfister et al. 2010). Landsat TIR imagery has enabled the application of the same concepts to large scale aquatic systems (Lalot et al. 2015, Handcock et al. 2006, Wawrzyniak et al. 2012, Breman 2002, Wilson & Rocha 2012, Tcherepanov et al. 2005). A successful transference of Landsat TIR imagery to a terrestrial system was introduced by Sass et al. (2014) to identify groundwater discharge zones. Since the launch of the first Landsat with a TIR band in 1984, satellite TIR imagery offers a cost effective tool, However no previous study has used this tool to perform a long-term study to characterize groundwater flow in terrestrial ecosystems. Additionally, no study could be found where Landsat TIR imagery has been used to characterize peatland areas in temperate areas. Peatland systems offer appropriate conditions for this type of analysis as the ecosystem's physiochemical and biotic functions are controlled by water saturation conditions.

2 Hypothesis

The ultimate purpose of this study is to infer GHG emissions from peatland areas in Baden-Württemberg, Germany, based on their water saturation conditions. In order to achieve this, this study first needs to examine the use of Landsat TIR imagery to estimate the groundwater level in peatland areas. This approach tries to fill a research gap, by applying a cost-effective method in a long-term study to assess not only static water saturation conditions in a peatland area, but also to determine water saturation changes over time.

This study hypothesizes that: 1) In the study region, temperature differences between groundwater and soil surface can be used to differentiate groundwater saturated peatland from drained peatland. 2) If large temperature differences between the peatland and its surrounding area are detected by satellite TIR imagery during the summer and the winter, then the peatland area is saturated by groundwater, else the GWL lies deeper and the peatland area is partially to fully drained. The change in groundwater saturation conditions could then be compared from year to year, based on the magnitude of temperature differences.

In order to validate this hypothesis, temperature differences can be correlated to in situ GWL measurements. If a significant correlation is found, the correlation's function can be used to estimate GWL on scenarios where no in situ GWL data is available. Such correlation could be used to estimate carbon emissions based on GWL.

For the delimitation of the peatland and surrounding areas, this study makes use of the Baden-Württemberg peatland cadastre. The study assumes that by definition, the GWL to be expected within the defined peatland areas is close to the ground level, while the GWL outside peatland boundaries lies deeper. Because temperature values derived from Landsat TIR imagery are dependent on the land cover, peatland and peatland surrounding areas are to be compared using a land cover present in both areas.

3 Material and Methods

This section will present the data sources and the study region, followed by the methodology used in this study. The methods presented here make an attempt to: 1) Determine if there is a temperature difference between groundwater and air or soil temperature in the study region. 2) Determine the criteria for the Landsat data selection. 3) Define and delimit the zones to be used for this analysis. 4) Explain how to extract thermal data from Landsat imagery. 5) Determine how to measure temperature contrasts between zones. 6) Describe the process to correlate GWL to temperature contrasts. No further methodology for the determination of GHG emissions based on GWL is presented here, because the GWL could not be predicted.

3.1 Data

This study relies on a variety of data from different sources, by combining this data, this study seeks to have a basis to test and verify the validity of the methodology proposed here. In this section, a brief overview of the data sources will be presented according to two sub categories: Primary and secondary data sources.

3.1.1 Primary data sources

Primary data sources include data which is essential for the analysis method proposed in this study. Primary data includes:

1. The peatland cadastre map from Baden-Württemberg published by the State's Institute for Environment, Measurements and Nature Conservation "Landesanstalt für Umwelt, Messungen und Naturschutz Baden-Württemberg" (LUBW) and made available through the online interactive data service "Umwelt-Daten und -Karten Online"

(UDO) (udo.lubw.baden-wuerttemberg.de). This map includes the geographical location, name, description, area, and peatland type of all peatland areas in the state of Baden-Württemberg, Germany. Peatland types are classified into three categories: 1) Peatland (Niedermoor), 2) Raised bog (Hochmoor), 3) Transition mires (Anmoor) (LUBW 2014).

2. Satellite thermal imagery from the Landsat-5 Thematic Mapper (TM) available from March 1984 to May 2012 on a 16-day repeat cycle. For its greater portion, this data is made available by the United States Geological Survey (USGS) through the "Earth-Explorer" user interface (earthexplorer.usgs.gov). In the absence of data in the USGS database, additional satellite data for the study area can be attained through the "International Cooperator" ground station, in this case, represented by the European Space Agency (ESA). ESA manages an on-line catalogue and ordering service, "Earth Observation Link" (EOLi), where additional data relevant to this study was downloaded.

3. Groundwater level data. The State Office for Geology, Raw Materials and Mining "Landesamt für Geologie, Rohstoffe und Bergbau" (LGRB) in cooperation with LUBW, provide an overview of the location of GWL measuring points in the peatland areas of Baden-Württemberg. This source includes information on the measuring period of each gauge, the ground level and measuring point elevation in m a.s.l., a brief characterization of the regular degree of water saturation in the station, and a reference to the regional council managing the groundwater data in question. The GWL data relevant for this study was acquired directly through the regional council of Tübingen. The groundwater station with the longest data acquisition period covers a time frame between 1994 and 2011.

3.1.2 Secondary data sources

Secondary data sources include data which either helps deliver preliminary results or serves to verify the suitability of the primary data. Secondary data include:

1. Air and soil temperature from a local weather station. The Climate Data Center (CDC) offers free access to the many of the climate data from the German Weather Service "Deutscher Wetterdienst" (DWD) via an FTP server (ftp://ftp-cdc.dwd.de/pub/CDC/). This study made use of air and soil temperature records from station #3927 in Pfullendorf, Baden-Württemberg (47.9301 °N, 9.2898 °W), the closest station to the main

study area. This station counts with daily mean air temperature data from 1958 to 2014, and daily mean soil temperature at 5 cm depth from 1988 to 2015.

2. Groundwater temperature data from 2008 to 2011 for one of the main groundwater stations. The source for this data is the same as the one referred on section 3.1.1.3.

3. Land use map resources. This study makes use of three sources for the characterization of land use coverage: 1) Land use maps for 1990, 2000 and 2006 in the Water and Soil Atlas for Baden-Württemberg "Wasser- und Bodenatlas Baden-Württemberg" (WaBoA). The input data for the WaBoA land use maps are Landsat TM and 1:100.000 topographic maps, complemented by an analysis of 1:50.000 topographic maps as well as aerial and satellite photography. The land use forms in this map were identified according to the land use classification system established by the Coordination of Information on the Environment (CORINE). While these maps provide a useful initial overview of the land use forms in Baden-Württemberg, their resolution is limited, as units smaller than 25 ha are added to their respective neighboring areas (WaBoA 2012). 2) A higher resolution land use map is made available by the Official Topographic Cartographic Information System "Amtliches Topographisch-Kartographisches Informationssystem" (ATKIS) (www.adv-online.de) (Harbeck 2001). ATKIS data contains national peatland land use forms, information which was further refined by the University of Stuttgart for the region of upper Swabia and Donauried (Weinzierl & Waldmann 2014). The zones defined in this map can be smaller than 20 ha and the classification system used in these maps is more detailed than the one used in WaBoA. However, this map covers only the peatland areas of Baden-Württemberg, no information on the land use of the peatland surrounding area is available. 3) Google Earth satellite imagery from 2014. Even though Google does not provide a vector based map of land use, the visualization of this high resolution raster imagery, which is roughly 65 cm pan-sharpened (65 cm panchromatic at nadir, 2.62 m multispectral at nadir) (Mohammed et al. 2013), provides an additional tool for delimiting land use zones.

4. A study carried by LGRB, which estimated the longtime CO_2 emissions of peatland areas in upper Swabia, based on historical and current water levels (Weinzierl & Waldmann 2014), providing some general background information and a source for validation purposes.

3.2 Study region

The study region is located in Baden-Württemberg, Germany (Sub-figure 3.1 (a)). The state of Baden-Württemberg counts with a peatland area of approximately 45.000 ha (LUBW 2015). The peatland areas in this study were selected from the south-eastern corner of the state. In this area, the pre-Alpine hill-land and the Iller-Lech Plateau natural regions concentrate approximately 87 % of the state's peatland area (LUBW 2015). Most of this highly peatland dense area is covered by the 27^{th} row on the 194^{th} path of the Landsat-5 satellite image. Only peatland areas which were fully contained within this path and row, were selected for this analysis.

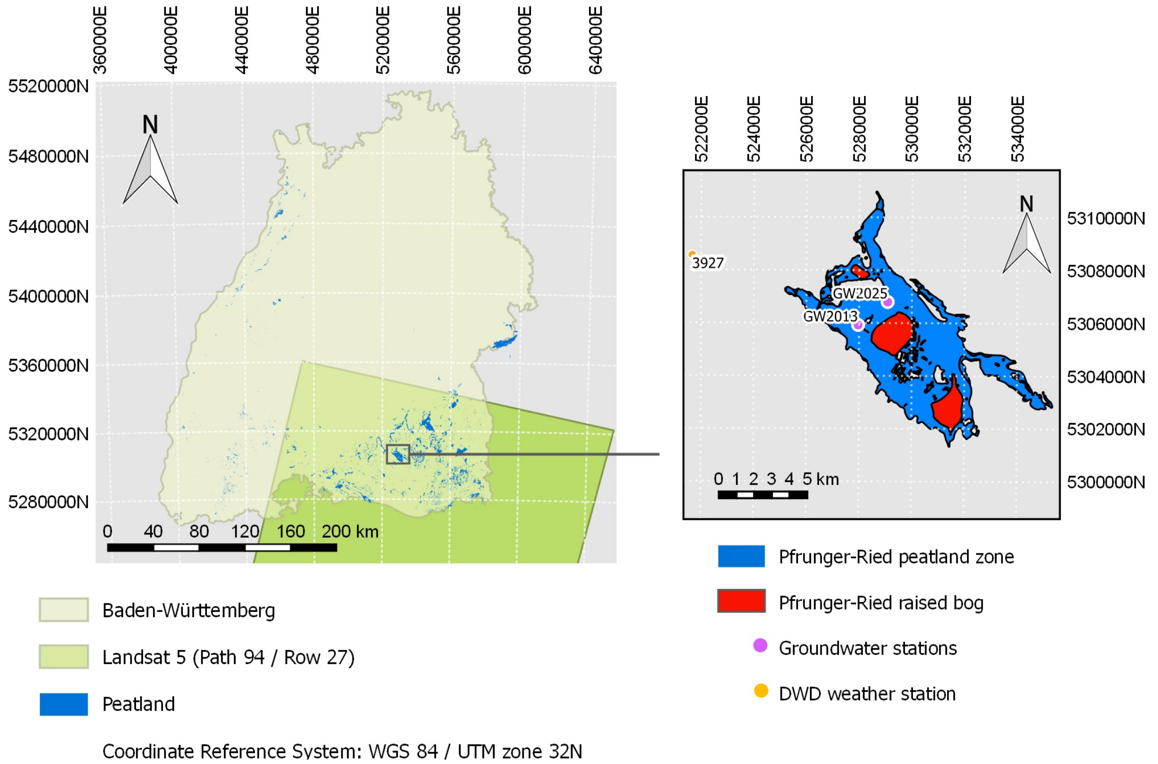

(a) Baden-Württemberg peatland cadastre and upper corners of Landsat-5 path 194 / row 27 scene coverage

(b) Pfrunger-Ried peatland with two groundwater and one weather station

Figure 3.1: Study Area.

Pfrunger-Ried

The primary peatland area for this study is centered in the Pfrunger-Ried peatland (47.9 °N, 9.4 °W) (Sub-figure 3.1(b)). The Pfrunger-Ried, with approximately 2.600 ha, is the second largest peatland area in south-west Germany (LUBW 2015). It consists of several peatland sub-areas such as: raised bogs, transition mires, and fens as well as the Ostrach river valley (BfN 2015). As early as the time of the foundation of the Wilhelmsdorf settlement around 1820, much of the peatland sub-areas were drained, to a great degree for peat extraction and for intensive agriculture. Some sub-areas in the central region of the peatland were preserved. From 2002 to 2015 a great portion of the Pfrunger-Ried began a process of renaturalization under the conservation project "chance.natur", carried out by the "Stiftung Naturschutz Pfrunger - Burgweiler Ried". Under this project, starting in 2005, approximately 610 ha peatland were rewetted in order to restore the original hydrology of the peat-forming ecosystems. In the peatland peripheral zone, in an area of approximately 300 ha, grassland pastures were established by local farmers (LUBW 2015).

The Pfrunger-Ried was selected for this study because of quantity and quality of supporting data available for this peatland. The primary data source being the longest available period of groundwater measurements in the main study area. Also, the availability of a climate station managed by the DWD in the immediate vicinity of the Pfrunger-Ried, offers the opportunity to validate partial results in this study. Additionally, a study by Weinzierl & Waldmann (2014), which examined the longtime CO_2 emissions based on historical and current water levels in this peatland area, provides the possibility to compare the results of said study to ones achieved in this one. The presence of raised bogs in the Pfrunger-Ried enables an inspection into possible differences between peatland forms. A further advantage of this peatland is that the land use form extends from inside the peatland to the outer peripheral zones, which enables a comparison of peatland to non-peatland zones using the same land use. Finally, while the large size of this peatland area might present challenges due to the variability of peatland zones, it might also present advantages, as the Satellite thermal imagery used here has a resolution of 60 x 60 m, and the reliability of average results increases as the area which they cover increases. Overall, the Pfrunger-Ried was selected as the primary peatland area site because the quantity of available data enable an in-depth analysis for this site.

Other peatland areas

Aside from the primary study area in the Pfrunger-Ried, nine other peatland areas in the main study area were selected for this analysis. The peatland areas are: Fetzach-Taufach, Arrisrieder, Reicher, South-west of Goettlishofen, Isnyer, bei Rengers, Chrisatzhofen, Oberweihermoor and Roemerkastell. Table 3.1 contains details about the location and area of these peatlands. These sites do not have the same amount of supporting data as the Pfrunger-Ried does. However, with them, this study seeks to test the replicability of results attained on the Pfrunger-Ried. These peatland areas were selected by surveying the WaBoA land use map, and selecting peatland areas which were either partially or entirely covered by grassland, and which also had the same land cover in the surrounding area.

Table 3.1: Peatland details ordered after peatland surface area.

Peatland	Coordinates	Peatland surface area
Pfrunger-Ried	(47.9 °N, 9.4 °W)	2549 ha
Fetzach-Taufach	(47.75 °N, 10.03 °W)	265 ha
Arrisrieder	(47.75 °N, 9.88 °W)	140 ha
Reicher	(47.76 °N, 9.74°W)	116 ha
SW of Goettlishofen	(47.72 °N, 9.945 °W)	30 ha
Isnyer	(47.70 °N, 10.020 °W)	16 ha
bei Rengers	(47.72 °N, 10.062 °W)	7 ha
Christazhofen	(47.72 °N, 9.957 °W)	5 ha
Oberweihermoor	(47.726 °N, 10.024 °W)	4 ha
Roemerkastell	(47.696 °N, 10.065 °W)	2 ha

3.3 Groundwater and soil surface temperature difference

As mentioned previously, groundwater is less susceptible to seasonal temperature fluctuations such as ambient temperature, solar radiation, currents and wind (Breman 2002), maintaining a relatively constant temperature all year round. Given that the study area is located in a temperate region defined by a yearly seasonal cycle, with warmer temperatures in the summer and colder temperatures in the winter, the temperature difference between the constant groundwater temperature and the yearly fluctuating soil surface temperature should also have a yearly cycle. In order to test this premise, this study examined the yearly cycle of groundwater temperature, as well as the yearly cycle of temperature difference between groundwater temperature and unsaturated soil temperature at 5 cm depth (Equation 3.1). This temperature difference was calculated using data from matching dates.

$$\Delta_T = T_{GW} - T_G \tag{3.1}$$

Where the Δ_T is the temperature difference of groundwater to soil, T_{GW} is the mean daily groundwater temperature in groundwater station "2025/570-5" (GW2025) in Pfrunger-Ried, and T_G is the mean daily soil temperature at 5 cm depth in the DWD weather station #3927 in Pfullendorf. This study assumed that a comparison using data from these two sites was possible, despite their relative distance of 12 km, because groundwater temperatures are relatively constant.

3.4 Landsat Satellite imagery

The Landsat Program is a joint effort from the U.S. Geological Survey (USGS) and the National Aeronautics and Space Administration (NASA). Having launched their first Landsat mission in 1972, this database provides an important archive of remotely sensed data worldwide. For the purposes of this study, data from the three Landsat missions which contain a thermal band came into question: Landsat-4 and -5, Landsat-7 and Landsat-8. Table 3.2 contains an overview of launch and decommission dates for these Landsat missions. As this study seeks to obtain a result which outlines the evolution of soil moisture conditions in peatland areas, the criteria for the Landsat selection was that it should have the longest uninterrupted data coverage period, and the time line for the data coverage should overlap the available GWL data. The Landsat-5 promised to fulfill these requirements and was therefore chosen for this study. The Landsat-4 could have been used to fill possible gaps in the Landsat-5 data range, however the amount of usable Landsat-4 images for this study was too small. An initial search for Landsat-4 images in the EarthExplorer database delivered only twelve results from 1988 to 1990, from which only three images were partially cloud-free in the main study area. The Landsat-7 was considered as source for filling in possible missing data from the Landsat-5 data. However, in May 2003 the ”Scan Line Corrector” of Landsat-7 failed, rendering the data from that point on, inadequate for this study. An analysis of Landsat-8 data was discarded from this study, as it covers a time-frame which does not overlap with the available GWL data.

The Landsat-5 TM orbits at 705 km altitude and has a 16-day full-Earth-coverage cycle. The scene selected for this study corresponds to the 27^{th} row of the 194^{th} path, which is recorded in a 16 day cycle between 09:35 and 09:45 a.m. Greenwich Mean Time (GMT), i.e., between 10:35 and 10:45 a.m. Local Time (LT) in the winter and 11:35 and 11:45 a.m. LT in the summer. The approximate scene size is of 170 km north-south by 183 km east-west (USGS 2015*b*). The multispectral TM includes bands in the visible, near-infrared, and short-wave infrared, as well as a single thermal band (Barsi et al. 2007). The Band-6 (TIR band) is the

Table 3.2: Landsat mission dates.

Satellite	Launch	Decommissioned
Landsat-4	July 16, 1982	June 15, 2001
Landsat-5	March 1, 1984	June 5, 2013
Landsat-7	April 15, 1999	Operational
Landsat-8	February 11, 2013	Operational

Table adapted from USGS (2012)

basis for the thermal mapping and estimation of soil moisture in this study. This spectral band covers the spectral wavelength between 10.40 and 12.50 µm. Band-6 was acquired at 120-meter resolution, but the downloadable product from USGS or ESA has a 30-meter resampled resolution (USGS 2015*b*).

All images for Landsat-5, path 194 and row 27, available in the EarthExplorer archive were carefully examined using a preview of the TM and the coordinates for the Pfrunger-Ried peatland area. If an approximate peatland area of more than 50 % was free of clouds or cloud shadows, the image was downloaded using the EarthExplorer's bulk download system. The "Level 1" product, which includes all seven bands of the Landsat-5 images and their corresponding metadata, was downloaded. When available, the higher-level cloud-masking data record (cfmask), was also downloaded. The cfmask was developed at the Boston University in a Matrix Laboratory (MATLAB) environment to automate cloud, cloud shadow, and snow masking for Landsat TM and ETM+ images (USGS 2015*c*).

Considering the fact that the Landsat-5 was launched on March 5, 1984, decommissioned on July 5, 2013, and that it has a return cycle of 16 days, the total of images available for each path and row should amount to 647 records for the entire mission's period. However only 194 images were available in the EarthExplorer USGS archive. USGS indicates that while many scenes collected worldwide are available in the archive, each ground station in the "International Cooperator" network is the primary source for distributing the captured data in their area. USGS states that if some data is not found in the USGS archive, missing data may be available from the ground station that collected the data (USGS 2015*a*). The ground station responsible for the records used in this study is represented by ESA. Making use of ESA's ordering catalogue "EOLi", the missing data was searched for and, when available, acquired. Here, an additional set of 180 images (using the same path and row) were found. Joining images retrieved from the USGS and ESA sources still leaves a remaining of 253 missing images. The ESA support team was notified of the missing images, they offered to reprocess and attempt to recover the Landsat-5 gaps for the requested scene. However, this process will not be finished before the first quarter of 2016. An overview of the unavailable, available and usable Landsat-5 data, along with the sources providing this data for the 27^{th} row on the 194^{th} path, is presented in figure 3.2.

The selection process to download images from the EOLi database was the same as the one used in the EarthExplorer database. Images were selected according to the degree of cloud coverage visible in preview images, with particular attention to the Pfrunger-Ried peatland area. The EOLi ordering services provides all the processed image bands and metadata,

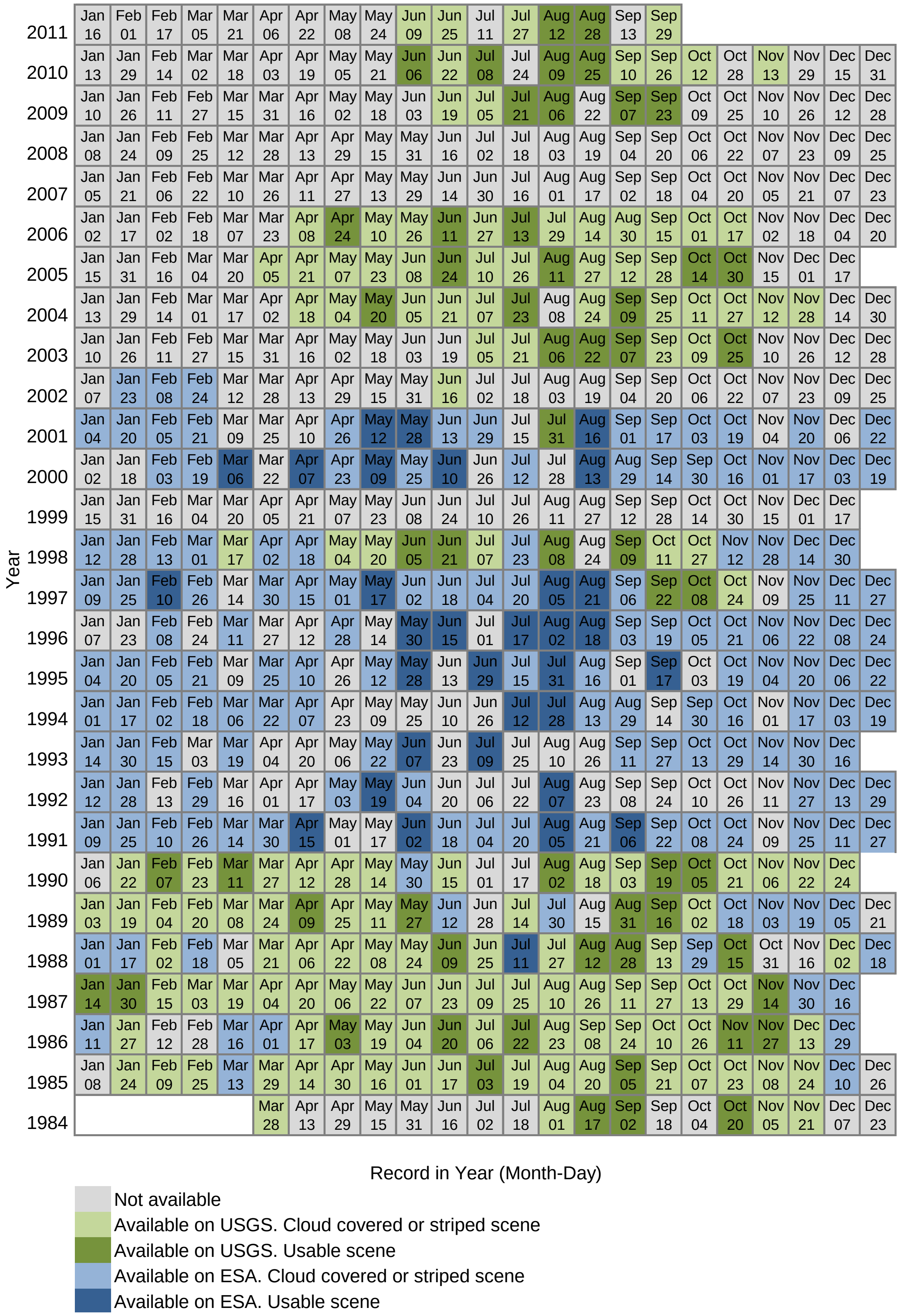

Figure 3.2: Overview of available and usable Landsat-5 data for the 27^{th} row on the 194^{th} path.

however, a cfmask is not available for download on this source. For the Landsat images downloaded from EOLi, a vector based map defining cloud and shadow zones was drawn for each individual image in the Pfrunger-Ried area. All bands were combined and used as visual aid for the definition of cloud and shadow zones.

After the images were downloaded, the thermal band was carefully examined. Some images presented an anomaly known as "striping". This defect shows itself as visible stripes crossing the entire thermal band with a regular pattern. These stripes show a deviation from their neighboring cells (Figure 3.3). On personal correspondence, the ESA support team explained the cause for this defect as follows: "Unlike visible and NIR bands, the calibration processing of the thermal band data uses in-flight values. When the in-flight values recorded by the internal calibrator are corrupted, the resulting 'image record' cannot be calibrated correctly and only a partial/no calibration is applied and the entire pass is degraded somewhat. As a result of the lack of telemetry, it is not possible to extract temperatures. A side effect of this issue, can be striping in the image." The ESA support team stated that it is currently not possible to correct this defect and suggested that scenes with this anomaly should not be converted to temperature values as results may be unreliable.

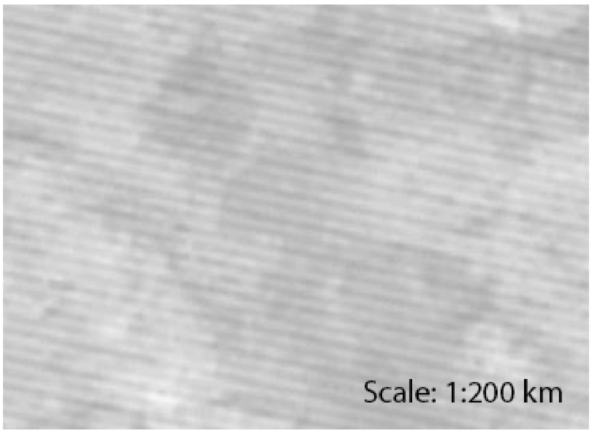

Figure 3.3: Extract of Band-6 of Landsat-5 image LT51940271989323ESA00 showing striping defect.

Finally, from a total of 374 available images (joining USGS and ESA data sets), 274 images were excluded from this study because of cloud coverage and 13 because of damage in the thermal band due to striping. This leaves a final set of only 87 images which could be used for this study. The files corresponding to these 87 dates were downloaded. Then, a rectangular area covering the peatland area which was to be analysed, plus a surrounding buffer area of at least half of the maximal east to west distance in the peatland area, was defined. The purpose of this rectangular area, or 'mask', was to delimit the area to be clipped from each Landsat scene, in order to reduce the size of input files and simplify later computing steps. This mask was defined for each one of the peatland areas considered in this study, and it was defined in such a way as to cut the raster images exactly through the borderlines between pixels. The clipping of the Landsat thermal band and cfmask was automatized using the Geospatial Data Abstraction Library (GDAL).

3.5 Land use definition and zonification

This study seeks to compare the land surface temperature of groundwater saturated land (peatland) and non groundwater saturated land (peatland surrounding). In order to attain temperature measures which best reflect soil emissivity under these two conditions, inadequate land cover usages need to be dismissed and equal land cover needs to be used for the temperature comparison. Urban areas with buildings and paved streets were excluded, as these surfaces heat up considerably under the sunlight and the signal they emit to the thermal band reflects the properties of materials present in urban areas, and not the water saturation conditions of the underground. An analogous situation is given with forested areas, where primarily during the vegetative period, canopy covered surfaces dominate the emissivity signal. In addition to urban, and forest areas, open water areas such as lakes and ponds were excluded from this analysis. For the purposes of this study, the ideal land cover would be barren soil, however this land cover is not represented in this area. Therefore, a land use with a vegetative cover closest to the ground was chosen. The land use forms which came into consideration were grassland and farmland. As sufficient grassland surface area existed both inside and in the surrounding peatland area, this land cover was chosen for this study.

The grassland zones were defined in a two step process. First, the grassland area, as defined on the WaBoA 1990 land use map, was selected. As noted in section 3.1.2 , this map has a rather low resolution, which meant that areas smaller than 25 ha were included into the grassland zone despite having a different land cover. In order to compensate for this low resolution a second step was implemented. In this next step, the WaBoA grassland zone was superimposed with the latest available Google Earth satellite imagery in the area. Then, all forest, urban or open water areas in the Google Earth image, were excluded from the grassland zone. By doing this, the definition of the grassland zone was refined, and material for grassland definition for both 1990 and 2014 was taken into account, thus covering a larger time range. A higher resolution map describing the land use forms in peatland areas, first provided by the ATKIS data source and further refined within a project carried out by the University of Stuttgart, was available for this study. However upon closer consideration it was opted to leave out this source, because this study requires to use the same criteria for land use definition both inside and outside the peatland to ensure an appropriate comparison. Since this source only contains information about the area within the peatland, it is not optimal for this study. On the land use definition for the raised bogs areas an exception was made, because no grassland cover existed inside these areas. Raised bogs are typically covered by peat swamp forests and their characteristic Sphagnum moss vegetation cover (Joosten & Clarke 2002). Therefore, in this case, areas with thick forest cover or open water surfaces were excluded and areas with lower vegetation cover (Sphagnum moss) were used for the comparison. These zones were defined using the Google Earth satellite imagery. Additionally, Google Earth imagery served as a visual tool to check the geographical alignment for all Landsat images, using urban areas and lakes as reference points.

Apart from defining the land use zones, the peatland zones for the comparison were defined using the Baden-Württemberg peatland cadastre. Peatland and raised bog limits were simply adopted from the peatland cadastre. Transition mire zones defined in the peatland cadastre were excluded from the comparison, as these zones have soils with less than 30 % organic matter and/or less than 30 cm in thickness (LUBW 2015), and they cover rather thin peatland border areas from which not enough pixel values could be extracted to make a meaningful comparison. For the definition of the surrounding area, a buffer zone running along the borders of the peatland area was defined. The thickness of this buffer zone was defined in such a way that it would cover approximately the same area as the peatland area. The distance from the outer border buffer line to the peatland border line was approximately the same as the average distance of the peatland borderline to the central region of the peatland.

Because the Pfrunger-Ried covers a large area (2.600 ha), the recorded GWL from one station might not be representative for the entire peatland area. This, in turn may represent a challenge for the interpretation of results. For this reason, a smaller area close to the groundwater stations with the longest available recording period, was defined. These groundwater stations are: Station "2025/570-5" (GW2025) and station "2013/570-8" (GW2013). Ideally, these small areas would have been located directly on top of the groundwater stations. However, because these stations are located in a forested area, two circular areas with a 200 m radius, placed in the closest grassland area to the stations, were defined. These are called "proxy groundwater station" zones and they are located within the peatland area. Proxy zone for groundwater station GW2025 was anchored at a distance of 350 m in north-east direction (GW2025pr) and proxy zone for groundwater station GW2013 was anchored at a distance of 420 m in south-west direction (GW2013pr). Additionally, two zones of the same area were defined at the corresponding closest grassland peatland surrounding area. One in the eastern side and the other in the western side. These are referred as the "East Comparison Zone" (EastCZ) and the "West Comparison Zone" (WestCZ). The EastCZ represents the comparison zone for GW2025pr, and the WestCZ represents the comparison zone for GW2013pr. Table 3.3 lists the central coordinates for these smaller areas.

Table 3.3: Proxy groundwater stations and comparison zones in Pfrunger-Ried

Station name	Center coordinates
GW2025pr	(47.914843 °N, 9.392408 °W)
GW2013pr	(47.902749 °N, 9.371149 °W)
EastCZ	(47.923466 °N, 9.39649 °W)
WestCZ	(47.901432 °N, 9.366617 °W)

The defined comparison zones are: 1) Peatland grassland against peatland surrounding grassland (peatland vs. surrounding). 2) When a raised bog area was present, moos cover in the raised bog against grassland in the peatland surrounding (raised bog vs. surrounding). For the Pfrunger-Ried peatland: 3) GW2025pr inside the peatland grassland area against the EastCZ in the peatland surrounding grassland (GW2025pr vs. EastCZ). 4) GW2013pr inside the peatland grassland area against the WestCZ in the peatland surrounding grassland (GW2013pr vs. WestCZ).

3.6 Satellite thermal imagery data extraction and transformation process

In order to simplify subsequent computing processes, the spatial raster data was exported into a matrix format. In this matrix, each raster data pixel was represented by its central east and north coordinates and the pixel's digital number (DN). The DN is a value in a range between 0 and 255. This was done for all available clipped Landsat and cfmask files. The zones defined on the previous steps were transferred into point values following the same format as the Landsat images, i.e. using the central cell coordinates in a grid conformed of 30 x 30 m cells. This way each cell can be assigned to the categories mentioned on the previous section. The land use and the zone for each cell in the grid, can be identified.

In order to obtain a temperature value in °C for each pixel, this study followed a process outlined in Sass et al. (2014), adapted from Markham & Barker (1986) and Barsi et al. (2003), whereby the DN of each pixel is converted to a temperature value in a two step process. First, a calibrated radiance is obtained using the DNs, and the Bias and Gain values specific to each Landsat scene were used according to equation 3.2.

$$L_{cal} = Gain \cdot DN + Bias \tag{3.2}$$

where L_{cal} is the calibrated radiance in W/(m^2·sr·µm), Gain ((W/(m^2·sr·µm)))/counts) and Bias (W/(m^2·sr·µm)) are rescaling factors provided in the Landsat scene metadata, and DN is the digital number for each pixel in the thermal image.

In a second step, an at-sensor temperature in K was attained using the calibrated radiance and the calibration constants K_1 and K_2 as shown in equation 3.3.

$$T = K_2/[ln(K_1/L_{cal} + 1)] \tag{3.3}$$

where T is the effective at-sensor temperature in units of K assuming an emissivity of one; K_2 is the calibration constant 2 in units of K; K_1 is the calibration constant 1 in units of W/(m^2·sr·µm); and L_{cal} is the calibrated radiance in units of W/(m^2·sr·µm). The calibration constants of 607.76 and 1260.56 for K_1 and K_2, were taken from (Markham & Barker 1986, Sass et al. 2014). Finally, the resulting temperature in K was transformed to °C.

As described on Wubet (2003), this effective at-sensor temperature depends on two factors: "1) Surface temperature, which is an indication of the thermodynamic state resulting from the energy balance of the fluxes between the atmosphere, surface and sub surface soil. 2) The surface emissivity, which is the efficiency of the surface for transmitting the radiant energy generated in the soil in to the atmosphere. It depends on the composition, surface roughness and physical parameters of the surface[...]. Thus, to make a quantitative estimate of the absolute surface temperature, one needs to separate the effects of temperature and emissivity in the observed radiation as measured by satellites" (p.1). Li et al. (2004) outlines a method to convert effective at-sensor temperature to absolute surface temperatures by atmospherically correcting Landsat data using a radiative transfer model with atmospheric profile data, and an approach to estimate the emissivity for Landsat thermal bands by the vegetation cover.

However, this study adopted the same approach as the one taken by Sass et al. (2014), where stable atmospheric conditions were assumed and where the effective at-sensor temperature was not converted to absolute surface temperature. This step was not considered necessary for two reasons: First, because the primary application of this method is to analyze the spatial pattern and difference of surface temperatures and not their absolute value. Second, given the fact that only zones with the same land cover are compared, it is not necessary to account for the effect that different vegetation covers have on the intensity of the recorded temperature. If the atmospheric conditions are stable, cloud-free, and the land cover is the same, we can assume that temperature differences are caused by soil moisture conditions.

In this study, the plausibility of the computed effective at-sensor temperature data was verified with two methods. The first was to observe the distribution of the mean temperature $\overline{T}$ of a defined cloud-free zone (e.g. grassland peatland) in the month and day they were taken at, and check if the overall temperatures were higher in the summer season and lower in the winter season. The Standard Deviation (SD) for the same zone was also computed to account for general patterns of variation. The second method was to compare the average at-sensor temperature for the DWD station #3927 in Pfullendorf against the average air and soil temperature measurements taken at the same station the same day of the Landsat scene acquisition. The area representing the DWD station #3927 in the Landsat scene was defined by selecting the raster cell where the DWD station is located and a buffer zone of one raster cell distance around that station. Raster cells which were cloud covered were excluded from the averaging calculation. Landsat at-sensor temperature and daily mean temperature values registered in the ground were correlated with a linear regression. The strength of the relationship was measured by the coefficient of determination (R^2) at a significance level of 0.005.

3.7 Difference between temperature means and z-score

To calculate temperature differences between zones two approaches were taken. The first was to get the difference between temperature means ($\Delta_{\overline{T}}$) by calculating the mean temperatures for each zone and simply subtracting the mean temperature in the zone outside the peatland area from the mean temperature in the peatland or raised bog area (Equation 3.4).

$$\Delta_{\overline{T}} = \overline{T_P} - \overline{T_S} \tag{3.4}$$

Where $\overline{T_P}$ is the mean temperature inside the peatland or raised bog area and $\overline{T_S}$ is the mean temperature in the surrounding area.

The second approach was to standardize temperature differences between zones by calculating the standard score (z-score). The z-score is a dimensionless quantity which indicates how far a value is from the population mean, and expresses this difference in terms of the number of standard deviations by which it differs (Lundberg 2007, Kirkwood & Sterne 2003) (Equation 3.5).

$$z = \frac{x - \mu}{\sigma} \tag{3.5}$$

Where z is z-score, x is the sample or single value, μ is the mean of the population and σ is the standard deviation of the population. In this study, z-scores were used for comparing the mean temperature in a partial area (i.e. peatland area or raised bog area) and the total area (i.e. peatland and surrounding or raised bog and surrounding area). The z-score was adapted so that the single value x represents the mean temperature in the partial area, while μ represents the mean temperature in the total area and σ represents the standard deviation of temperature values in the total area. Z-score values calculated in these study will be referred using the abbreviation pattern: ”A vs. A & B”, where A and B refer to different zones. Using the nomenclature of equation 3.5, this can be interpreted as follows: z = A vs. A & B, x = mean temperature in A, μ = mean temperature in A & B, σ = standard deviation in A & B.

To maintain consistency with $\Delta_{\overline{T}}$, the partial area was represented by the peatland or raised bog area. Thus, for $\Delta_{\overline{T}}$ and z-score values computed in this study, positive values imply warmer conditions in the water saturated area (peatland or raised bog) while negative values imply colder conditions in the same area. In this sense, $\Delta_{\overline{T}}$ and z-score provide analogous information, nevertheless, both were computed to identify which measure best reflects the distribution of these temperature contrasts throughout the year. If the hypothesis proposed in this study is accurate, we should observe positive $\Delta_{\overline{T}}$ and z-score values in the winter and negative values in the summer. This difference should be more pronounced when the GWL is near surface level (Sub-figure 3.4(a)) and the amplitude of this signal should attenuate if the GWL lies deeper (Sub-figure 3.4(b)).

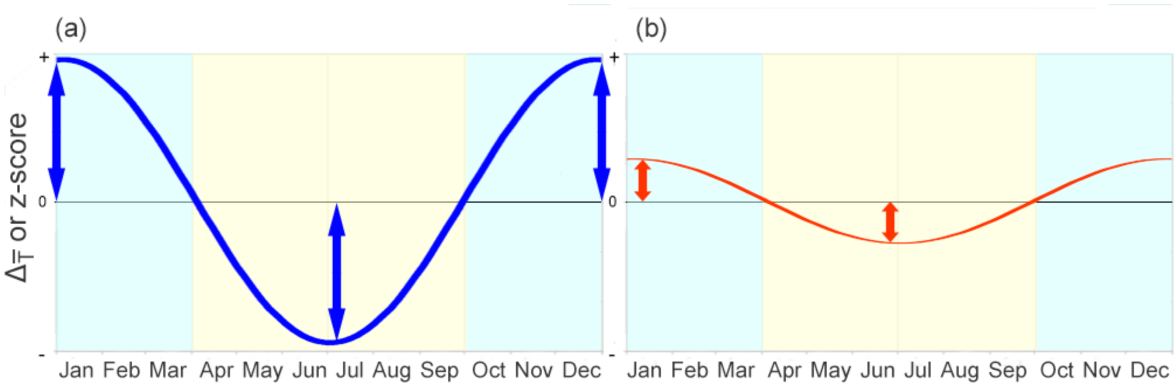

Figure 3.4: Hypothetical temperature contrast wave in a year's cycle with: (a) Near-surface GWL and (b) deep GWL.

3.8 Groundwater level and its correlation to temperature difference or z-score

According to the LGRB register of groundwater stations in Baden-Württemberg, there is a total of 111 groundwater stations in the Pfrunger-Ried peatland. Only four of those stations cover a continuous time range longer than six years (Table 3.4). These stations were used to identify yearly patterns in the GWL cycle. Of those four stations, only two could be used for the correlation between GWLs and temperature contrasts expressed as $\Delta_{\overline{T}}$ and z-score, because only for these stations a nearby proxy station located at less than 500 m distance could be defined. GWL measurements for each station were originally provided in m a.s.l., with the ground level for each station also in m a.s.l.. These GWL measurements were subtracted form the station's ground level to produce GWL measurements relative to the ground level. Thus, resulting negative values represent meters below ground surface level (b.g.s.l.) while positive values represent meters above ground surface levels (a.g.s.l.). These are the GWL measurements this study used on further steps.

Table 3.4: Groundwater stations in Pfrunger-Ried covering a period longer than six years.

Station Name	Time frame	Coordinates
2013/570-8 (GW2013)*	1994-2003 / 2009-2011	(47.906007 °N, 9.37423 °W)
2025/570-5 (GW2025)*	1994-2012	(47.913823 °N, 9.389253 °W)
2056/570-0 (GW2056)	1994-2001	(47.908807 °N, 9.401803 °W)
2064/570-5 (GW2064)	1995-2003	(47.901098 °N, 9.399497 °W)

* Stations used for temperature contrast vs. GWL correlation

Available GWL data for stations GW2013 and GW2025 present inconsistent measurement intervals. For the period between 2008 and 2011 station GW2025 has daily GWL measurements, but for the remaining time there measurements are taken on a weekly basis. When the date of acquisition of Landsat imagery used in this study (hereinafter "Landsat date") matched an available groundwater measurement, Landsat derived results and GWL were directly correlated to each other. However, when this was not the case, the GWL data used for the correlation was the result of a linear interpolation between the two closest groundwater measurement dates available (one in the past one in the future). A maximum limit of seven days in both directions in time was set for the linear interpolation. The interpolation was the result of a weighted average between these two dates. The weighted average was calculated with inverse distance weighting (Equation 3.6), so that the GWL measured on the date with the smallest distance in time to the Landsat date contributes more to the interpolated groundwater level (GWL') than the GWL measurement taken on the date farther away as described on equation 3.6.

$$\mathrm{GWL}' = \left(1 - \frac{\Delta_1}{\Delta_1 + \Delta_2}\right) \cdot \mathrm{GWL}_1 + \left(1 - \frac{\Delta_2}{\Delta_1 + \Delta_2}\right) \cdot \mathrm{GWL}_2 \tag{3.6}$$

Where GWL' is the interpolated groundwater level on the Landsat date, Δ_1 and Δ_2 are the absolute distance in days from the Landsat date to the two closest dates when groundwater data was available. GWL_1 and GWL_2 stand for the groundwater level measured on dates 1 and 2.

Finally, Landsat derived $\Delta_{\overline{T}}$ or z-score were correlated to the GWL'. Two separate correlations were done, one for positive $\Delta_{\overline{T}}$ or z-score values with GWL' and another for negative $\Delta_{\overline{T}}$ or z-score values with GWL'. An alternative would have been to correlate absolute $\Delta_{\overline{T}}$ or z-score values to GWL' values, however, it was opted against this alternative as a differentiation between positive and negative $\Delta_{\overline{T}}$ or z-score values might offer an insight into possible differences caused by seasonal changes. If the Hypothesis proposed in this study is accurate, we should observe $\Delta_{\overline{T}}$ or z-score close to zero when the GWL' is deep and have those values become more distant to zero as the GWL' approximates the surface level, so that the nearer the GWL' is to the surface level, the farther $\Delta_{\overline{T}}$ or z-score are from zero (Figure 3.5).

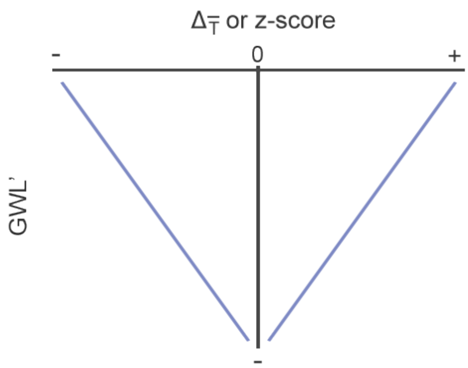

Figure 3.5: Sketch of the hypothetical relationship between temperature contrast and interpolated groundwater level.

4 Results

4.1 Groundwater, soil and air temperature

Groundwater temperature

The yearly groundwater temperature cycle is presented in figure 4.1. Groundwater temperature data for LGRB station GW2025 is available from March 2008 to October 2011. Groundwater temperature values oscillate between approx. 5 and 11 °C, reaching minimum temperatures in March and maximum temperatures in October. Overall, registered temperatures follow a smooth pattern which repeats itself in a cyclic yearly pattern, without abrupt changes from day to day. Small differences can be seen from the winter 2009/2010 to the winter 2010/2011 when temperatures are about 1 °C colder. The first fifteen measurements taken in March 2008 deviate from the pattern visible for the same period in other years. First they decrease abruptly, approximately by 1 °C in 15 days, afterwards they start gradually increasing at a rate comparable to data acquired during the next years.

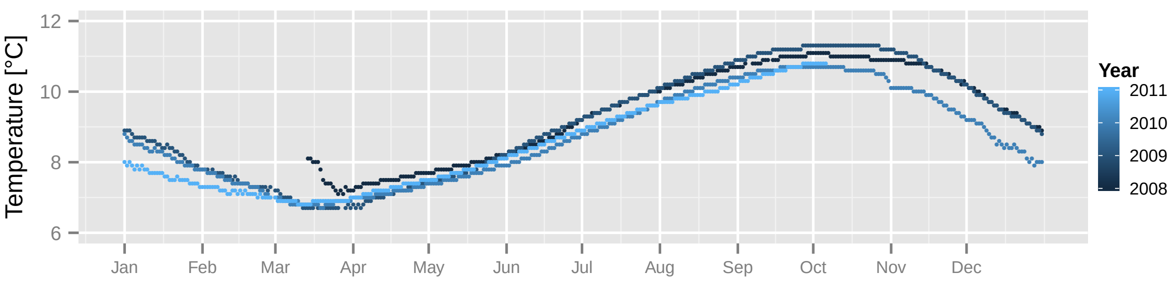

Figure 4.1: Yearly groundwater temperature cycle.

Soil and air temperature

The yearly soil and air temperature cycle is presented in figure 4.2, using daily average values for soil and air temperatures, taken at DWD station #3927 in Pfullendorf, Germany.

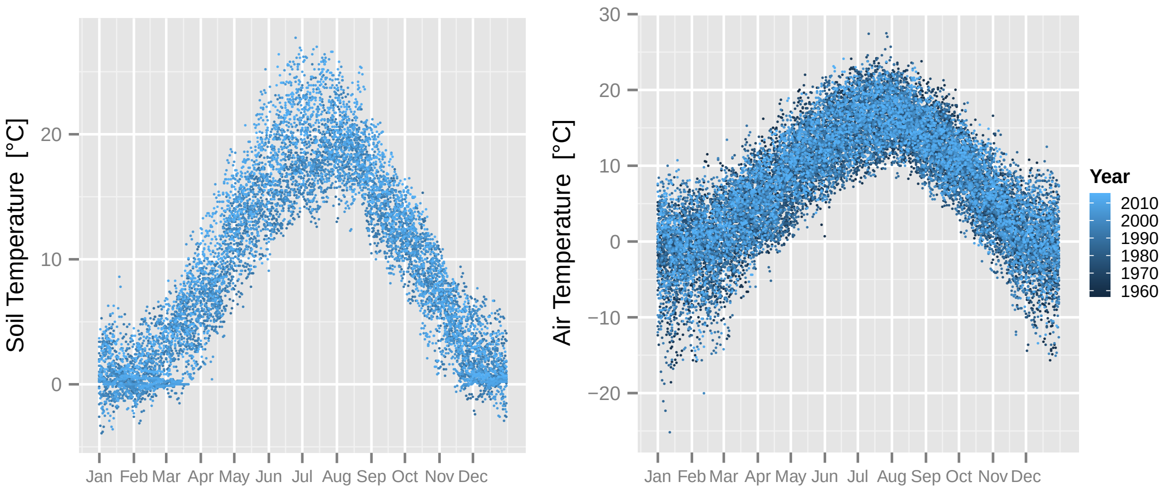

(a) Soil temperature 5 cm b.g.s.l. at DWD station #3927.

(b) Air temperature at DWD station #3927.

Figure 4.2: Yearly air and soil temperature measurements in the study site.

Soil temperatures recorded at 5 cm b.g.s.l. from 1988 to 2014, are presented in sub-figure 4.2(a). Maximum soil temperatures were primarily registered in July, in that month, temperatures range from 13 °C to 28 °C. Thus, the temperatures in the warmest month of the year vary within a maximum range of 15 °C. Minimum soil temperatures were primarily registered in January, in that month, temperatures range from -4 °C to 8 °C, Thus, the temperatures in the coldest month of the year vary within a maximum range of 12 °C.

Air temperatures were recorded at 2 m a.g.s.l. from 1958 to 2014 and are presented in sub-figure 4.2(b). Maximum air temperatures were primarily registered in July, in that month, temperatures range from 8 °C to 28 °C, whereby only five measurements exceed 25 °C. This means, that most temperatures in the warmest month of the year vary within a maximum range of 17 °C. Minimum air temperatures were primarily registered in January, in that month, temperatures range from -25 °C to 10 °C, whereby only six measurements lie below -18 °C. Thus, most temperatures in the coldest month of the year vary within a maximum range of 28 °C.

Groundwater temperature to soil and air temperature difference

Temperature differences (Δ_T) between groundwater and air or soil are represented in figure 4.3. Δ_T is calculated using mean daily records for the period between 2008 and 2011. Points are color coded according to the year in which the measurements were recorded.

Sub-figure 4.3(a) shows the groundwater temperature at LGRB groundwater station GW2025 minus the soil temperature at DWD station #3927 [Δ_T (GW T - Soil T)]. Absolute maximum Δ_T (GW T - Soil T) reaches 17.9 °C during the summer and only 12.2 °C during winter. The

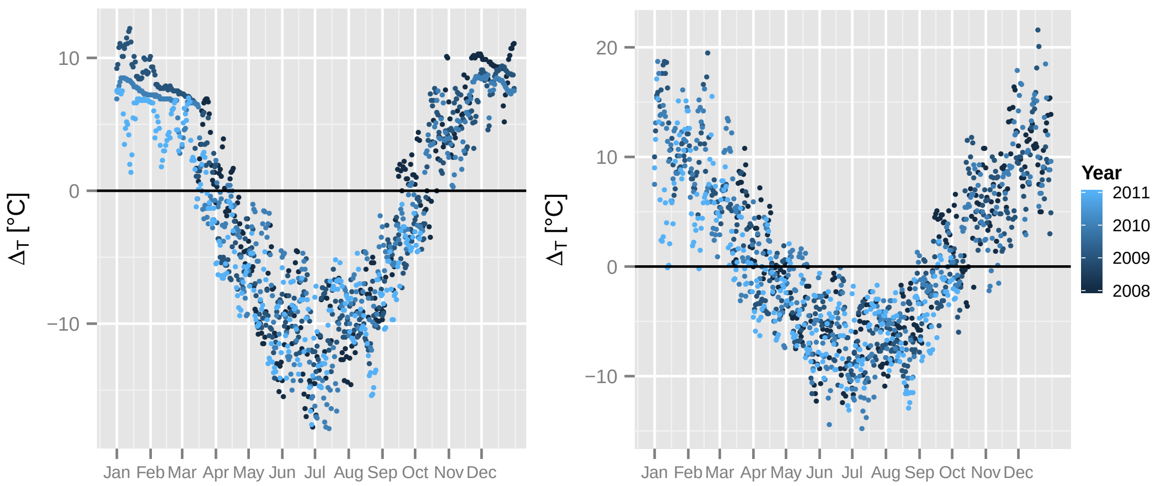

(a) Δ_T (GW T - Soil T): Groundwater to soil temperature difference.

(b) Δ_T (GW T - Air T): Groundwater to air temperature difference.

Figure 4.3: Yearly groundwater to soil (or air) temperature difference.

range of negative Δ_T (GW T - Soil T) values is greater than the range of positive Δ_T (GW T - Soil T) values, particularly for measurements taken from June to August, when Δ_T (GW T - Soil T) values range from -5 to -18 °C. During the winter months, from December to February, positive Δ_T (GW T - Soil T) values range only from 6 to 12 °C. Only between January 4^{th} - 16^{th}, 2011 and between February 2^{nd} - 17^{th}, 2011, there is a deviation from this pattern, where some Δ_T (GW T - Soil T) values approximate zero.

Sub-figure 4.3(b) shows the groundwater temperature at LGRB groundwater station GW2025 minus the air temperature at DWD station #3927 [Δ_T (GW T - Air T)]. Absolute maximum Δ_T (GW T - Air T) reaches only 14.8 °C during the summer and 21.6 °C during winter. The maximum absolute range of values Δ_T (GW T - Air T) can take, in any month of the year, is of approximately 15 °C and relatively constant throughout the year. The first two months in 2011 present an exemption, as Δ_T (GW T - Air T) reaches values close to zero around the 15^{th} of January and the 12th of February, a pattern which deviates from the pattern visible in previous years.

Relationship between in situ temperature measurements

A simple linear regression was calculated to predict soil temperature at 5 cm b.g.s.l. based on air temperature in DWD station #3927 (Figure 4.4). A significant regression equation was found ($f_{(x)}$=0.93x-2.58, $p < 0.005$), with a coefficient of determination (R^2) of 0.888. For air temperatures over 0 °C, paired values lie close to the one to one line; whereby more than 50 % of those values lie slightly over the one to one line. For air temperatures under 0 °C this relationship is distorted, so that soil temperatures remain on a range between -4 °C and

4 °C despite decreasing air temperatures. The distance of paired values to the regression line increases with air temperatures below -5 °C.

Paired data in the soil (or air) temperature to groundwater temperature correlation in figure 4.5 form a circular pattern. Soil (or air) temperatures are warmer than groundwater temperatures during the summer and colder during winter. In both relationships, paired values rarely approximate the one to one line, when they do so, it is only during the transition months between winter and summer (March and April) and during the transition months between summer and winter (September and October). A simple linear regression between soil temperature at 5 cm b.g.s.l. and groundwater temperature (Sub-figure 4.5(a)) resulted in an R^2 of 0.073 ($f_{(x)}$=0.05x+8.4, $p < 0.005$). A simple linear regression between air temperature at 2 m a.g.s.l. and groundwater temperature (Sub-figure 4.5(b)) resulted in an R^2 of 0.088 ($f_{(x)}$=0.06x+8.5, $p < 0.005$). Soil temperatures for December and January cover a smaller range than air temperatures for the same months.

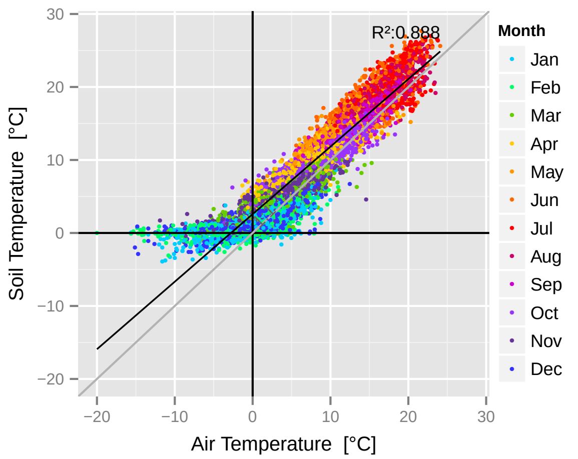

Figure 4.4: Relationship between air and soil temperature.

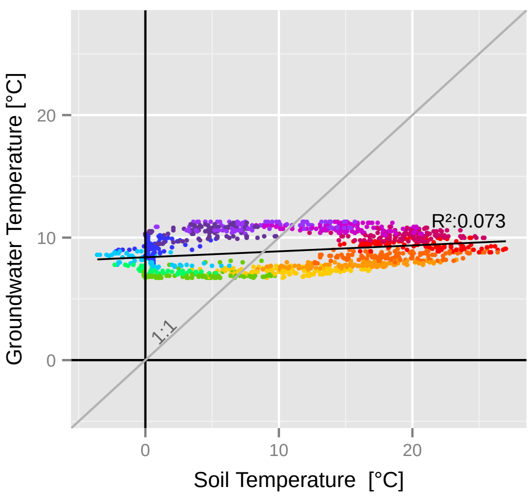

(a) Relationship between soil and groundwater temperature.

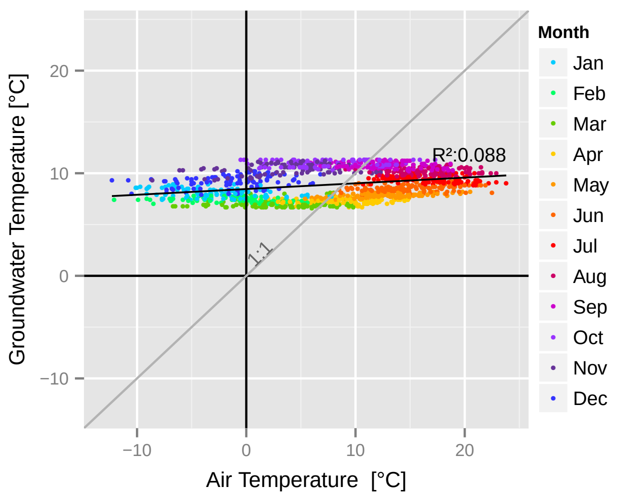

(b) Relationship between air and groundwater temperature.

Figure 4.5: Relationship between soil (or air) temperature and groundwater temperature.

4.2 Land use zonification

Figure 4.6 shows the Pfrunger-Ried study area with peatland and raised bog areas as defined on the peatland cadastre (LUBW 2014). This map includes the peatland surrounding zone defined in this study, which extends over a buffer zone at a distance of 700 m from the external peatland border. Groundwater stations GW2013 and GW2025, as well as proxy groundwater station zones GW2013pr and GW2013pr along with their corresponding comparison zones EastCZ and WestCZ, are shown in the map. Proxy groundwater zones and comparison zones each cover an area of approximately 12 ha, raised bogs cover an area of approximately 324 ha, peatland covers an area of approximately 2225 ha and surrounding buffer zone cover an area of approximately 2969 ha.

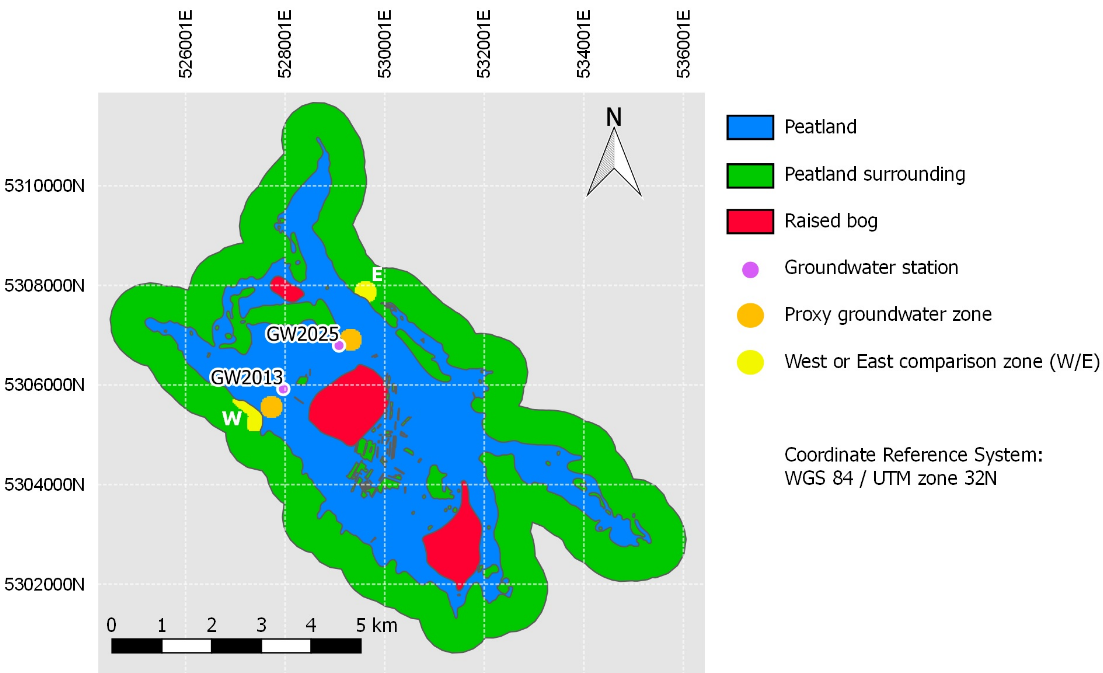

Figure 4.6: Peatland and surrounding buffer zones for Pfrunger-Ried.

The starting point for the selection of grassland areas in the Pfrunger-Ried is presented in sub-figure 4.7(a), with a Google Earth image recorded the 18^{th} of August, 2014. In the northern and southern edges of the map, urban areas are recognizable. Dark green areas, mainly located in the central region of the peatland, are forested areas. Sub-figure 4.7(b) presents the result of the grassland zonification process where only the grassland cover is visible. Less than 50 % of the original area is defined as grassland and can be used for a zonal temperature comparison.

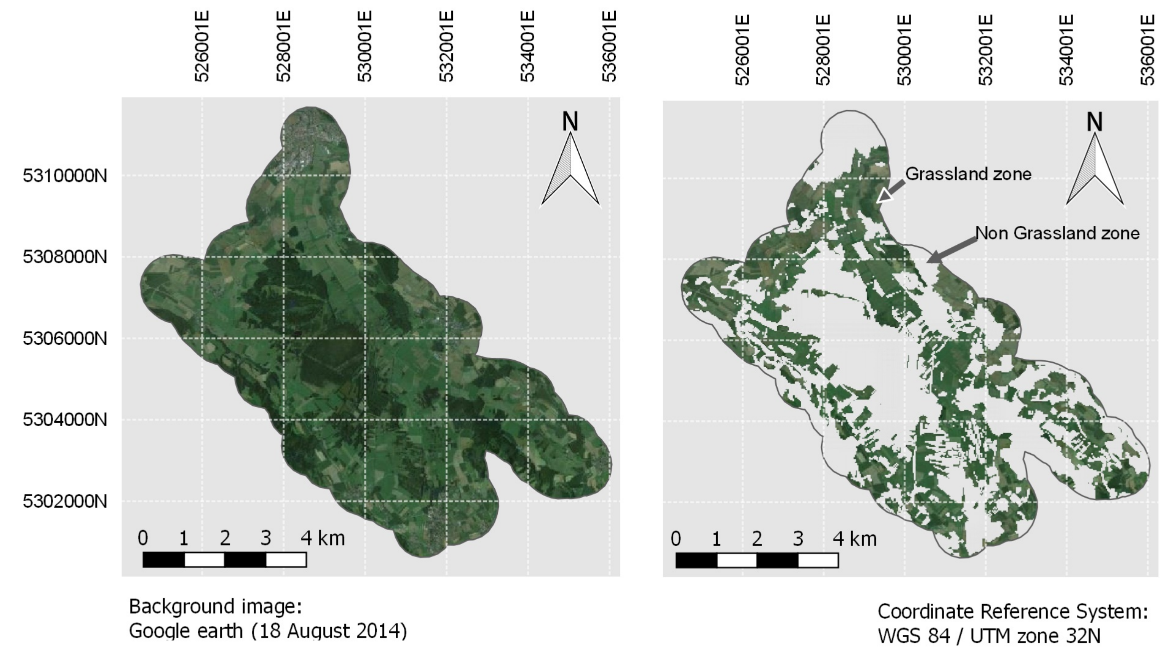

(a) Pfrunger-Ried peatland and surrounding in Google Earth satellite imagery.

(b) Pfrunger-Ried peatland and surrounding grassland in Google Earth satellite imagery.

Figure 4.7: Pfrunger-Ried grassland zone definition.

Figure 4.8 presents the results for the grassland zonification overlapped with the peatland zonification. Most of the raised bog area and the central peatland area is excluded because forest is the dominant land cover there. Each colored area in this map represents the zones upon which mean zonal temperatures are to be computed i.e., without taking into account

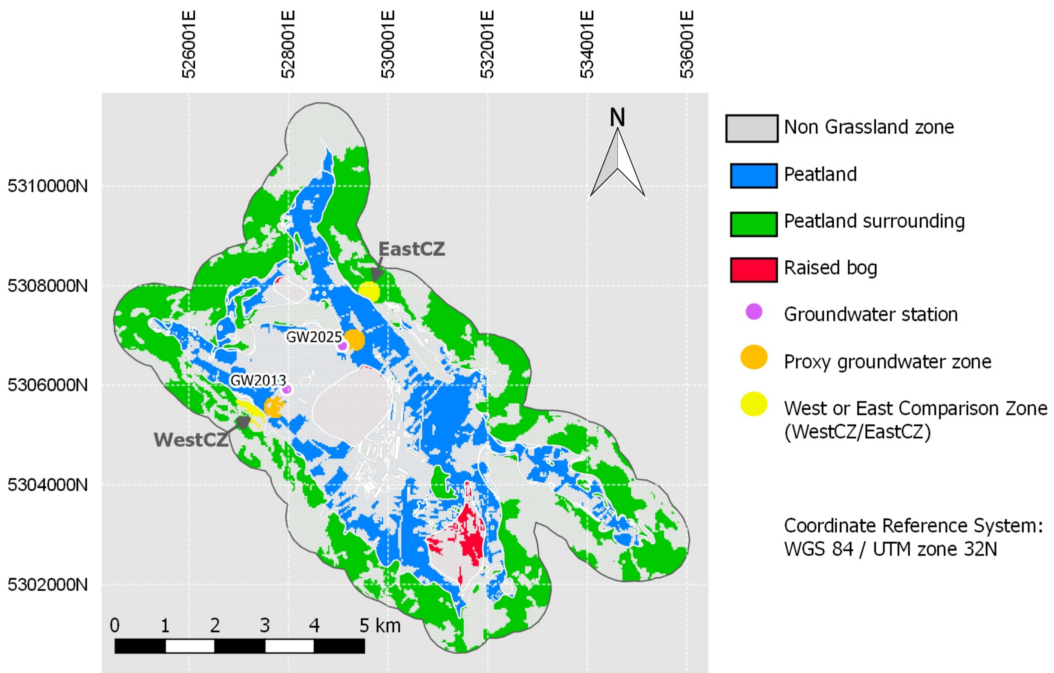

Figure 4.8: Grassland peatland and surrounding zonification for Pfrunger-Ried.

the cloud, cloud shadow or snow covered areas which were also excluded from each Landsat image.

Figure 4.9 presents the results for the grassland zonification overlapped with peatland zonification in the peatland areas: Fetzach-Taufach, Arrisrieder, Reicher, SW of Goettlishofen, Isnyer, bei Rengers, Christazhofen, Oberweihermoor, Roemerkastell. According to the WaBoA

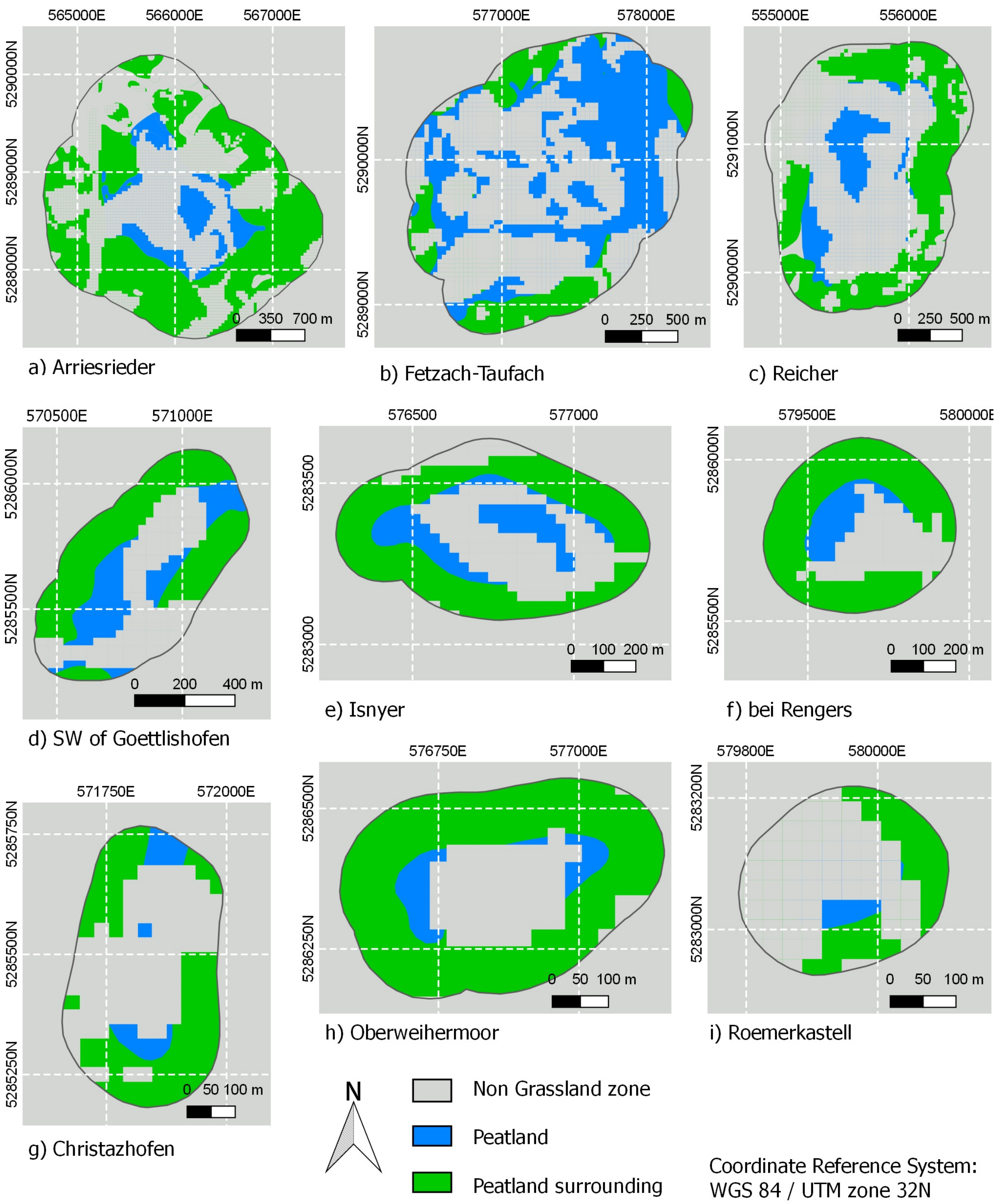

Figure 4.9: Grassland peatland and surrounding zonification for a) Fetzach-Taufach, b) Arrisrieder, c) Reicher, d) SW of Goettlishofen, e) Isnyer, f) bei Rengers, g) Christazhofen, h) Oberweihermoor, i) Roemerkastell.

land use map, these peatland areas and their surrounding area have a grassland land use, however upon closer examination on Google Earth, the grassland zone is smaller for all peatland forms. In all of the selected peatland areas there is presence of forest within the peatland area. In some cases, the presence of the forest land use ends close to the peatland borders, as is the case for the peatland areas shown in sub-figures 4.9 (c), (e), (f), (g), (h) and (i). When the peatland is particularly small, and a great portion of the peatland area is excluded due to a differing land use, the peatland areas are represented by limited number of pixels. In Roemerkastell only three pixels, representing a ground area of 30 x 30 m, characterize the peatland area, in Christazhofen twelve and in Oberweihermoor sixteen.

4.3 Landsat Thermal Infrared imagery

Availability of Landsat imagery

A list of dates with available and usable Landsat imagery for this study was presented in figure 3.2. Further analysis revealed that this data set had to be further reduced. In some cases because, the cfmask assigned cloud or snow coverage to the entire zone which was to be used to compute a zonal mean temperature. Table 4.1 presents the dates when no pixels in the grassland zones in Pfrunger-Ried were free of clouds, cloud shadows or snow.

Table 4.1: Pfrunger-Ried unavailable Landsat imagery due to cloud or snow coverage in selected areas.

Date	Peatland	Raised bog	Surround	GW2013pr	GW2025pr	EastCZ	WestCZ
July 4^{th}, 1985	x	x	x	x	x	x	x
January 14^{th}, 1987	x	x	x	x	x	x	x
January 30^{th}, 1987		x	x	x	x	x	x
August 28^{th}, 1988					x		
September 19^{th}, 1990	x	x	x	x	x	x	x
Sepember, 22^{nd}, 1997				x			x
October, 8^{th}, 1997				x	x		
June 5^{th}, 1998	x	x	x	x	x	x	x
June 10^{th}, 2000						x	
August 16^{th}, 2001						x	
September 7^{th}, 2003				x	x	x	x
June 24^{th}, 2005				x	x		x
September 7^{th}, 2009					x	x	
August 9^{th}, 2010				x			x
August, 12^{nd}, 2011				x	x	x	x
August 28^{th}, 2011				x			

Distribution of mean temperatures derived from Landsat TIR Imagery for Pfrunger-Ried peatland and surrounding grassland zone

Figure 4.10 presents the yearly cycle of at-sensor mean temperatures ($\overline{T}$) derived from the Landsat TIR sensor. $\overline{T}$ were averaged for the grassland peatland and surrounding zones shown in figure 4.8. The pattern of at-sensor $\overline{T}$s shows overall warmer temperatures in the summer months and colder temperatures in the winter months. Maximum $\overline{T}$s were reached August 8^{th}, 2003 with 35 °C in the peatland area and 37 °C in the surrounding area. Minimum $\overline{T}$ was reached January 30^{th}, 1987 with -1 °C in the peatland area, and November 27^{th}, 1986 with 11 °C in the surrounding area. $\overline{T}$ for January, 1987 could not be computed for the surrounding area as the entire area was either snow or cloud covered. The highest amount of $\overline{T}$ results is concentrated in the summer months, no $\overline{T}$s could be calculated for December, $\overline{T}$s for November could be computed only for 1986 and 1987 and $\overline{T}$s for February could only be computed for 1990 and 1997. Overall, the standard deviation (SD) for the summer measurements tend to be greater than the SD for the winter measurements. $\overline{T}$s in the peatland and in the surrounding area are very similar, and differences are not immediately discernible upon comparison of these two plots. The only relevant difference which could be reported about the remaining plots is that SDs showed a general tendency to become smaller when the area they represented became smaller too. Yearly $\overline{T}$s for each zone in each of the peatlands analyzed in this study were examined, some of them were also included in the appendix section. The appendix also includes Boxplots for Pfrunger-Ried peatland grassland temperatures.

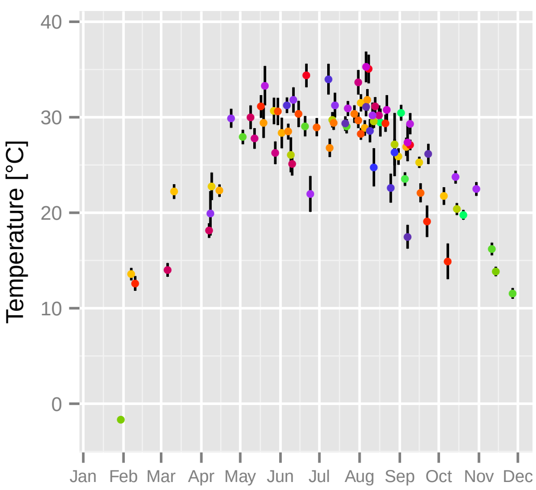

(a) At-sensor $\overline{T}$ in Pfrunger-Ried peatland

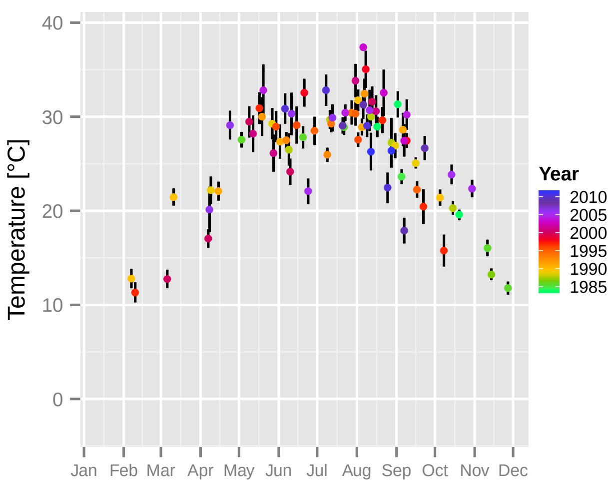

(b) At-sensor $\overline{T}$ in Pfrunger-Ried surrounding

Figure 4.10: Yearly cycle of at-sensor mean temperatures and standard deviations for Pfrunger-Ried peatland and surrounding zones.

Relationship between at-sensor temperatures and in situ measurements

To validate the accuracy of at-sensor temperature, the relationship of these results to soil (or air) temperatures measured in situ was examined (Figure 4.11). At-sensor temperatures are derived from the pixels surrounding DWD station #3927, where soil and air daily $\overline{T}$ measurements are available. Landsat temperatures correspond to records taken between between 10:35 and 10:45 a.m. LT in the winter and 11:35 and 11:45 a.m. LT in the summer, and in situ measurements represent daily means.

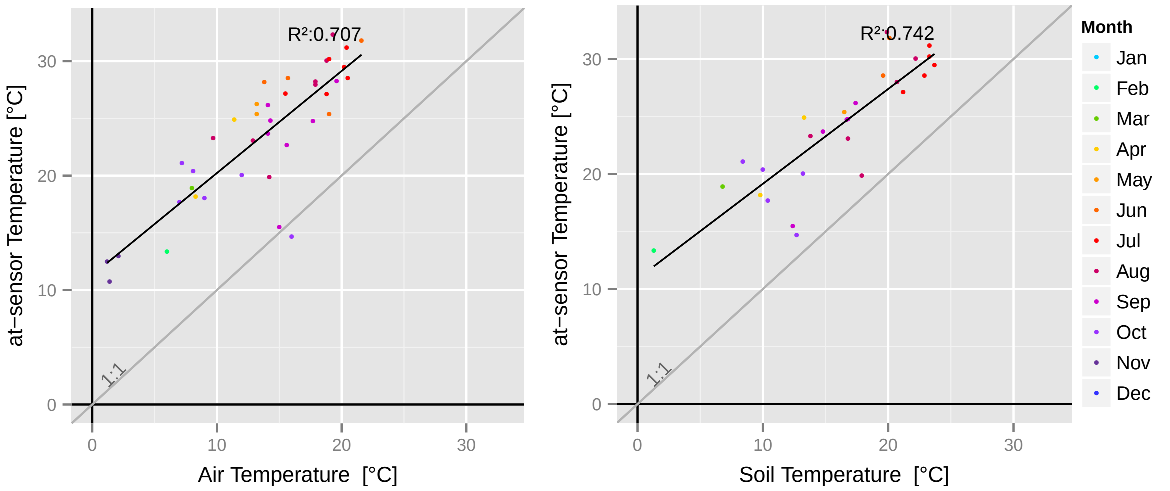

(a) Daily mean air temperature vs. at-sensor temperature.

(b) Daily mean soil temperature vs. at-sensor temperature.

Figure 4.11: Relationship between daily mean air (or soil) temperature and at-sensor temperature for DWD station #3927.

A simple linear regression was calculated to predict at-sensor temperatures based on air temperature, taken at 2 m a.g.s.l. (Sub-figure 4.11(a)). A significant linear regression equation was found ($f_{(x)}$=0.9x+11.3, $p < 0.005$), with an R^2 of 0.707. Only two measurements, taken in the months of September and October lie in the immediate proximity of the one to one line. Most at-sensor temperatures are about 11 °C higher than mean daily air temperatures. This correlation is conformed of 38 paired values corresponding to dates when Landsat (TIR imagery and cfmask) and air temperature data were available, and the area of the DWD station was not completely covered by clouds, cloud shadows or snow.

Another simple linear regression was calculated to predict at-sensor temperatures based on soil temperature, taken at 5 cm b.g.s.l. (Sub-figure 4.11(b)). A significant linear regression was found ($f_{(x)}$=0.8x+10.9, $p < 0.005$), with an R^2 of 0.742. Only two measurements, taken in the months of August, September and October lie close to the one to one line. All at-sensor temperatures are higher than mean daily soil temperatures, most of them approximately 11 °C higher. This correlation is conformed of 27 paired values corresponding to dates when

Landsat (TIR imagery and cfmask) and soil temperature data was available, and the area of the DWD station was not completely covered by clouds, cloud shadows or snow.

4.4 Temperature difference between means and z-score

The following results (Figures: 4.12 to 4.17) present yearly cycles of differences between temperature means ($\Delta_{\overline{T}}$) and z-score, with a color coding for the years in which measurements were acquired. Figures 4.12 to 4.15 present temperature contrasts in the Pfrunger-Ried peatland, while figures 4.16 and 4.17 present temperature differences between peatland and surrounding in the remaining nine peatland areas (Arrisrieder, Fetzach-Taufach, Reicher, SW of Göttlishofen, Isnyer, bei Rengers, Christazhofen, Oberweihermoor and Roemerkastell). $\Delta_{\overline{T}}$ values presented in this section were computed by substracting the assumed water saturated zone from the drained zone, and z-score values were computed by comparing the assumed water saturated zone vs. the joined water saturated and drained zone. This way, negative values represent colder (positive values represent warmer) conditions in the peatland area.

$\Delta_{\overline{T}}$ and z-score in Pfrunger-Ried

Figure 4.12 presents the temperature contrast between peatland and surrounding expressed as $\Delta_{\overline{T}}$ and z-score. Between mid July and October approximately 80 % of the results are negative, during the remaining time, approximately 80 % of the results are positive. There is no discernible pattern in the distribution of $\Delta_{\overline{T}}$ and z-score values according to the year in which they were acquired. Sub-figure 4.12(a) presents the difference between peatland $\overline{T}$ and surrounding $\overline{T}$. Minimum $\Delta_{\overline{T}}$ is reached in August, 2005 with -2.1 °C; $\Delta_{\overline{T}} < 1$ °C occurs only during the months of August and September. Maximum $\Delta_{\overline{T}}$ is reached in June, 2000 with 1.8 °C; $\Delta_{\overline{T}} > 1$ °C occurs from February to mid July. Sub-figure 4.12(b) presents the z-score of peatland vs. peatland & surrounding. Minimum z-score is reached in August, 2011 with -0.61; Z-score < 0.4 occurs only during the months of August and September. Maximum z-score is reached in March, 2000 with 0.7; Z-score > 0.4 occurs from February to August and in November.

Figure 4.13 presents the temperature contrast between raised bog and peatland expressed as $\Delta_{\overline{T}}$ and z-score. In this comparison, the peatland $\overline{T}$ is subtracted from the raised bog $\overline{T}$. In this case, negative values represent colder (positive values represent warmer) conditions in the raised bog area. Overall, negative values reach a greater distance to zero than positive values, and approximately 70 % of the results are negative values distributed throughout the

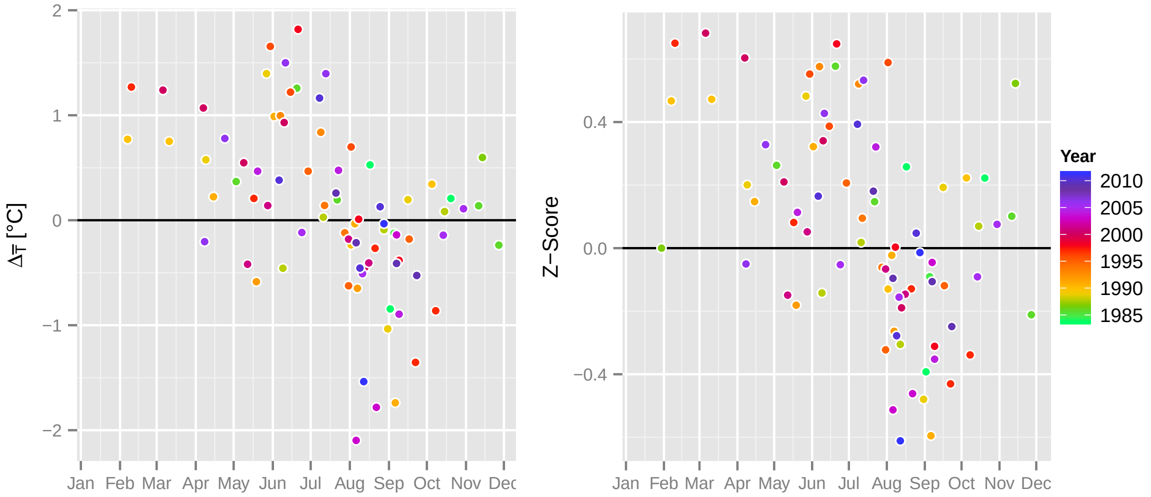

(a) $\Delta_{\overline{T}}$ (Peatland $\overline{T}$ - Surrounding $\overline{T}$) (b) z-score (Peatland vs. Peatland & Surrounding)

Figure 4.12: Pfrunger-Ried temperature contrast between peatland and surrounding expressed as $\Delta_{\overline{T}}$ and z-score.

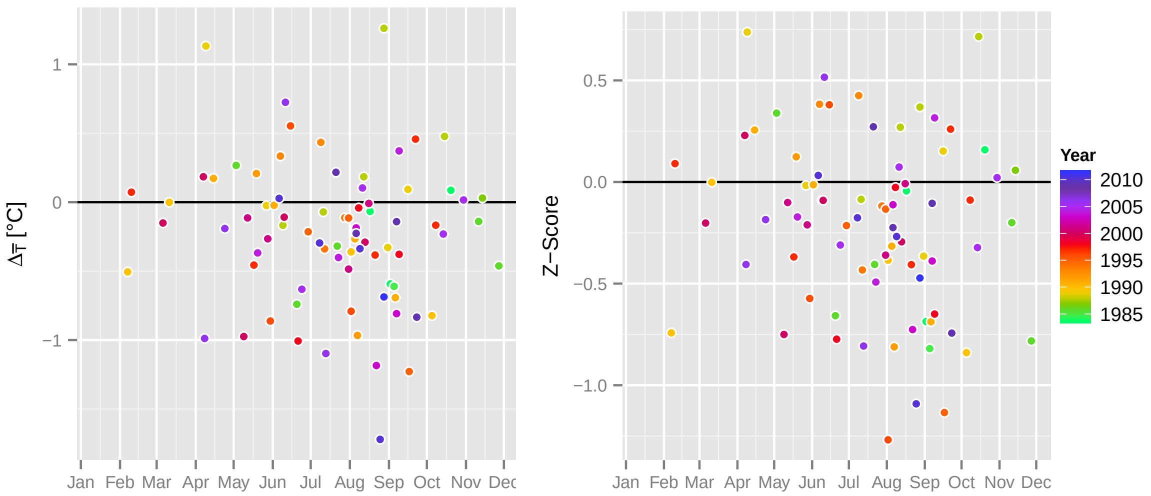

(a) $\Delta_{\overline{T}}$ (Raised Bog $\overline{T}$ - Peatland $\overline{T}$) (b) z-score (Raised Bog vs. Raised Bog & Peatland)

Figure 4.13: Pfrunger-Ried temperature contrast between raised bog and peatland expressed as $\Delta_{\overline{T}}$ and z-score.

entire year. There is no discernible pattern in the distribution of $\Delta_{\overline{T}}$ and z-score values according to the year in which they were acquired. Sub-figure 4.13(a) presents the difference between raised bog $\overline{T}$ and peatland $\overline{T}$. Minimum $\Delta_{\overline{T}}$ is reached in August, 2010 with -1.7 °C; $\Delta_{\overline{T}} < -1$ °C occurs only during the months between July and September. Maximum $\Delta_{\overline{T}}$ is reached in August, 1988 with 1.2 °C; $\Delta_{\overline{T}} > 1$ °C occurs only in April and in August. Sub-figure 4.13(b) presents the z-score of raised bog vs. raised bog & peatland. Minimum z-score is reached in August, 1996 with -1.5; Z-score < -1 occurs only during the months of August and September. Maximum z-score is reached in April, 1991 with 0.75; Z-score > 0.5 occurs in April, June and October.

Figure 4.14 presents the temperature contrast between the proxy zone for groundwater station 2025 (GW2025pr) and the east comparison zone (EastCZ) located in the surrounding area, expressed as $\Delta_{\overline{T}}$ and z-score. Slightly over 50 % of the results are positive values, evenly distributed throughout the year's cycle. There is no discernible pattern in the distribution of $\Delta_{\overline{T}}$ and z-score values according to the year in which they were acquired. Sub-figure 4.14(a) presents the difference between GW2025pr $\overline{T}$ and EastCZ $\overline{T}$. Minimum $\Delta_{\overline{T}}$ is an outlier value reached in April, 2006 with -5.7 °C; $\Delta_{\overline{T}} <$ -2 °C occurs only during the months between April and May. Maximum $\Delta_{\overline{T}}$ is reached in May, 1989; May, 2001 and June, 1986 with approximately 2.1 °C. Sub-figure 4.12(b) presents the z-score of GW2025pr vs. GW2025pr & EastCZ. Minimum z-score is an outlier value reached in July, 1985 with -4 and maximum z-score is also an outlier value reached in September, 1997 with 1.9. The remaining positive and negative values are evenly distributed throughout the year.

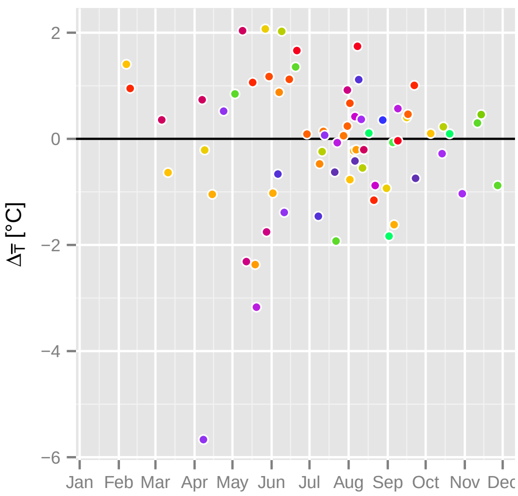

(a) $\Delta_{\overline{T}}$ (GW2025pr $\overline{T}$ - EastCZ $\overline{T}$)

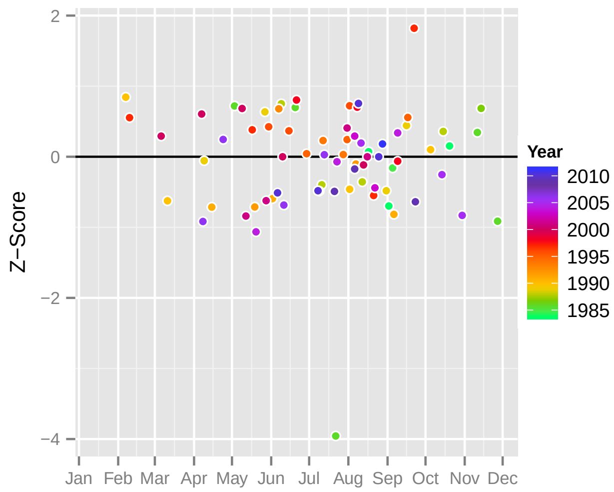

(b) z-score (GW2025pr vs. GW2025pr & EastCZ)

Figure 4.14: Pfrunger-Ried temperature contrast between GW2025pr and EastCZ expressed as $\Delta_{\overline{T}}$ and z-score.

Figure 4.15 presents the temperature contrast between the proxy zone for groundwater station 2013 (GW2013pr) and the west comparison zone (WestCZ) located in the surrounding area, expressed as $\Delta_{\overline{T}}$ and z-score. Approximately 60 % of the results are positive values, evenly distributed throughout the year. Negative values occur between March and September. There is no discernible pattern in the distribution of $\Delta_{\overline{T}}$ and z-score values according to the year in which they were acquired. Sub-figure 4.15(a) presents the difference between GW2013pr $\overline{T}$ and WestCZ $\overline{T}$. Minimum $\Delta_{\overline{T}}$ is an outlier value reached in May, 2004 with -6 °C; $\Delta_{\overline{T}} <$ -1 °C occur during May, June, August and September. Maximum $\Delta_{\overline{T}}$ is reached in June, 2000 and August, 1998 with approximately 1.6 °C. Sub-figure 4.15(b) presents the z-score of GW2013pr vs. GW2013pr & WestCZ. Minimum z-score is an outlier value reached in September, 1995 with -2, followed by another outlier value reached in May, 2004 with -1.7. Maximum z-score value is reached in August, 1984 with 0.8, closely followed by several other results taken between the months of February and October. The remaining positive and negative values are evenly distributed in the year.

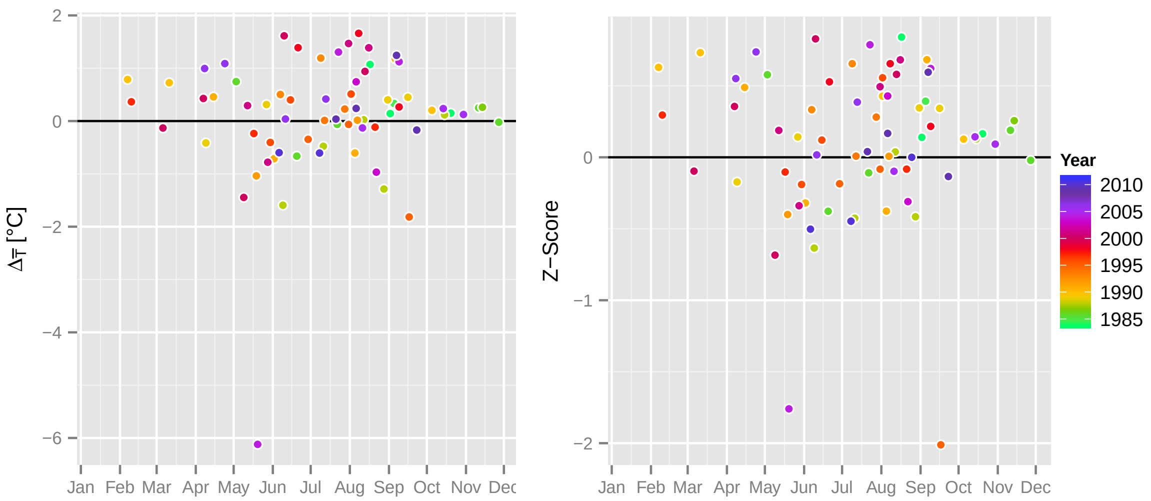

(a) $\Delta_{\overline{T}}$ (GW2013pr $\overline{T}$ - WestCZ $\overline{T}$) (b) z-score (GW2013pr vs. GW2013pr & WestCZ)

Figure 4.15: Pfrunger-Ried temperature contrast between GW2013pr and WestCZ expressed as $\Delta_{\overline{T}}$ and z-score.

$\Delta_{\overline{T}}$ in other peatland areas (Arrisrieder, Fetzach-Taufach, Reicher, SW of Göttlishofen, Isnyer, bei Rengers, Christazhofen, Oberweihermoor and Roemerkastell)

Temperature contrasts in other peatland areas are presented only as $\Delta_{\overline{T}}$ values as for smaller areas, z-score outliers were generated more often than using $\Delta_{\overline{T}}$ measurements. Figure 4.16 presents $\Delta_{\overline{T}}$ values for peatlands $\geq$ 30 ha, while figure 4.17 presents $\Delta_{\overline{T}}$ values for peatland areas $<$ 30 ha.

Figure 4.16 presents $\Delta_{\overline{T}}$ values for peatland areas: a) Arrisrieder, b) Fetzach-Taufach, c) Reicher, d) SW of Göttlishofen. In sub-figures 4.16(a),(b),(d), more than 50 % $\Delta_{\overline{T}}$ of the values are negative, while in sub-figure 4.16(c) more than 50 % $\Delta_{\overline{T}}$ of the values are positive. In sub-figures 4.16(a) to (c) positive values are arranged in a way which suggests the formation of a peak in a certain time of the year. In these cases, the peak of the distribution can be interpreted by the maximal $\Delta_{\overline{T}}$ value. Maximal $\Delta_{\overline{T}}$ values are reached in May, 1986 with 1.4 °C for sub-figure 4.16(a), in May, 2004 with 2 °C for sub-figure 4.16(b), in May, 2001 and July, 2004 with 4 °C for sub-figure 4.16(c), and in September, 2004 with 0.6 °C for sub-figure 4.16(d). The distribution of negative $\Delta_{\overline{T}}$ values is more scattered. Sub-figures 4.16(a) &

(b) show greater negative $\Delta_{\overline{T}}$ values between August and September. Sub-figure 4.16(c) shows greater negative $\Delta_{\overline{T}}$ values between November and February and in sub-figure 4.16(d) between April and July. Minimal $\Delta_{\overline{T}}$ values are reached in July, 2010 with -1.1 °C for sub-figure 4.16(a), in July, 2010 with -1.7 °C for sub-figure 4.16(b), in November, 1986 with -1.6 °C for sub-figure 4.16(c), and in May, 2004 with -1.4 °C for sub-figure 4.16(d). Overall, the distribution of scatter plots in sub-figures 4.16(a) to (d) follow no recognizable pattern, neither is there a discernible pattern in the distribution of $\Delta_{\overline{T}}$ values according to the year in which they were acquired.

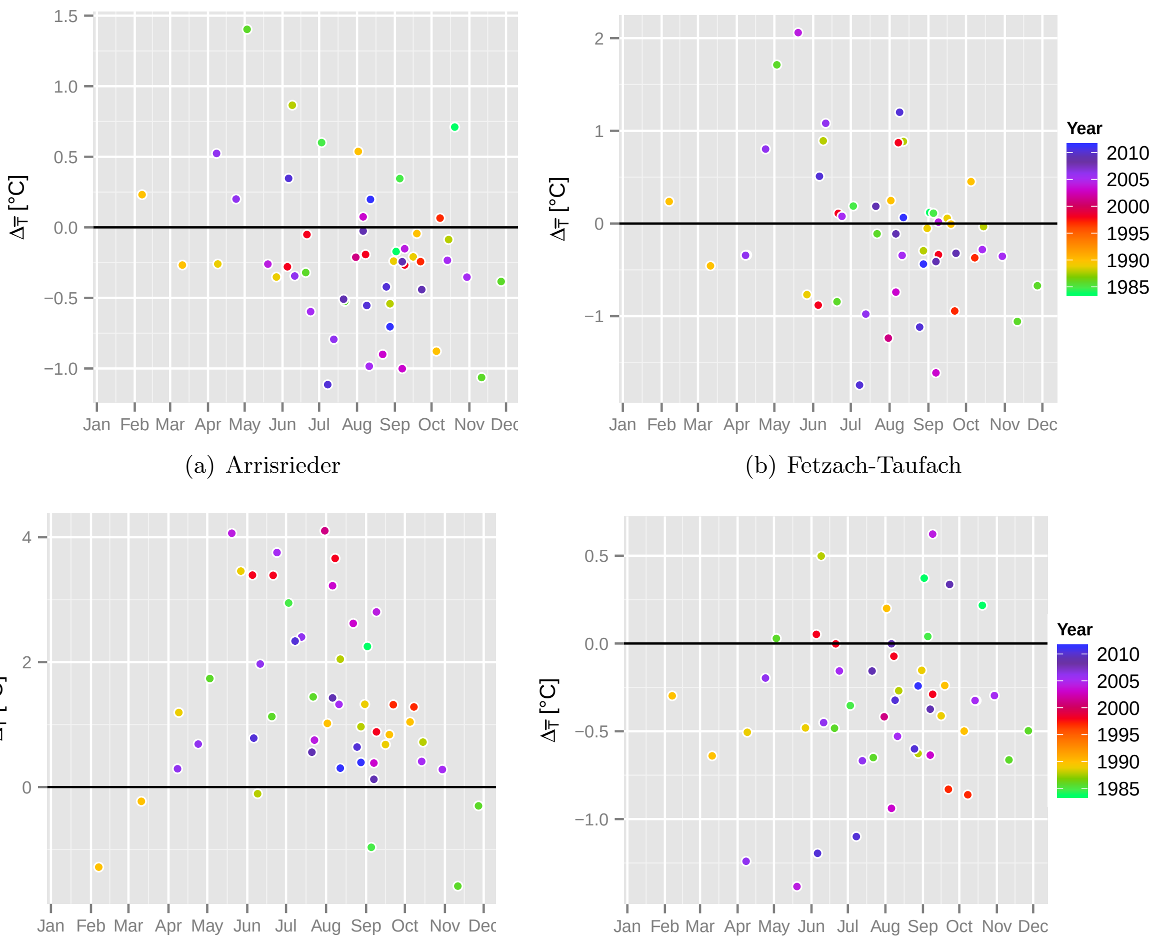

(a) Arrisrieder (b) Fetzach-Taufach

(c) Reicher (d) SW of Göttlishofen

Figure 4.16: $\Delta_{\overline{T}}$ (Peatland $\overline{T}$ - Surrounding $\overline{T}$): Difference between peatland $\overline{T}$ and surrounding $\overline{T}$.

Figure 4.17 presents $\Delta_{\overline{T}}$ values for peatland areas: a) Isnyer, b) bei Rengers, c) Christazhofen, d) Oberweihermoor and e) Roemerkastell. In sub-figures 4.17(b),(c),(e), approximately 50 % of the $\Delta_{\overline{T}}$ values are negative and 50 % positive, while in figures 4.17(a) & (d) more than 78 % $\Delta_{\overline{T}}$ values are negative. In sub-figure 4.17(e) $\Delta_{\overline{T}}$ values are mostly negative between mid July and October and mostly positive for the remaining time. For sub-figures 4.17(a),(b),(c),(d) there is no discernible pattern for the distribution of $\Delta_{\overline{T}}$ values throughout the year, neither

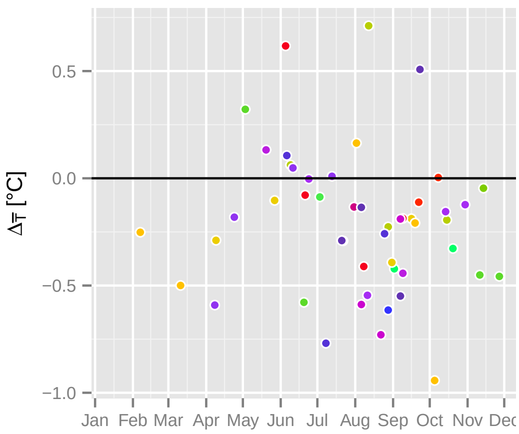

(a) Isnyer

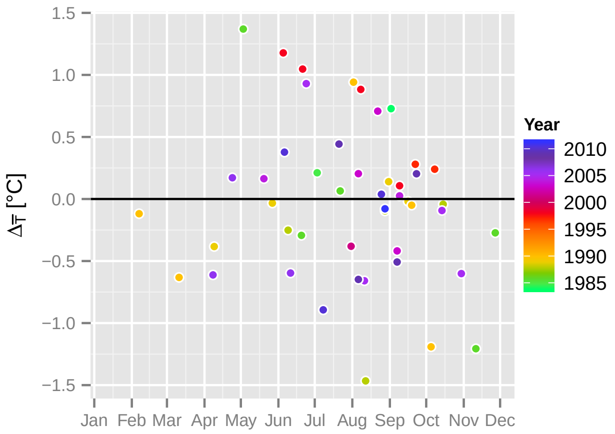

(b) bei Rengers

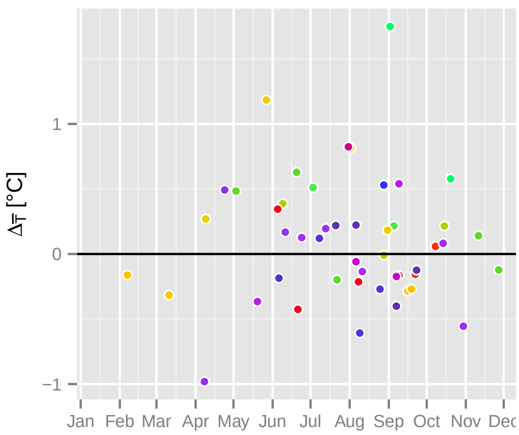

(c) Christazhofen

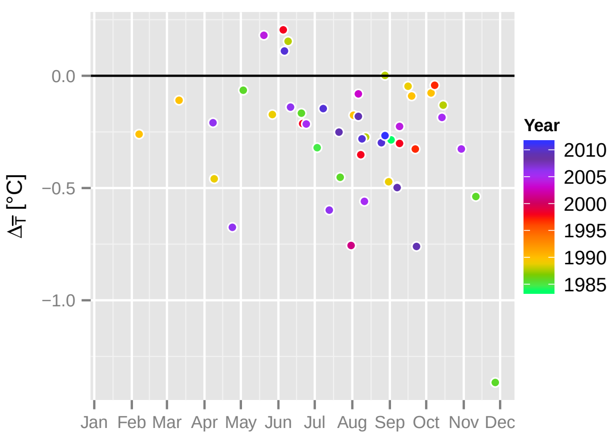

(d) Oberweihermoor

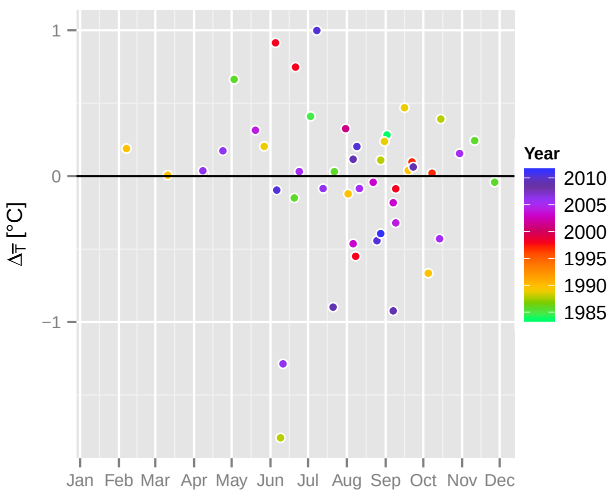

(e) Römerkastell

Figure 4.17: $\Delta_{\overline{T}}$ (Peatland $\overline{T}$ - Surrounding $\overline{T}$): Difference between peatland $\overline{T}$ and surrounding $\overline{T}$.

is there a discernible pattern in the distribution of $\Delta_{\overline{T}}$ values according to the year in which they were acquired. Maximal $\Delta_{\overline{T}}$ values are reached in August, 1988 with 0.7 °C for sub-figure 4.17(a); In September, 1988 with 1.5 °C for sub-figure 4.17(b); In June, 1984 with 1.8 °C for sub-figure 4.17(c); In June, 1998 with 0.2 °C for sub-figure 4.17(d); And in July, 2010 with

1 °C for sub-figure 4.17(e). Minimal $\Delta_{\overline{T}}$ values are reached in October, 1990 with -1 °C for sub-figure 4.17(a); In August, 1986 with -1.4 °C for sub-figure 4.17(b); In April, 2006 with -1 °C for sub-figure 4.17(c); In November, 1986 with -1.4 °C for sub-figure 4.17(d); And in June, 1988 with -1.8 °C for sub-figure 4.17(e).

4.5 Groundwater level

Figures 4.18 and 4.20 represent the yearly cycle of GWL for the stations with the longest registering period in Pfrunger-Ried. Figures 4.19 and 4.21 present the yearly cycle of interpolated groundwater levels (GWL') for the days when Landsat derived results are available. These also provide an overview of the amount of available data for a correlation between Landsat derived temperature contrasts and GWL' data, and the year and month for which they are available. Points are color coded according to the year in which they were taken. Zero represents the ground level at the measuring station, negative values represent the GWL in m b.g.s.l. and positive values represent GWL in m a.g.s.l..

Figure 4.18 presents the yearly GWL for groundwater station GW2025. Measurements are given in a weekly interval for the period between August, 1994 and March, 2008 (1^{st} phase), while from March, 2008 to December, 2011 (2^{nd} phase) measurements are given in a daily interval. There is an interruption of data collection between January and August, 1997. Overall, a downward shift in GWL values from measurements taken in the 1^{st} to the 2^{nd} phase can be observed, as measurements in the 2^{nd} phase never reach values above -20 m b.g.s.l.. During the 1^{st} phase, GWLs range between a few cm a.g.s.l. to approximately -0.5 m b.g.s.l. in the months of January to mid June. Beginning from mid June, the distance of the GWL to the ground level starts to increase, reaching the deepest GWL during the months of August and September. From October to December, GWL progressively approach the ground level again. For the most part, values range from 0 to 0.75 m b.g.s.l. during this period, in some years reaching positive values towards the end of December. During the 2^{nd} phase of the data registering period measurements range from 0.25 to 0.5 m b.g.s.l. from January to the end of April. During 2008 and 2009 GWL start lowering in May and reach minimum levels of -1 m b.g.s.l. towards mid October, from there on, levels start to rise again reaching a level of approximately 0.5 m b.g.s.l. in December. Measurements taken in 2011 show a unique pattern, where minimum levels of 0.75 m b.g.s.l. are reached from mid June to mid July. Measurements taken in 2010 range between 0.25 to 0.6 m b.g.s.l. with the minimum values taken in July and maximum values taken in December.

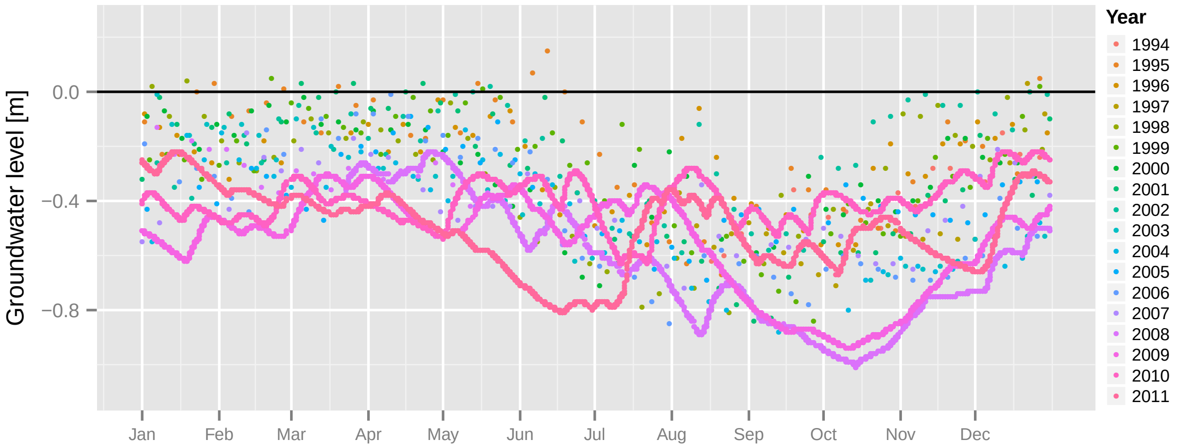

Figure 4.18: Yearly groundwater level cycle for station GW2025.

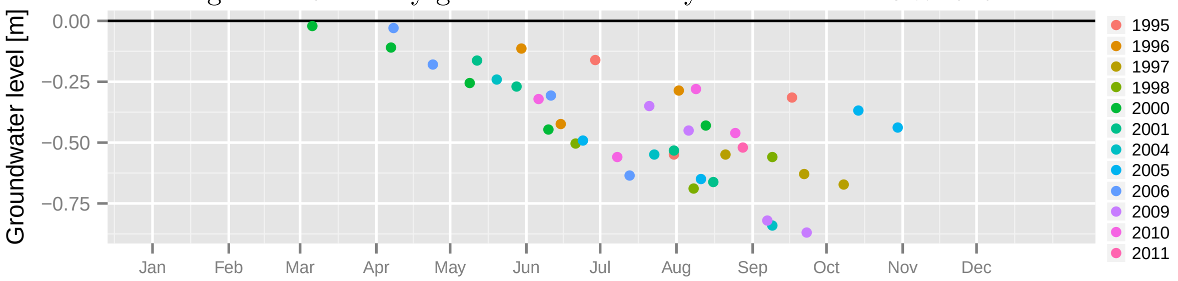

Figure 4.19: Yearly interpolated groundwater level for station GW2025.

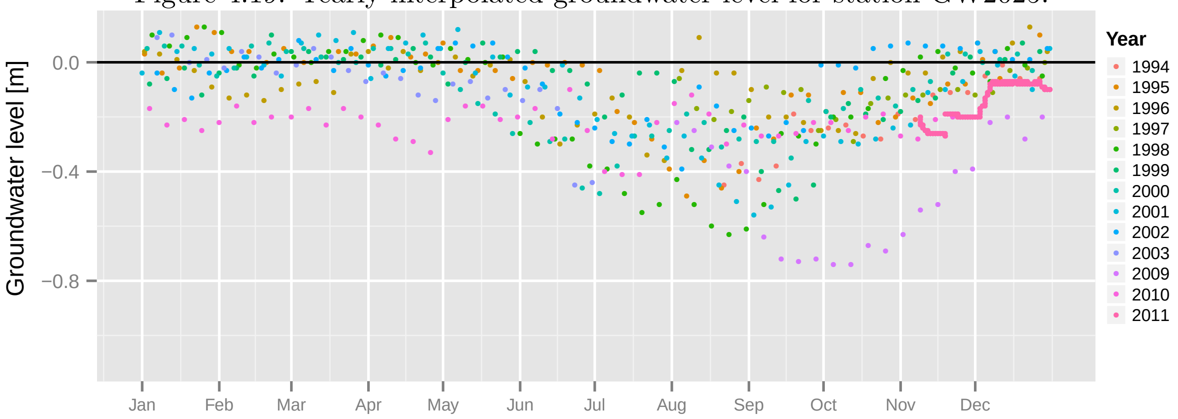

Figure 4.20: Yearly groundwater level cycle for station GW2013.

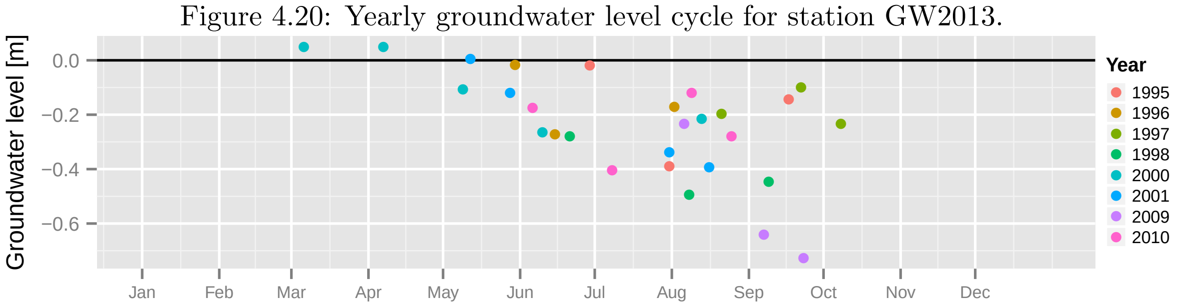

Figure 4.21: Yearly interpolated groundwater level for station GW2013.

Figure 4.20 presents the yearly GWL for station GW2013. Measurements are given in a five to ten day interval for the period between August, 1994 and June, 2003 and for the period between August, 2009 and January, 2011. From 2003 to 2009 data collection was interrupted. From November, 2011 to the end of December, 2011 measurements are given in a daily interval. For the data collected between 1994 and 2003, GWL range from -15 cm b.g.s.l. to 10 cm a.g.s.l. between January and mid May. From May on, GWL progressively decrease to reach minimum values below -0.5 m b.g.s.l. between mid July to mid September and then increases to reach maximum values again in December. GWL from 2009 reach minimum values between mid September and mid October, and values from 2010 are relatively low during the months of January to May compared to previous years.

Figure 4.19 presents GWL' for station GW2025. The available data covers the following range of years: 1995-1998, 2000-2001, 2004-2006, 2009-2011. Minimum GWL' is reached in September, and GWL' reaching ground surface level occur only during March and April. Figure 4.21 presents GWL' for station GW2013. The available data covers the following range of years: 1995-1998, 2000-2001, 2009-2010. Minimum GWL' is reached in September, and GWL' reaching ground surface level occur only from March to May. For both stations, no interpolated GWL' were computed for January, February, November and December, because no Landsat data for said months was available for the years when GWL measurements were taken.

Figure 4.22 shows the annual mean GWL for station GW2025 excluding years 1994 and 1997, when no data was available for certain months. Overall mean GWLs decrease, although this is not a monotonic fall. Annual mean GWL range between -20 cm b.g.l.s. and -60 cm b.g.l.s.

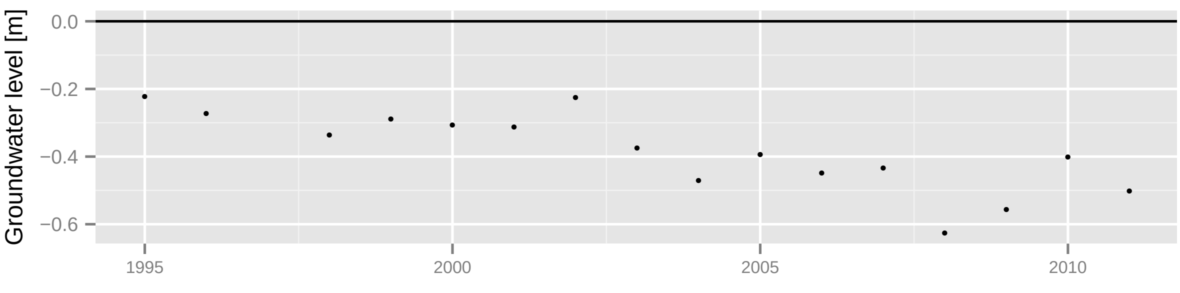

Figure 4.22: Mean annual groundwater level for station GW2025.

4.6 Relationship between temperature contrasts and groundwater level

Figures 4.23 to 4.27 show the relationship between temperature contrast ($\Delta_{\overline{T}}$ or z-score) and interpolated groundwater level (GWL') measurements from stations GW2025 or GW2013 in the Pfrunger-Ried peatland. Each graphic shows two simple linear regressions, one calculated to predict GWL' based on positive temperature contrast ($\Delta_{\overline{T}}$ or z-score) and another to predict GWL' based on negative temperature contrast (- $\Delta_{\overline{T}}$ or - z-score). The regression line is plotted along with its R^2 and the points in the scatter plot are color coded after the month in which the Landsat image was acquired.

The results in this section represent only a selection of possible correlations for the data available in the Pfrunger-Ried peatland, and they are laid out in a sequence which seeks to make the comparison between plots easier. Here are some generalities about the disposition of this section's results. Figures 4.23, 4.25, 4.26, 4.27 use $\Delta_{\overline{T}}$ as the independent variable. To compare how the GWL' correlates to z-score values, figure 4.24 uses z-score as independent variable and the same dependent variable used in figure 4.23. When comparing temperature contrasts between larger areas such as peatland and surrounding (Figures 4.23 & 4.24), or raised bog and peatland (Figure 4.25), one correlation using GWL' from station GW2025 (sub-figure (a)) and another using GWL' from station GW2013 (sub-figure (b)) are presented. When comparing a proxy groundwater station zone with the west or east comparison zone (Figure 4.26), only the GWL' from the groundwater station which corresponds to the proxy zone is presented. Available GWL' measuring points for these correlations in groundwater station GW2013 correspond to approximately 60 % of the available GWL' measuring points in groundwater station GW2025. Sub-figures 4.27(a) and (b) present the same correlation as figures 4.23(a) and 4.26(a) respectively, however, in this case, points corresponding to measurements taken in transition months are excluded. By transition months, the months between the winter and summer seasons (March and April) and between the summer and winter (September and October) seasons are meant. All linear regressions presented in this section are summarized with their corresponding function, p-value and R^2 in table 4.2.

The relationship between $\Delta_{\overline{T}}$ (Peatland $\overline{T}$ - Surrounding $\overline{T}$) and GWL' is presented in figure 4.23, using the GWL' at station GW2025 in sub-figure 4.23(a) and the GWL' at station GW2013 in sub-figure 4.23(b). There is approximately the same amount of negative x-values than there is of positive x-values in both sub-figures. The regression lines for positive x-values in both sub-figures have a positive slope and the regression line for negative x-values has a positive slope in sub-figure (a) and a negative slope in sub-figure (b). None of these correlations have a p-value under the significance level of 0.01, and all R^2 values lie below 0.1. The same is true for the figure 4.24 and the corresponding sub-figures (a) and (b). In figure 4.24, z-score values are used instead of $\Delta_{\overline{T}}$, which changes the distribution of measurements along the x-axis. This change does not reduce p-values under the significance level of 0.01 and an increase of R^2 over 0.1 occurs only for the correlation between positive z-score values and GWL' from station GW2013 in sub-figure 4.24 (b).

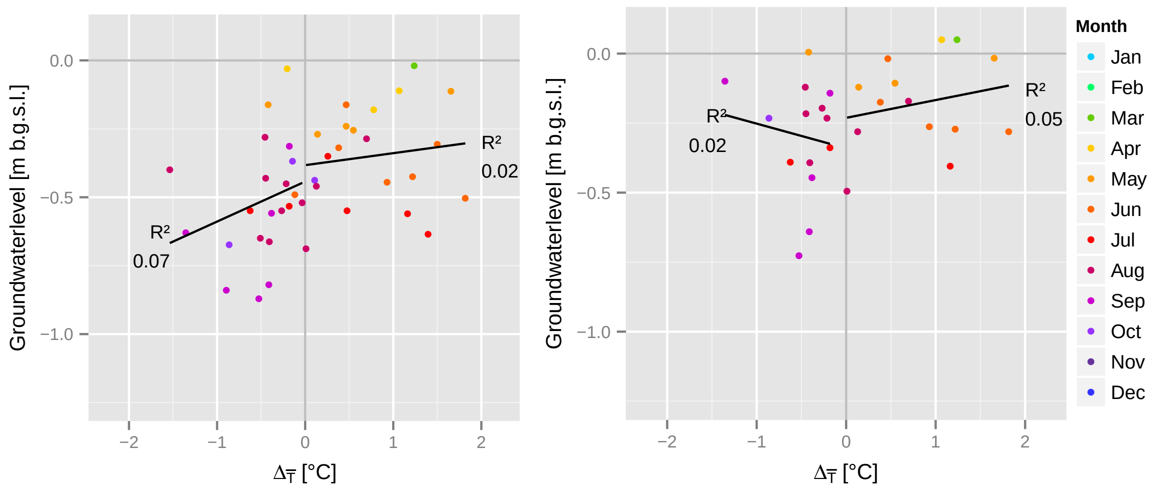

(a) $\Delta_{\overline{T}}$ (Peatland $\overline{T}$ - Surrounding $\overline{T}$) vs. GWL' at station GW2025

(b) $\Delta_{\overline{T}}$ (Peatland $\overline{T}$ - Surrounding $\overline{T}$) vs. GWL' at station GW2013

Figure 4.23: Relationship between $\Delta_{\overline{T}}$ (Peatland $\overline{T}$ - Surrounding $\overline{T}$) and interpolated groundwater level at stations GW2025 and GW2013.

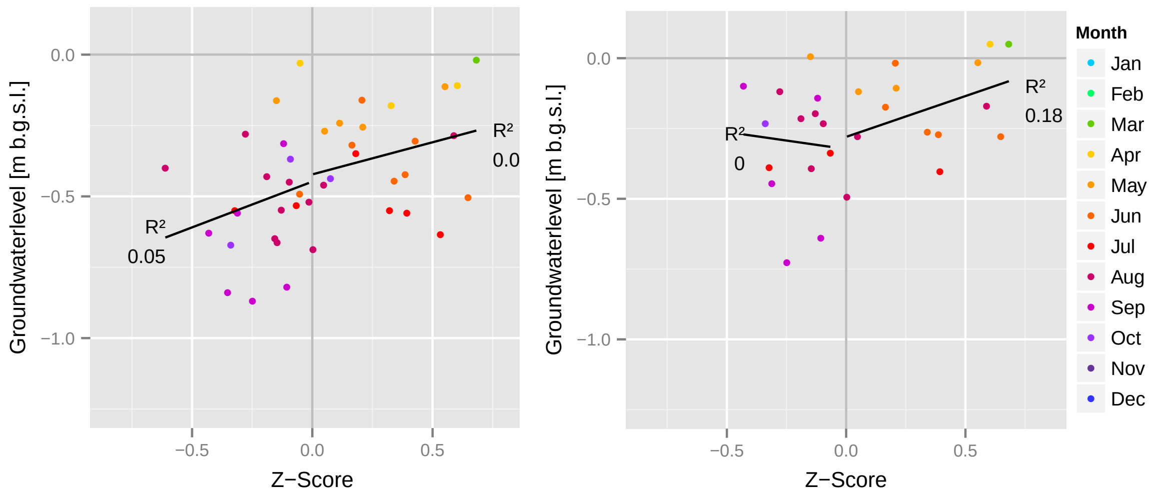

(a) z-sore (Peatland vs. Peatland & Surrounding) vs. GWL' at station GW2025

(b) z-sore (Peatland vs. Peatland & Surround) vs. GWL' at station GW2013

Figure 4.24: Relationship between z-sore (Peatland vs. Peatland & Surrounding) and interpolated groundwater level at stations GW2025 and GW2013.

The relationship between $\Delta_{\overline{T}}$ (Raised Bog $\overline{T}$ - Peatland $\overline{T}$) and GWL' is presented in figure

4.25, using the GWL' at station GW2025 in sub-figure 4.25(a) and the GWL' at station GW2013 in sub-figure 4.25(b). In sub-figure (a) approximately 79 % of all $\Delta_{\overline{T}}$ values are negative and 21 % are positive values, in sub-figure (b) approximately 85 % of all $\Delta_{\overline{T}}$ values are negative and 15 % are positive values. All regression lines in both sub-figures have negative slopes. Only one regression line (positive $\Delta_{\overline{T}}$ values in sub-figure (b)) has an R^2 over 0.1. However, said correlation uses only four measurements. Also, no regression line in figure 4.25 has a p-value under the significance level of 0.01.

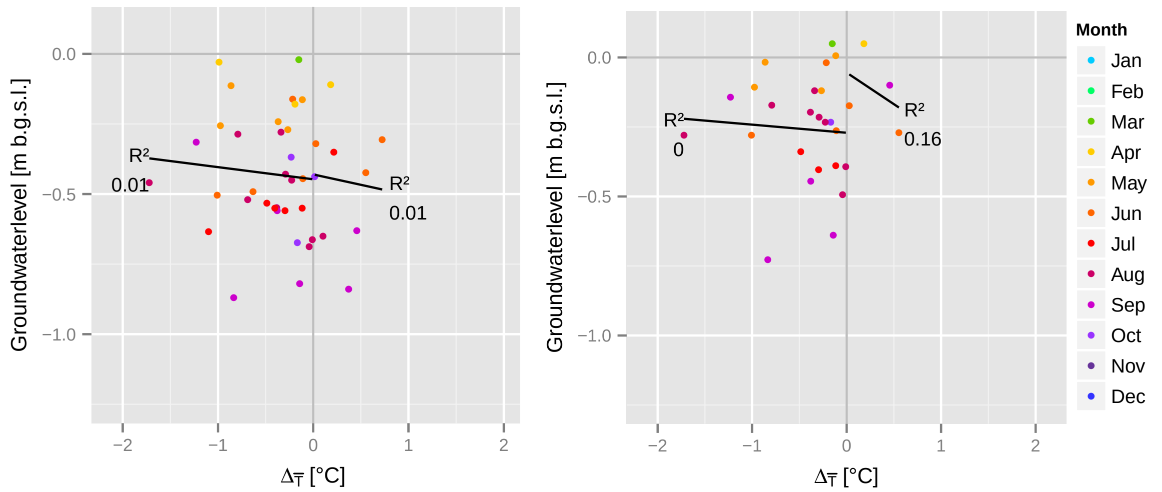

(a) $\Delta_{\overline{T}}$ (Raised Bog $\overline{T}$ - Peatland $\overline{T}$) vs. GWL' at station GW2025

(b) $\Delta_{\overline{T}}$ (Raised Bog - Peatland) vs. GWL' at station GW2013

Figure 4.25: Relationship between $\Delta_{\overline{T}}$ (Raised Bog $\overline{T}$ - Peatland $\overline{T}$) and interpolated groundwater level at stations GW2025 and GW2013.

The relationship between $\Delta_{\overline{T}}$ (GW2025pr $\overline{T}$ - EastCZ $\overline{T}$) and GWL' in station GW2025 is presented in sub-figure 4.26(a). There is approximately the same amount of negative $\Delta_{\overline{T}}$ values than there is of positive $\Delta_{\overline{T}}$ values. Both regression lines have a negative slope. The regression line using negative $\Delta_{\overline{T}}$ values has the highest R^2 ($R^2 = 0.45$) and lowest p-value ($p < 0.01$) found in the correlations presented here. However, for the correlation using positive $\Delta_{\overline{T}}$ values the R^2 sinks below 0.001 and the p-value is > 0.9. The relationship between $\Delta_{\overline{T}}$ (GW2013pr $\overline{T}$ - WestCZ $\overline{T}$) and GWL' in station GW2013 is presented in sub-figure 4.26(b). There is approximately the same amount of negative $\Delta_{\overline{T}}$ values than there is of positive $\Delta_{\overline{T}}$ values. Both regression lines have a negative slope. Only the regression line using positive $\Delta_{\overline{T}}$ values has an $R^2 > 0.2$, however both regressions have p-values over the significance level of of 0.01.

The results in sub-figure 4.27(a) should be compared against results in sub-figure 4.23(a), as both represent the same relationship. However, for the correlation presented in sub-figure 4.27(a), measurements taken during transition months were excluded. This change didn't result in higher R^2 values nor did it cause p-values to sink. The results in sub-figure 4.27(b) show the same relationship as the one shown in sub-figure 4.26(a). Similarly, measurements from transition months were excluded. This change resulted in a decrease of the R^2 value and increase of the p-value over the significance level of 0.01 for negative $\Delta_{\overline{T}}$ values. For positive $\Delta_{\overline{T}}$ values, the R^2 value increased slightly, still not reaching a value over 0.1 and p-values decreased slightly.

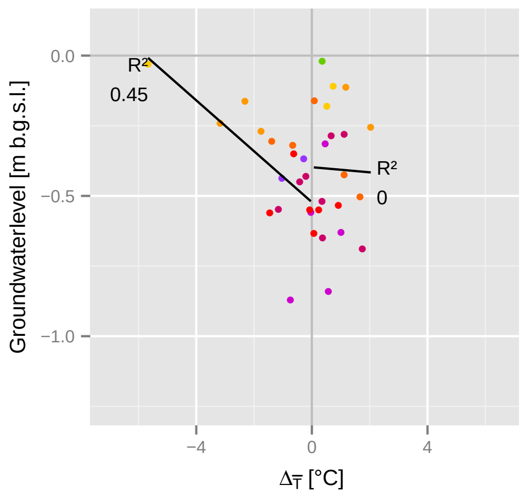

(a) $\Delta_{\overline{T}}$ (GW2025pr $\overline{T}$ - EastCZ $\overline{T}$) vs. GWL' at station GW2025

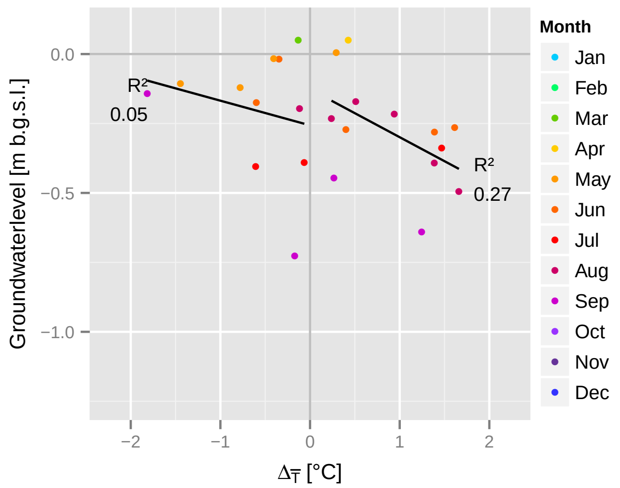

(b) $\Delta_{\overline{T}}$ (GW2013pr $\overline{T}$ - WestCZ $\overline{T}$) vs. GWL' at station GW2013

Figure 4.26: Relationship between $\Delta_{\overline{T}}$ [(GW2025pr $\overline{T}$ - EastCZ $\overline{T}$) or (GW2013 $\overline{T}$ - WestCZ $\overline{T}$)] and interpolated groundwater level at stations GW2025 or GW2013.

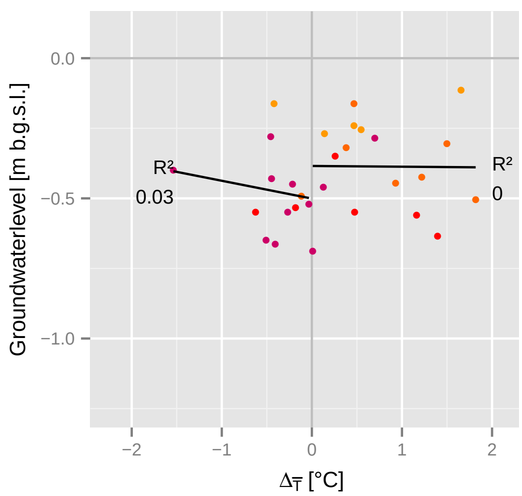

(a) $\Delta_{\overline{T}}$ (Peatland $\overline{T}$ - Surrounding $\overline{T}$) vs. GWL' at station GW2025, excluding transition months.

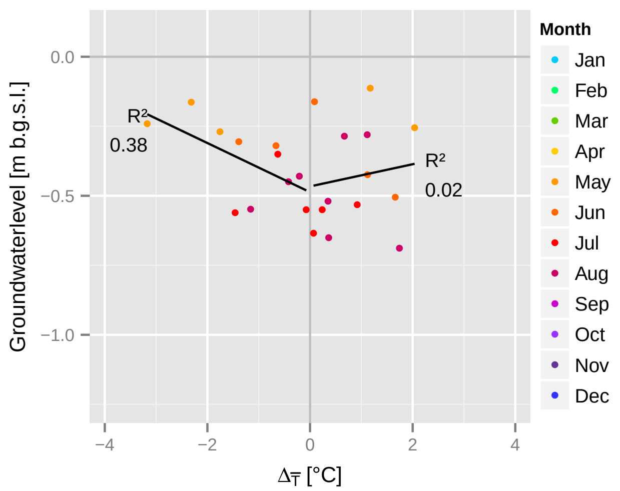

(b) $\Delta_{\overline{T}}$ (GW2025pr $\overline{T}$ - EastCZ $\overline{T}$) vs. GWL' at station GW2025, excluding transition months.

Figure 4.27: Relationship between $\Delta_{\overline{T}}$ and interpolated groundwater level at station GW2025 excluding measurements taken in transition months (March, April, September and October).

Table 4.2: Simple linear regression results for correlations between $\Delta_{\overline{T}}$ or z-score and GWL'

Figure	Dependent variable GWL' in station	Independent variable $\pm\Delta_{\overline{T}}$ or z-score	Function	p-value	R^2
4.23(a)	GW2025	$-\Delta_{\overline{T}}$ (Peatland $\overline{T}$ - Surrounding $\overline{T}$)	$f_{(x)}$= 0.15x-0.44	0.239	0.07
		$+\Delta_{\overline{T}}$ (Peatland $\overline{T}$ - Surrounding $\overline{T}$)	$f_{(x)}$= 0.04x-0.38	0.566	0.02
4.23(b)	GW2013	$-\Delta_{\overline{T}}$ (Peatland $\overline{T}$ - Surrounding $\overline{T}$)	$f_{(x)}$= -0.09x-0.34	0.65	0.02
		$+\Delta_{\overline{T}}$ (Peatland $\overline{T}$ - Surrounding $\overline{T}$)	$f_{(x)}$= 0.06x-0.23	0.447	0.05
4.24(a)	GW2025	- z-score (Peatland vs. Peatland & Surrounding)	$f_{(x)}$= 0.32x-0.45	0.323	0.05
		+ z-score (Peatland vs. Peatland& Surrounding)	$f_{(x)}$= 0.23x-0.43	0.238	0.07
4.24(b)	GW2013	- z-score (Peatland vs. Peatland & Surrounding)	$f_{(x)}$= -0.12x-0.32	0.824	0.004
		+ z-score (Peatland vs. Peatland & Surrounding)	$f_{(x)}$= 0.29x-0.28	0.134	0.18
4.25(a)	GW2025	$-\Delta_{\overline{T}}$ (Raised Bog $\overline{T}$ - Peatland $\overline{T}$)	$f_{(x)}$= -0.04x-0.45	0.653	0.01
		$+\Delta_{\overline{T}}$ (Raised Bog $\overline{T}$ - Peatland $\overline{T}$)	$f_{(x)}$= -0.07x-0.43	0.832	0.01
4.25(b)	GW2013	$-\Delta_{\overline{T}}$ (Raised Bog $\overline{T}$ - Peatland $\overline{T}$)	$f_{(x)}$= -0.03x-0.27	0.763	0.004
		$+\Delta_{\overline{T}}$ (Raised Bog $\overline{T}$ - Peatland $\overline{T}$)	$f_{(x)}$= -0.23x-0.05	0.594	0.16
4.26(a)	GW2025	$-\Delta_{\overline{T}}$ (GW2025pr $\overline{T}$ - EastCZ $\overline{T}$)	$f_{(x)}$= -0.09x-0.52	0.005	0.45
		$+\Delta_{\overline{T}}$ (GW2025pr $\overline{T}$ - EastCZ $\overline{T}$)	$f_{(x)}$= -0.01x-0.4	0.929	<0.001
4.26(b)	GW2013	$-\Delta_{\overline{T}}$ (GW2013pr $\overline{T}$ - WestCZ $\overline{T}$)	$f_{(x)}$= -0.09x-0.26	0.505	0.05
		$+\Delta_{\overline{T}}$ (GW2013pr $\overline{T}$ - WestCZ $\overline{T}$)	$f_{(x)}$= -0.17x-0.13	0.07	0.27
4.27(a)	GW2025	$-\Delta_{\overline{T}}$ (Peatland $\overline{T}$ - Surrounding $\overline{T}$)*	$f_{(x)}$= -0.06x-0.5	0.593	0.03
		$+\Delta_{\overline{T}}$ (Peatland $\overline{T}$ - Surrounding $\overline{T}$)*	$f_{(x)}$= -0.003x-0.38	0.972	<0.001
4.27(b)	GW2025	$-\Delta_{\overline{T}}$ (GW2025pr $\overline{T}$ - EastCZ $\overline{T}$)*	$f_{(x)}$= -0.09x-0.49	0.044	0.38
		$-\Delta_{\overline{T}}$ (GW2025pr $\overline{T}$ - EastCZ $\overline{T}$)*	$f_{(x)}$= 0.04x-0.47	0.656	0.02

* Measurements taken during transition months were excluded

5 Discussion

5.1 Groundwater, soil and air temperature

The results on differences between groundwater, soil and air temperature, in the study region, suggest the validity of the assumption that groundwater temperature could be used as a tracer, during the summer and winter months. In situ measurements taken in station GW2025 (Figure 4.1) demonstrated that groundwater temperatures were less susceptible to seasonal temperature fluctuation. While a seasonal pattern can still be recognized, this temperature signal is attenuated and the maximal difference between the coldest and warmest temperatures is of approximately 5 °C, as opposed to a maximal difference of approximately 30 °C between minimum and maximum soil temperatures, and of 45 °C between minimum and maximum air temperatures. The divergence from an otherwise consistent pattern in groundwater temperature in March, 2008, is probably a measuring error. It can be noted that the groundwater temperature pattern is delayed in about three months compared to the yearly air or soil temperature cycle (Figure 4.2). Maximum air or soil temperature occurs around July, while maximum groundwater temperature occurs in October. The same is true for the temperature minimum, which occurs around December for air or soil temperature, and in March for groundwater temperature. This demonstrates that changes in groundwater temperature take place gradually, rather slowly and delayed as opposed to soil or air temperature. It is due to this reduced susceptibility of groundwater to seasonal temperature fluctuations that the difference between groundwater and soil or air temperature in the summer and the winter is measurable (Figures 4.3), and that both measures have correlations with a very low coefficient of determination ($R^2 < 0.1$; Figure 4.5). The anomaly in Δ_T values around the 15^{th} of January and the 12^{th} of February, 2011 in figures 4.3, could be explained by a sudden rise in air (and soil) temperature around those days.

This study assumes that drained areas should be better represented by soil temperatures and saturated areas by groundwater temperatures. The distribution of Δ_T (GW T - Soil T) values in figure 4.4(a) would suggest that on certain occasions in the summer, stronger temperature contrasts could be detected. However, because of the greater variability given in that season, also smaller temperature differences may be given. On the other hand, Δ_T in winter are more stable, yet Δ_T rarely go over 10 °C. This pattern doesn't occur with Δ_T (GW T - Air T), where contrasts reach greater measures and have a consistent variability range throughout the year. For this reason the relationship between air and soil temperature was examined. Results presented in figure 4.4 demonstrated that both measurements correlate better for air temperatures over 0 °C. Under that threshold the correlation between both variables deteriorates with decreasing air temperatures which implies that for air temperature below 0 °C, soil temperatures remain rather stable. A similar pattern was reported in Sass et al. (2014), where the same correlation was examined. There, the correlation between soil and air temperatures also declined under the freezing mark. Sass et al. (2014) examined the response of the coefficient of determination for soil to air temperature correlations, below the freezing mark, to different snow depths. Results showed that without any snow, the coefficient of determination for soil vs. air was approximately 0.8, and that with increasing snow depth the coefficient of determination gradually decreased. This proved that soil temperatures, measured 5 cm b.g.s.l. correlated linearly with air temperature until the snow pack formed, then, soil temperatures were decoupled from the atmosphere. Thus, snow can have an isolating function. A snow cover could explain the rather constant soil temperatures below 0 °C observed in this study's results. Unfortunately, this study doesn't count with snow depth measurements, so it is not possible to prove if snow cover is the cause for this phenomenon. Another possible explanation would be that here, groundwater temperatures are having an effect on the soil temperatures, heating them up from below. The DWD measuring station where these measurements were recorded is outside the Pfrunger-Ried peatland, however, it is located within another, smaller peatland area. There are no GWL measurements in that area, however, just the fact that it is a peatland area opens up the possibility that soil temperature measurements taken in station #3927 may be already "warmed up" by the underlying groundwater.

Regardless of the reason for this anomaly, these results demonstrate that, in the study region, temperature contrasts between soil and groundwater temperature are given. These temperature contrasts are given primarily in the summer and the winter. During the transition months between winter and summer (March and April), and between summer and winter (September and October) the intensity of this contrast is reduced. Thus, using heat as a groundwater tracer should in principle be possible during summer and winter but not during the transition months.

5.2 Zonification process and Landsat imagery availability

The zonification process to delimit the areas for which mean temperatures were to be measured considered three main aspects: a) Zones which belonged to the peatland, raised bog or surrounding area, b) Grassland land cover, c) Cloud, cloud shadow or snow coverage. So, the zones to be compared where the intersection zones between 'a & b', excluding zones in 'c', for each Landsat image.

Definition of peatland surrounding area

The process for defining the surrounding zone, with a buffer area extending over the peatland borders, was fairly simple. While the method presented here didn't ensure the exact same surface area inside and outside the peatland, both areas had comparable sizes. For the most part, a larger divergence between surface areas inside and outside the peatland, occurred when taking the land cover into consideration. Most of the peatland areas in Baden-Württemberg showed an abrupt change in land cover from inside, to outside the peatland area. A great portion of the smaller peatland areas had a forest land cover inside the peatland and a different land cover surrounding the peatland. For starters, this characteristic made it difficult to find peatland areas on which to apply this study. Then, even when according to the WaBoA land use map, the adequate land use transition was found for a given peatland, upon closer examination using Google Earth imagery, it turned out that the land use did change from inside to outside the peatland as is the case in the peatland areas shown in sub-figures 4.9(e)-(i). This could be explained by the fact that with different water saturation levels, conditions for different vegetation covers are given. For the Pfrunger-Ried, most of the 'Raised bog' area had a forest cover and the peatland a grassland cover. The surrounding area also had a portion of grassland cover, but this area didn't extend much farther, and most of the grassland cover in this zone was close to the edges of the peatland.

Land cover, vegetative period and TIR image resolution

In the reference study by Sass et al. (2014), the land use classification was not as stringent as the one done in this study. In that study, only open water and urban areas were excluded from the thermal map, and diverse agricultural land use forms intermixed with forested areas were used for the thermal comparison. Yet, that study was done using imagery from the winter season, when the vegetation cover was at a minimum, exposing the ground surface in most of the study region. However, in the present study, temperatures are also compared during the vegetative period, and upon surveying the Landsat TIR images for the summer months it is evident that large differences between forest and non-forest areas are given. Thus, if a temperature contrast comparison is to be done during the summer as well as during the winter, it only makes sense to be as thorough as possible with regard to the definition of the land use. Because of the relatively low height of grassland vegetation, this study considered that this land use form maximized the possibility to read temperature differences due to groundwater influence.

The additional step done in this study, using Google Earth imagery to refine the definition of grassland cover zones, certainly reduced the probability of including forested, urban or open water areas in the calculation of mean temperatures. However, a grassland cover is not a homogeneous surface, and there are differences between parcels related to grass type, usage, cut, harvest periods etc., so it is possible that during the vegetative period we are comparing random differences related to the grassland type and not necessarily the underlying water saturation conditions. Other studies have used TIR imagery during the summer, e.g., (Mutiti et al. 2010, Tweed et al. 2007, Bobba et al. 1992). However, for the most part what those studies have done was to use TIR imagery to detect different types of vegetative cover and use those characteristics as predictors for groundwater presence, a process which might have more success in semi-arid places where the mere presence of certain vegetation is an indicator of more humid conditions. On a different aspect, Barron & Van Niel (2009) suggests the use of imagery taken at night or dawn, when land cover effects on surface skin temperatures are minimized. This wasn't possible for our study region, because Landsat-5 imagery for that scene was always taken at 10:50 a.m. LT in the winter and 11:50 a.m. LT in the summer.

Another aspect which should be taken into account has to do with the Landsat imagery resolution. The thermal band for Landsat-5 was acquired at 120-meter resolution, but the downloadable product was resampled to a 30-meter resolution to match the resolution of the remaining bands. This means that while this study uses a raster image where each pixel represents a ground area of 30 x 30 m, this is only a resampled product, and in the original product each pixel should represent an area of 120 x 120 m. While later Landsat-missions offered a better resolution, this study was bound to use Landsat-5, because the GWL data was only available for a period which overlapped the Landsat-5 mission's period. Alone this low resolution in Landsat-5 TIR imagery, limits the informative value for smaller areas. This means that when defining a zone, ideally this zone should extend over enough surface area so that it could be well represented by this imagery. When applying a similar method on open water surfaces, Handcock et al. (2006) suggested using only ”pure” water, i.e., water pixels situated more 5 than a pixel away from the river banks. For the present study, this would imply that pixels near the borders to a different land use should be excluded. By applying such suggestion, most of the results for the smaller peatland areas (Figure 4.9) should be discarded, and the defined zones in the Pfrunger-Ried (Figure 4.8) would become much smaller. The selection process done in this study was fairly conservative, avoiding areas where groups of trees were visible. However, it is still possible that some of the cells used here represent a mixed signal between grassland and other land covers. First, because of the resolution of the imagery and second, because land use border are mostly scattered and uneven.

Cloud or snow coverage

Considering all the points mentioned above, it would seem that this method should be applied only to winter TIR imagery. Unfortunately, for this study, the great majority of winter images were covered by clouds. Only four images between 1984 and 2011 were available, undamaged and partially free of clouds for the period between the beginning of December and the end of February. But even for those images, the areas either detected by the cfmask or manually delimited as cloud areas cut to great of a portion out of the final zone which was to be used for mean temperature calculation. And even for the rare, cloud free image, comparison surface needed to be free from snow coverage. Without in situ information on snow depth for the days when this imagery was acquired, no real useful information can be extracted from snow covered surfaces. First, because as shown in Sass et al. (2014), larger snow pack coverage might have an isolating effect on soil temperatures, making it more difficult to assign the cause for the change in soil temperature. Second, because the TIR imagery would be reading temperature measurements at the top of the snow layer without delivering any information on the actual soil temperature.

5.3 Landsat Thermal Infrared imagery

One of the greater challenges in this study was the reduced amount of usable Landsat imagery. The original goal of this study was to present the trend for mean temperatures, temperature contrasts, and the relationship of temperature contrasts vs. GWL on a yearly basis, and to compare these results from year to year. However, at best, there were some years with four usable images, while for other years there would be no usable images. Also, these images were mostly not evenly distributed in different months, but for the most part they were concentrated in the summer, so that no trend could be observed from a yearly plot. It is because of this lack of images that all points were presented on a yearly cycle with color coding according to year to detect changes from a range of years to another. Some of the now unavailable images might become available after the first quarter of 2016, as the ground station ESA offered to reprocess the missing data. If missing data can be recovered, there exists the possibility to have access to an extra set of about 200 Landsat images, which could be interesting if future studies should be done in this area. However, there is still the possibility that a portion of those images have either a large cloud coverage or are damaged.

The results for Landsat mean temperatures in figure 4.10, show that at-sensor temperatures are plausible, as they follow the same yearly pattern as soil and air temperatures. Figure 4.11 confirms that Landsat derived temperatures are correlated to mean daily air or soil temperatures, whereby the correlation to soil temperature is slightly better. In general, Landsat derived temperatures are overestimated, but then again, in situ measurements represent daily means while at-sensor temperatures reflect temperature conditions at the time of Landsat image acquisition. It is possible that correlating Landsat temperatures to in situ measurements taken at the same time of the image acquisition could deliver better correlation measurements, but a higher temporal resolution for ground data was not available for the study region. Nevertheless the absolute accuracy of temperature measurements is not crucial for this study, but the spatial contrast between these measurements is. The fact that measurements show a significant linear correlation with an $R^2 > 0.7$ demonstrates that temperature contrasts can be appropriately approximated using Landsat TIR imagery.

5.4 Temperature difference between means and z-score

Temperature contrasts between peatland and surrounding areas expressed as $\Delta_{\overline{T}}$ and z-score (Figures 4.12 to 4.17), don't present a pattern which resembles the hypothetical temperature contrast wave postulated by this study (Figure 3.4). Because of the limited amount of measurements per year, points were color coded according to the year in which they were taken, so that if a change should occur from a period to another, this should be visually discernible. However, no structured pattern in the distribution of colors could be recognized. I.e., no pattern, which could be interpreted by a sequence of waves with varying amplitudes, could be observed.

Because there exists no reference as to what measurement, $\Delta_{\overline{T}}$ or z-score, would be more suitable for this analysis, both measurements were tested here. Generally, comparisons using z-score values generated more outliers, which occurred when the SD of the comparison zones was particularly small, a scenario which is likely to occur when a large portion of the comparison zones is covered by clouds or snow. However, neither variable ($\Delta_{\overline{T}}$ or z-score) showed a consistent pattern where it could be said that it approximated the hypothetical wave more than the other.

The first results in the Pfrunger-Ried (Peatland vs. Surround in Figure 4.12) showed a distribution where, for the months between August and mid October, there were mainly negative values, and for the remaining time there were mainly positive values. Minimum negative $\Delta_{\overline{T}}$ and z-score values reached in August, and maximum z-score values reached between February and March, suggested a correspondence to the hypothesis presented by this study. On the other hand, positive $\Delta_{\overline{T}}$ values were reached in June, and a great portion of both positive z-score and $\Delta_{\overline{T}}$ values occur until the end of July, a summer month where warmer conditions within the peatland can't be explained by the same hypothesis. It was with the purpose of determining if this particular distribution was caused by random effects, or if there is a pattern which can be reproduced, that smaller areas in the Pfrunger Ried area and other peatland areas were compared as well. However, the distribution of the Pfrunger-Ried peatland vs. surround temperature contrast was never repeated nor approximated by other examples. Additional examples used either smaller areas in the same peatland (e.g. GW2025pr vs. WestCZ or GW2013pr vs. EastCZ) or they used the same zonal comparison in nine other peatlands. Sub-figure 4.12(a) shows the distribution which, even when in a somewhat skewed fashion, most approximated the hypothetical wave. However, the fact that this pattern was not approximated on other comparisons suggests that such distribution could have generated for reasons outside the ones presented by this study's hypothesis.

5.5 Groundwater level and its correlation to temperature contrast

While the Pfrunger-Ried counts with 111 groundwater stations distributed in the northern half of the peatland area, only the two stations which covered a period long enough to make a comparison with the Landsat TIR images, were used for this study. If more groundwater stations would have covered the same period, a spatial interpolation of GWLs, using ordinary or universal kriging as shown in Gundogdu & Guney (2007), could have been applied. Because this was not possible, the GWL for the two available stations was examined separately.

Groundwater level interpolation method

GWL measurements taken from 2008 to 2011 in station 4.18 almost resemble a line, because of the proximity between points representing daily measurements. From this high temporal resolution can be recognized that the daily GWL signal has a rather irregular course. The temporal resolution for the GWL data between 1994 and 2007, permitted modeling GWL' using the two closest measuring points, which were at a maximum relative distance of seven days (with the Landsat date somewhere between those two dates). Despite the irregular pattern of GWL changes, and thanks to the temporal resolution of measurements recorded from 2008 to 2011, the approach adopted in this study to interpolate GWL seems to be adequate enough. Judging by the sequence of daily GWL measurements, a deviation from GWL' to the real GWL greater than 5 cm is unlikely to occur.

Groundwater level downward shift

The perceived downward shift from the first to the second phase of GWL recordings in station GW2025 (Figure 4.18) could be more of a progressive sinking in GWL. There appears to be an overall sequence, where points closer to the ground level are mostly from earlier years, and points towards the bottom range of GWL are mostly from more recent years. This can be confirmed by a downward trend in annual mean GWL for the same station (Figure 4.22). For station GW2013 (Figure 4.21) there is less data and an interrupted time sequence. Nevertheless, measurements taken between September and December, 2009 and between January and May, 2010, lie visibly lower than other years, which would suggest that the downward shift in GWL is not unique to station GW2025. These in situ recordings suggest there is an overall sinking of the groundwater table. This confirms that an assessment tool to approximate long-term changes in the groundwater table is relevant.

Interpolated groundwater level and Landsat imagery paired dataset

It should be considered that the paired dataset, which this study uses to identify a possible correlation between temperature contrasts and GWL, is a just fraction of what was originally estimated. First, only 374 Landsat images from 647 were available to download. Then only 87 could be downloaded because they were partially free of clouds and undamaged. For the Pfrunger-Ried peatland vs. surround comparison only 82 images could be used for a temperature contrast. And finally, for the GWL' to temperature contrast correlation, only 41 Landsat derived temperature contrast measurements could be matched to GWL' for station GW2025, and only 28 could be matched to GWL' for station GW2013. This selection process left a data set without any points for the winter months from the beginning of November to the end of February. So, any possible correlations occurring during the winter are not represented here. Summer data on the other hand is well represented, however, there is only one interpolated measurement in station GW2013 where GWL' reaches the ground surface level in July. In general, GWL tends to lie deeper during the summer. Not only stations GW2025 and GW2013, but other groundwater stations in this peatland area also show a similar pattern (Figures included in the appendix). Some measurements in the paired dataset correspond to GWL' at, or within 10 cm distance from the ground level, however, for the most part these occur between March and April, which are transition months between winter and summer. This means that, even if water saturation conditions are given, it is possible that the real temperature contrast between groundwater temperature and soil temperature is too small to reveal water saturation conditions based on temperature difference.

Correlation results

None of the linear regressions for the correlation between GWL' and temperature contrast match the hypothetical relationship postulated by this study (Figure 3.5). The first approach attempted to predict GWL' in stations GW2025 and GW2013 based in the temperature contrasts between the peatland and surrounding area in the Pfrunger-Ried. The same zonal comparison which produced the yearly temperature contrast distribution that most approximated the hypothetical wave postulated by this study. However, none of these correlations produced a linear regression with a p-value under the 0.01 significance level, regardless if $\Delta_{\overline{T}}$ or z-score were used as a temperature contrast measurement. One possible explanation is that temperature contrast measurements taken in the transition months from the summer to winter and from winter to summer were included in the correlation. As reported by (Pfister et al. 2010), the identification of spatial patterns is rendered extremely difficult in circumstances where the temperature difference is low. If groundwater and soil temperature are similar, as it is likely to be the case during transition months, temperature contrasts might not be revealing water saturation conditions. In a next step, transition months were excluded from those correlations, in order to examine if the correlation could benefit from excluding measurements taken during the months where pronounced temperature differences between groundwater and soil were not given. However, all examples for the same zonal comparison, made without transition months, showed no significant linear regression either (all p-values > 0.1). Another possible explanation for this lack of a correlation is that the temperature contrast between the Pfrunger-Ried peatland vs. surrounding zone could not be represented by the GWL' of a single groundwater station. This would make sense because, these zones, represent a rather large and variable area, and so the GWL might also variate within the peatland. So, the next step consisted in comparing the temperature contrast of smaller areas close to the points where groundwater measurements were available (i.e., proxy groundwater stations), against other small areas in the surrounding area (i.e., the East and

West comparison zones). By doing this, we can assume that the GWL' measurements are representative for the corresponding proxy zones. This was done using all available measuring points, as well as excluding values from transition months. Also, all correlations were done using both $\Delta_{\overline{T}}$ and z-score, not all were included in the results section, but some additional comparisons are included in the appendix. , even when not all these were presented in the results section. Only for the negative portion of $\Delta_{\overline{T}}$ (GW2025pr - EastCZ) against GWL' in station GW2025 was there a significant linear regression ($p < 0.01$) with an R^2 of 0.45 which also had orientation hypothesized in this study. However, it is likely that this regression is skewed by an outlier $\Delta_{\overline{T}}$ value measured in April, 2006, which also has a GWL' at ground level. When removing transition months, the linear regression is no longer significant under the 0.01 level, and the R^2 value is reduced. Also, the positive temperature contrast in the same correlation is in both cases not significant. Despite several approaches to examine the relationship between temperature contrast and GWL', results were both positive and negative temperature contrast measurements formed a significant linear regression with the GWL', matching the relationship this study hypothesized, never occurred.

6 Conclusion

This study tried to test a new method, which potentially would be able to estimate GWLs by using a long-term database of Landsat TIR imagery. The first hypothesis postulated in this study, stating that groundwater saturated soil and drained soil have a contrasting temperature signature in summer and in winter could be confirmed. This is based on the fact that differences between groundwater and soil temperature during the summer and the winter were given for the study region. However, the second hypothesis, postulating that the groundwater saturation degree in a peatland area could be derived from temperature differences detected by Landsat TIR imagery in the summer and winter had to be rejected. Despite the fact that temperature measurements derived from Landsat TIR imagery approximated surface temperatures on the ground, it is likely that temperature contrasts are only giving information on skin surface temperatures and not on the underlying ground water saturation conditions. While this study chose the best available land cover, which could translate ground temperatures more directly, it is possible that even in this case, the vegetation cover dominates the signal. Given that most of the Landsat images, which could be used in this region, were available during the vegetative period, to limit results to the winter season was not an option.

Many of the limitations this study encountered lied in a data set which was being continuously reduced. If this method should be tested again, results in this study showed that the following aspects should be taken into account: 1) A study site with sufficient cloud free and snow free winter imagery should be chosen. 2) A site where there is no abrupt change of vegetation between the water saturated area and the surrounding area. This aspect might not be as important outside the vegetative period, but even in the winter, it could be problematic if a forest (particularly an evergreen coniferous forest) is represented in one zone and grassland or farmland is represented in the other. 3) To adequately validate this method, GWL data for the same region should be available for the same period as the Landsat TIR imagery is available, 4) A site where variable GWL is given, so that there is a reference of conditions with GWL reaching the surface and also with a GWL lying deep. 5) A better resolution in the TIR band, as is the one given in Landsat-8, might deliver more accurate results. 6) For validation purposes "Radar" data could be used to approximate water saturation conditions. 7) GWL measurements in the surrounding area could serve to confirm if the surrounding area has a lower GWL. This study made that assumption based in the fact that if it were not so, these areas would have also been included within the peatland area delimitation in the peatland cadastre. However, having GWL measurements outside the peatland areas could help validate this assumption.

This study could not find a consistent pattern or a reliable regression function, by means of which GWL could be approximated either for other regions, or for other periods in time when Landsat imagery was available and in-situ GWL measurements were not. Because GWL could not be modeled, CO_2 emissions could not be calculated. However, despite the fact that the method presented here could not be proved, there is reason to believe that this method, or an adaptation thereof, could work given enough appropriate winter imagery and GWL data. Further research, under conditions which could enable successful testing of the ideas presented here, is encouraged.

Bibliography

Anderson, M. P. (2005), 'Heat as a ground water tracer', *Groundwater* **43**(6), 951–968.

Barron, O. & Van Niel, T. G. (2009), 'Application of thermal remote sensing to delineate groundwater discharge zones', *International Journal of Water* **5**(2), 109–124.

Barsi, J. a., Hook, S. J., Schott, J. R., Raqueno, N. G. & Markham, B. L. (2007), 'Landsat-5 thematic mapper thermal band calibration update', *IEEE Geoscience and Remote Sensing Letters* **4**(4), 552–555.

Barsi, J. A., Schott, J. R., Palluconi, F. D., Helder, D. L., Hook, S. J., Markham, B. L., Chander, G. & O'Donnell, E. M. (2003), 'Landsat tm and etm+ thermal band calibration', *Canadian Journal of Remote Sensing* **29**(2), 141–153.

Bechtold, M., Tiemeyer, B., Laggner, A., Leppelt, T., Frahm, E. & Belting, S. (2014), 'Large-scale regionalization of water table depth in peatlands optimized for greenhouse gas emission upscaling', *Hydrology and Earth System Sciences* **18**(9), 3319–3339.

Becker, M. W. (2006), 'Potential for satellite remote sensing of ground water', *Ground Water* **44**(2), 306–318.

Berglund, Ö. & Berglund, K. (2011), 'Influence of water table level and soil properties on emissions of greenhouse gases from cultivated peat soil', *Soil Biology and Biochemistry* **43**(5), 923–931.

BfN, B. f. N. (2015), 'Naturschutzgroßprojekte', *chance.natur* . Last accessed: 2015-09-15. **URL:** *https://www.bfn.de/0203_grossprojekte.html*

Bobba, a., Bukata, R. & Jerome, J. (1992), 'Digitally processed satellite data as a tool in detecting potential groundwater flow systems', *Journal of Hydrology* **131**(1-4), 25–62.

Breman, J. (2002), Gis analysis of landsat 7 thermal data to identify submarine springs, *in* 'Marine geography: GIS for the oceans and seas', ESRI, Inc., chapter 6, p. 49.

Cartwright, K. (1974), 'Tracing shallow groundwater systems by soil temperatures', *Water Resources Research* **10**(4), 847–855.

Charman, D. (2002), *Peatlands and environmental change.*, John Wiley & Sons Ltd.

Couwenberg, J., Dommain, R. & Joosten, H. (2010), 'Greenhouse gas fluxes from tropical peatlands in south-east asia', *Global Change Biology* **16**(6), 1715–1732.

Furukawa, Y., Inubushi, K., Ali, M., Itang, A. M. & Tsuruta, H. (2005), 'Effect of changing groundwater levels caused by land-use changes on greenhouse gas fluxes from tropical peat lands', *Nutrient Cycling in Agroecosystems* **71**(1), 81–91.

Gundogdu, K. S. & Guney, I. (2007), 'Spatial analyses of groundwater levels using universal kriging', *Journal of Earth System Science* **116**(1), 49–55.

Hahn-Schöfl, M., Zak, D., Minke, M., Gelbrecht, J., Augustin, J. & Freibauer, A. (2011), 'Organic sediment formed during inundation of a degraded fen grassland emits large fluxes of ch4', *Biogeosciences* **8**(6), 1539–1550.

Handcock, R. N., Gillespie, A. R., Cherkauer, K. A., Kay, J. E., Burges, S. J. & Kampf, S. K. (2006), 'Accuracy and uncertainty of thermal-infrared remote sensing of stream temperatures at multiple spatial scales', *Remote Sensing of Environment* **100**(4), 427–440.

Harbeck, R. (2001), '15 jahre atkis und die entwicklung geht weiter', pp. 3–14.

Huntley, D. (1978), 'On the detection of shallow aquifers using thermal infrared imagery', *Water Resources Research* **14**(6), 1075–1083.

Jaenicke, J., Rieley, J. O., Mott, C., Kimman, P. & Siegert, F. (2008), 'Determination of the amount of carbon stored in indonesian peatlands', *Geoderma* **147**(3), 151–158.

Jarasius, L., Matuleviciute, D., Pakalnis, R., Sendzikaite, J. & Lygis, V. (2014), 'Drainage impact on plant cover and hydrology of aukstumala raised bog (western lithuania)', *Botanica Lithuanica* **20**(2), 109–120.

Joosten, H. & Clarke, D. (2002), *Wise use of mires and peatlands*, Vol. 4.

Kirkwood, B. B. & Sterne, J. (2003), *Essential medical statistics.*

Kopp, B. J., Fleckenstein, J. H., Roulet, N. T., Humphreys, E., Talbot, J. & Blodau, C. (2013), 'Impact of long-term drainage on summer groundwater flow patterns in the mer bleue peatland, ontario, canada', *Hydrology and Earth System Sciences* **17**(9), 3485–3498.

Lalot, E., Curie, F., Wawrzyniak, V., Schomburgk, S., Piegay, H. & Moatar, F. (2015), 'Quantification of the beauce's groundwater contribution to the loire river discharge using satellite infrared imagery', *Hydrology and Earth System Sciences Discussions* **12**(2), 2047–2080.

Levy, P. E., Burden, A., Cooper, M. D. A., Dinsmore, K. J., Drewer, J., Evans, C., Fowler, D., Gaiawyn, J., Gray, A. & Jones, S. K. (2012), 'Methane emissions from soils: synthesis and analysis of a large uk data set', *Global Change Biology* **18**(5), 1657–1669.

Li, F., Jackson, T. J., Kustas, W. P., Schmugge, T. J., French, A. N., Cosh, M. H. & Bindlish, R. (2004), 'Deriving land surface temperature from landsat 5 and 7 during smex02/smacex', *Remote sensing of environment* **92**(4), 521–534.

LUBW (2014), 'Moorkataster'. Last accessed: 2015-07-31.
URL: *http://brsweb.lubw.baden-wuerttemberg.de*

LUBW (2015), Moorschutzprogramm baden-württemberg, Technical report.

Lundberg, J. (2007), 'Lifting the crown—citation z-score', *Journal of Informetrics* **1**(2), 145–154.

Markham, B. L. & Barker, J. L. (1986), 'Landsat mss and tm post-calibration dynamic ranges, exoatmospheric reflectances and at-satellite temperatures', *EOSAT Landsat technical notes* **1**(1), 3–8.

Mohammed, N. Z., Ghazi, A. & Mustafa, H. E. (2013), 'Positional accuracy testing of google earth', *International Journal of Multidisciplinary Sciences and Engineering* **4**(6).

Moore, T. R. & Roulet, N. T. (1993), 'Methane flux: water table relations in northern wetlands', *Geophysical Research Letters* **20**(7), 587–590.

Mutiti, S., Levy, J., Mutiti, C. & Gaturu, N. S. (2010), 'Assessing ground water development potential using landsat imagery', *Groundwater* **48**(2), 295–305.

Pfister, L., McDonnell, J. J., Hissler, C. & Hoffmann, L. (2010), 'Ground-based thermal imagery as a simple, practical tool for mapping saturated area connectivity and dynamics', *Hydrological Processes* **24**(21), 3123–3132.

Regina, K., Nykänen, H., Silvola, J. & Martikainen, P. J. (1996), 'Fluxes of nitrous oxide from boreal peatlands as affected by peatland type, water table level and nitrification capacity', *Biogeochemistry* **35**(3), 401–418.

Roulet, N. T. (2000), 'Peatlands, carbon storage, greenhouse gases, and the kyoto protocol: prospects and significance for canada', *Wetlands* **20**(4), 605–615.

Sander, P., Chesley, M. M. & Minor, T. B. (1996), 'Groundwater assessment using remote sensing and gis in a rural groundwater project in ghana: lessons learned', *Hydrogeology Journal* **4**(3), 40–49.

Sass, G. Z., Creed, I. F., Riddell, J. & Bayley, S. E. (2014), 'Regional-scale mapping of groundwater discharge zones using thermal satellite imagery', *Hydrological Processes* **28**(23), 5662–5673.

Schuetz, T. & Weiler, M. (2011), 'Quantification of localized groundwater inflow into streams using ground-based infrared thermography', *Geophysical Research Letters* **38**(3), 1–5.

Schweikle, V. (2001), Moore in baden-württemberg - eigenschaften, inventur und funktionen, Technical report.

Tanneberger, F. & Wichtmann, W. (2011), *Carbon credits from peatland rewetting: climate, biodiversity, land use*, Schweizerbart Science Publishers, Stuttgart. 223pp.

Tcherepanov, E. N., Zlotnik, V. A. & Henebry, G. M. (2005), 'Using landsat thermal imagery and gis for identification of groundwater discharge into shallow groundwater dominated lakes', *International Journal of Remote Sensing* **26**(17), 3649–3661.

Tweed, S. O., Leblanc, M., Webb, J. a. & Lubczynski, M. W. (2007), 'Remote sensing and gis for mapping groundwater recharge and discharge areas in salinity prone catchments, southeastern australia', *Hydrogeology Journal* **15**(1), 75–96.

USGS (2012), 'Landsat — a global land-imaging mission', *U.S. Geological Survey Fact Sheet* **3072**, 4.

USGS (2015*a*), 'Availability of landsat scenes in earthexplorer archive', *Frequently Asked Questions about the Landsat Missions* . Last accessed: 2015-08-15.
URL: *http://landsat.usgs.gov/Are_all_collected_Landsat_scenes_held_in_the_USGS_Landsat_archive.php*

USGS (2015*b*), 'Landsat band designations', *Frequently Asked Questions about the Landsat Missions* . Last accessed: 2015-08-15.
URL: *http://landsat.usgs.gov/band_designations_landsat_satellites.php*

USGS (2015*c*), 'Product guide landsat 4-7 climate data record (cdr) surface reflectance'.

WaBoA (2012), Landnutzung, Technical report.

Wawrzyniak, V., Piégay, H. & Poirel, A. (2012), 'Longitudinal and temporal thermal patterns of the french rhône river using landsat etm+ thermal infrared images', *Aquatic sciences* **74**(3), 405–414.

Weinzierl, W. & Waldmann, F. (2014), Ermittlung langjähriger co2 -emissionen und beurteilung der moore oberschwabens auf basis historischer und aktueller höhennivellements, Technical report.

Wilson, J. & Rocha, C. (2012), 'Regional scale assessment of submarine groundwater discharge in ireland combining medium resolution satellite imagery and geochemical tracing techniques', *Remote Sensing of Environment* **119**, 21–34.

Wubet, M. T. (2003), 'Estimation of absolute surface temperature by satellite remote sensing', *International Institute for Geoinformation Science and Earth Observation, Netherlands* . M.Sc. thesis.

Younger, P. L. (2009), Groundwater and freshwater ecosystems, *in* 'Groundwater in the environment: an introduction', John Wiley & Sons, chapter 6, pp. 135–136.

Zhou, Y., Li, N., Grace, J., Yang, M., Lu, C., Geng, X., Lei, G., Zhu, W. & Deng, Y. (2014), 'Impact of groundwater table and plateau zokors (myospalax baileyi) on ecosystem respiration in the zoige peatlands of china', *PloS one* **9**(12), e115542.

Appendix

A Boxplots for Pfrunger-Ried peatland grassland temperatures

The following figures represent the available at-sensor temperatures of Landsat derived temperatures for the grassland peatland area in the Pfrunger-Ried, excluding clout temperature measurements. Visualizing them as box plots allows for a detailed observation of the set of temperatures measured, and which were later expressed as mean temperatures. Plots are arranged after the year in which they were acquired.

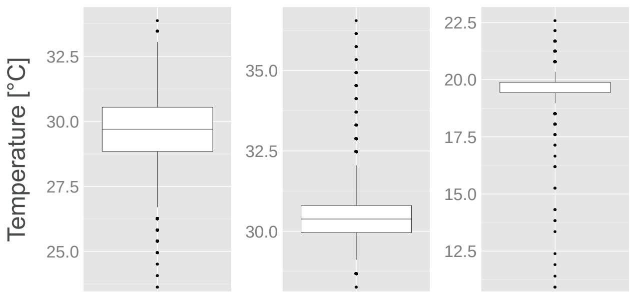

(b) Aug 17 (c) Sep 02 (d) Oct 20

Figure A.1: Boxplots for Pfrunger-Ried peatland grassland temperatures in 1984

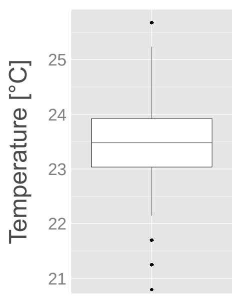

(b) Sep 05

Figure A.2: Boxplot for Pfrunger-Ried peatland grassland temperatures in 1985

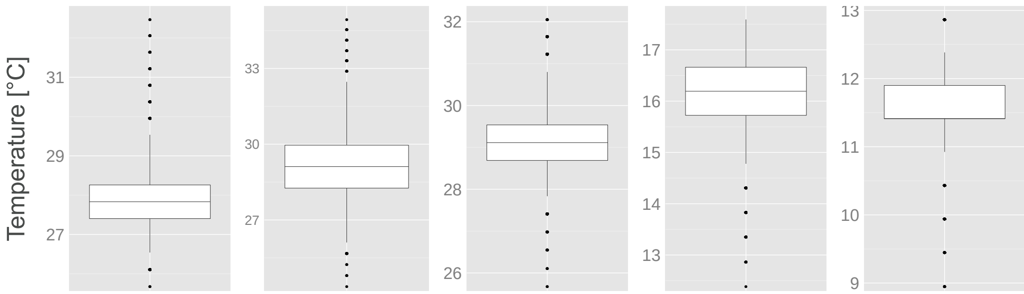

(b) May 03 (c) Jun 20 (d) Jul 22 (e) Nov 11 (f) Nov 27

Figure A.3: Boxplots for Pfrunger-Ried peatland grassland temperatures in 1986

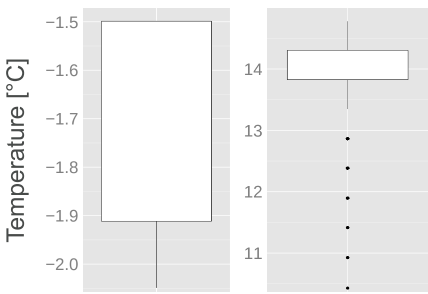

(b) Jan 30 (c) Nov 14

Figure A.4: Boxplots for Pfrunger-Ried peatland grassland temperatures in 1987

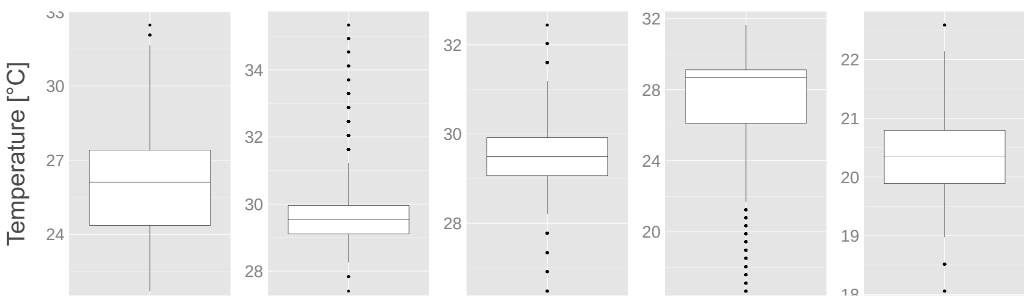

(b) Jun 09 (c) Jul 11 (d) Aug 12 (e) Aug 28 (f) Oct 15

Figure A.5: Boxplots for Pfrunger-Ried peatland grassland temperatures in 1988

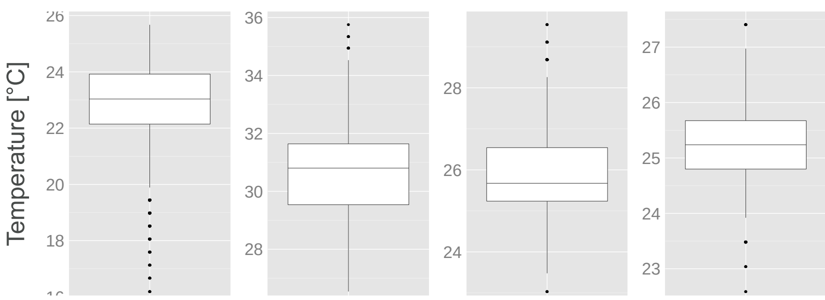

(b) Apr 09 (c) May 27 (d) Aug 31 (e) Sep 16

Figure A.6: Boxplots for Pfrunger-Ried peatland grassland temperatures in 1989

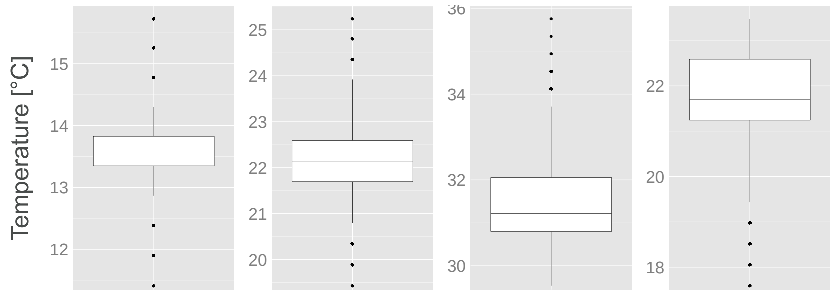

(b) Feb 07 (c) Mar 11 (d) Aug 02 (e) Oct 05

Figure A.7: Boxplots for Pfrunger-Ried peatland grassland temperatures in 1990

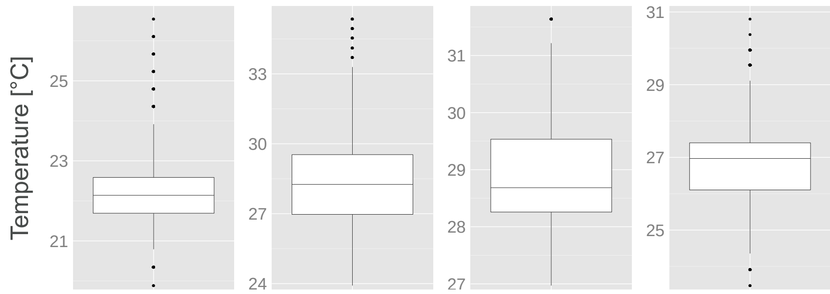

(b) Apr 15 (c) Jun 02 (d) Aug 05 (e) Sep 06

Figure A.8: Boxplots for Pfrunger-Ried peatland grassland temperatures in 1991

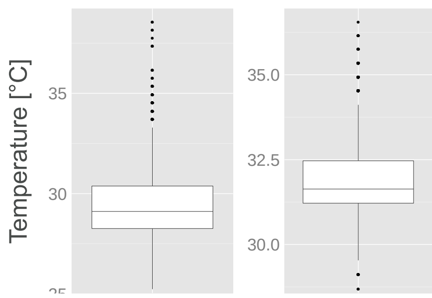

(b) May 19 (c) Aug 07

Figure A.9: Boxplots for Pfrunger-Ried peatland grassland temperatures in 1992

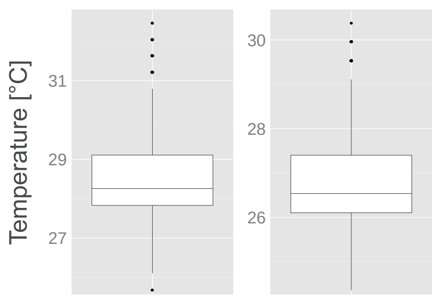

(b) Jun 07 (c) Jul 09

Figure A.10: Boxplots for Pfrunger-Ried peatland grassland temperatures in 1993

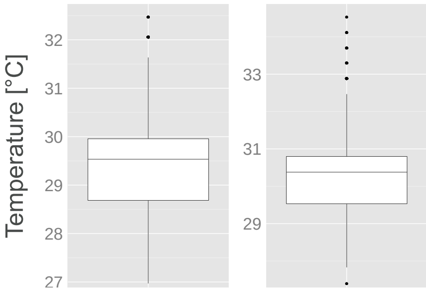

(b) Jul 12 (c) Jul 28

Figure A.11: Boxplots for Pfrunger-Ried peatland grassland temperatures in 1994

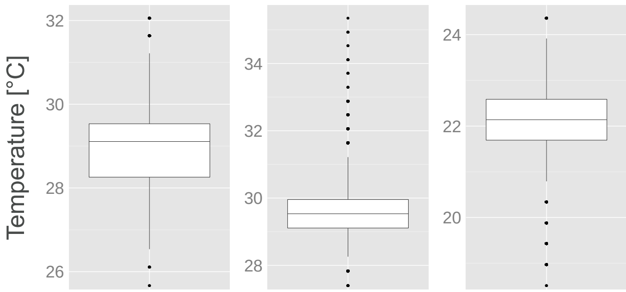

(b) Jun 29 (c) Jul 31 (d) Sep 17

Figure A.12: Boxplots for Pfrunger-Ried peatland grassland temperatures in 1995

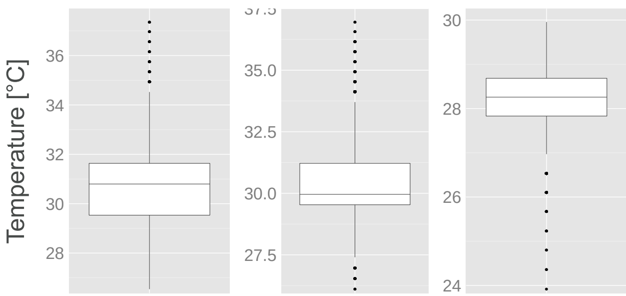

(b) May 30 (c) Jun 15 (d) Aug 02

Figure A.13: Boxplots for Pfrunger-Ried peatland grassland temperatures in 1996

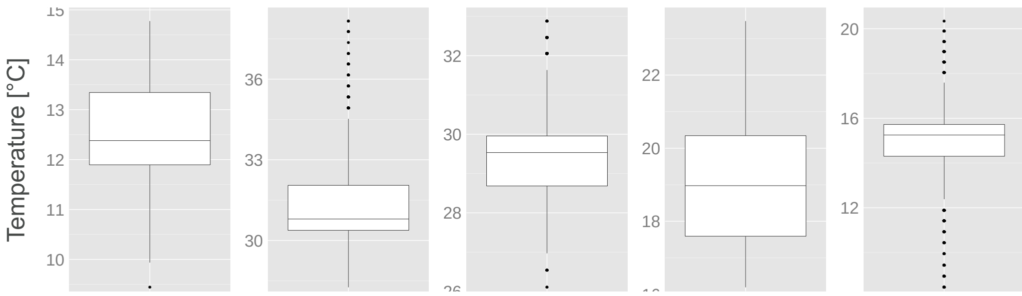

(b) Feb 10 (c) May 17 (d) Aug 21 (e) Sep 22 (f) Oct 08

Figure A.14: Boxplots for Pfrunger-Ried peatland grassland temperatures in 1997

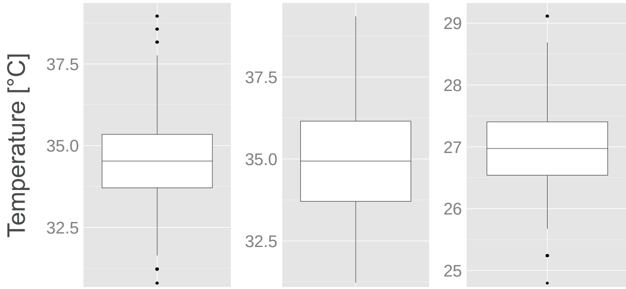

(b) Jun 21 (c) Aug 08 (d) Sep 09

Figure A.15: Boxplots for Pfrunger-Ried peatland grassland temperatures in 1998

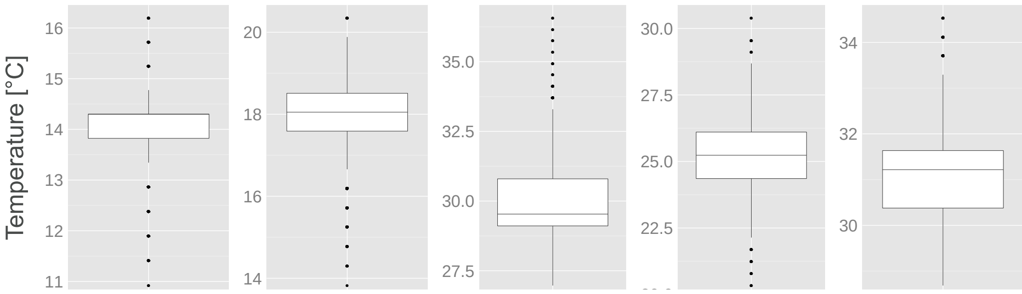

(b) Mar 06 (c) Apr 07 (d) May 09 (e) Jun 10 (f) Aug 13

Figure A.16: Boxplots for Pfrunger-Ried peatland grassland temperatures in 2000

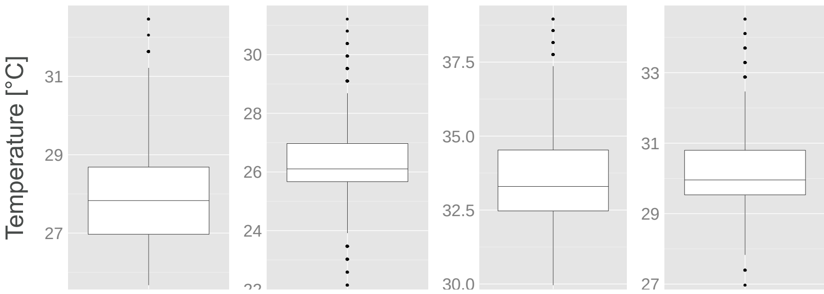

(b) May 12 (c) May 28 (d) Jul 31 (e) Aug 16

Figure A.17: Boxplots for Pfrunger-Ried peatland grassland temperatures in 2001

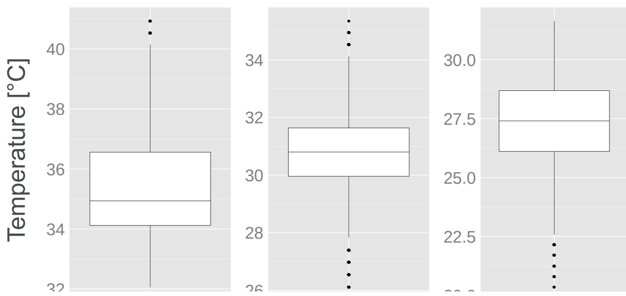

(b) Aug 06 (c) Aug 22 (d) Sep 07

Figure A.18: Boxplots for Pfrunger-Ried peatland grassland temperatures in 2003

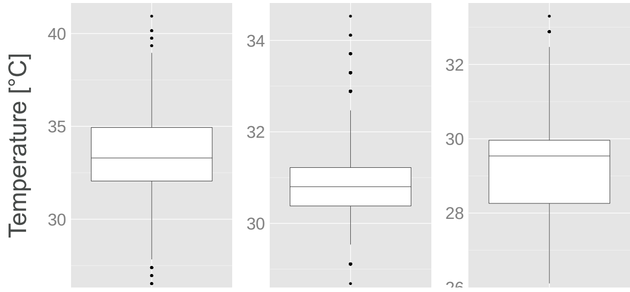

(b) May 20 (c) Jul 23 (d) Sep 09

Figure A.19: Boxplots for Pfrunger-Ried peatland grassland temperatures in 2004

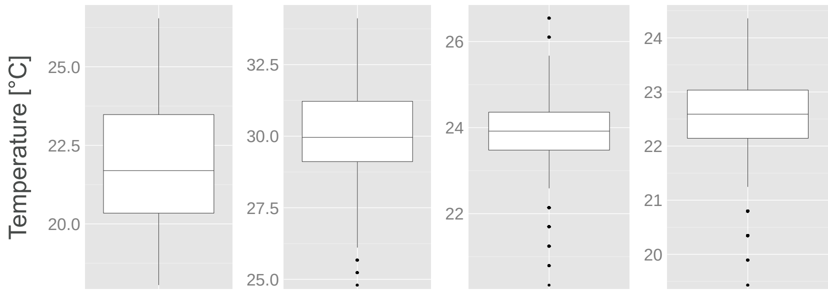

(b) Jun 24 (c) Aug 11 (d) Oct 14 (e) Oct 30

Figure A.20: Boxplots for Pfrunger-Ried peatland grassland temperatures in 2005

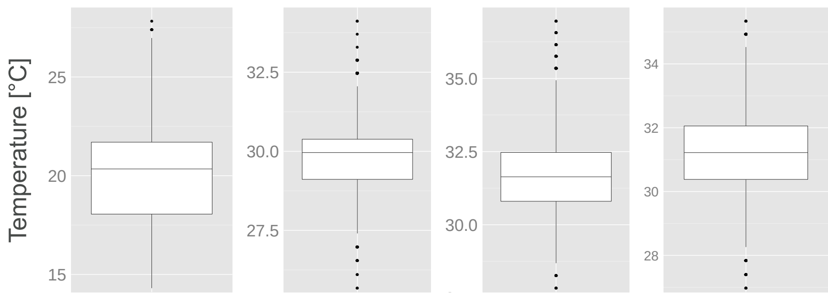

(b) Apr 08 (c) Apr 24 (d) Jun 11 (e) Jul 13

Figure A.21: Boxplots for Pfrunger-Ried peatland grassland temperatures in 2006

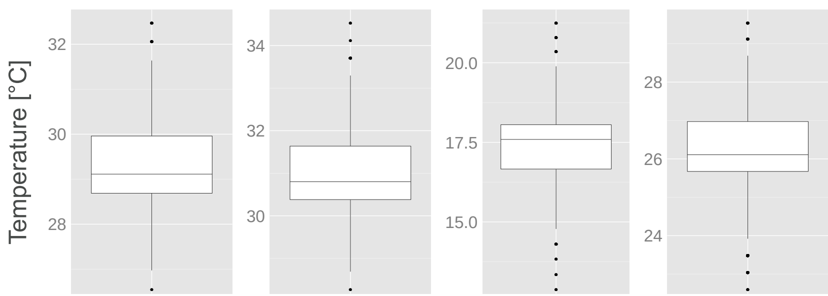

(b) Jul 21 (c) Aug 06 (d) Sep 07 (e) Sep 23

Figure A.22: Boxplots for Pfrunger-Ried peatland grassland temperatures in 2009

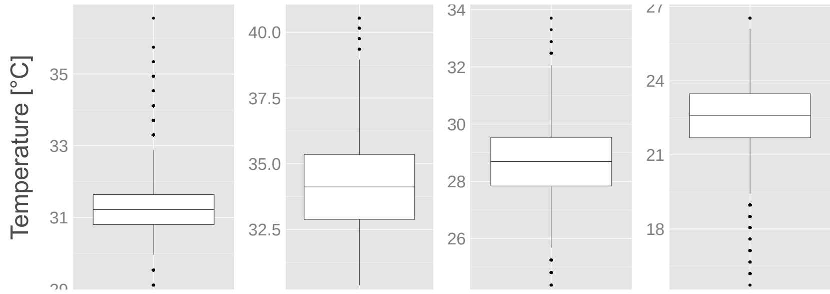

(b) Jun 06 (c) Jul 08 (d) Aug 09 (e) Aug 25

Figure A.23: Boxplots for Pfrunger-Ried peatland grassland temperatures in 2010

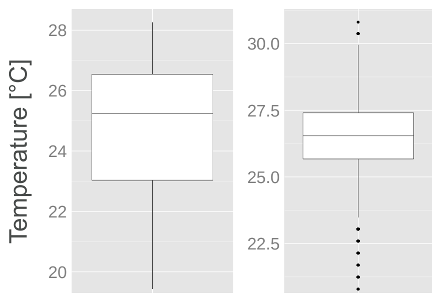

(b) Aug 12 (c) Aug 28

Figure A.24: Boxplots for Pfrunger-Ried peatland grassland temperatures in 2011

B Additional figures

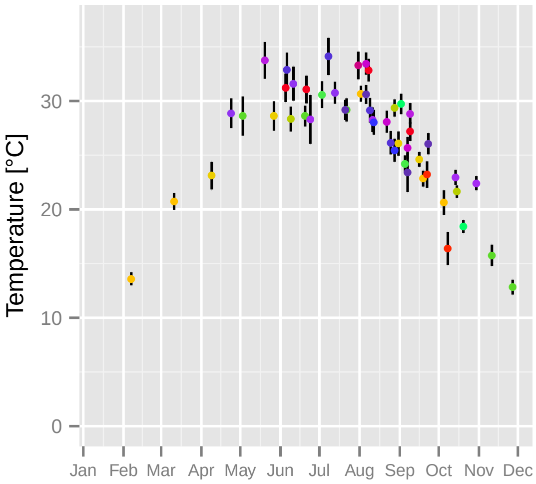

(a) $\overline{T}$ in Arrisrieder peatland

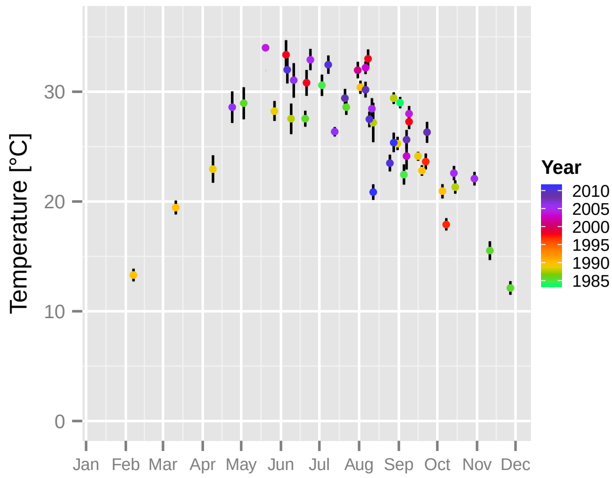

(b) $\overline{T}$ in Fetzach-Taufach peatland

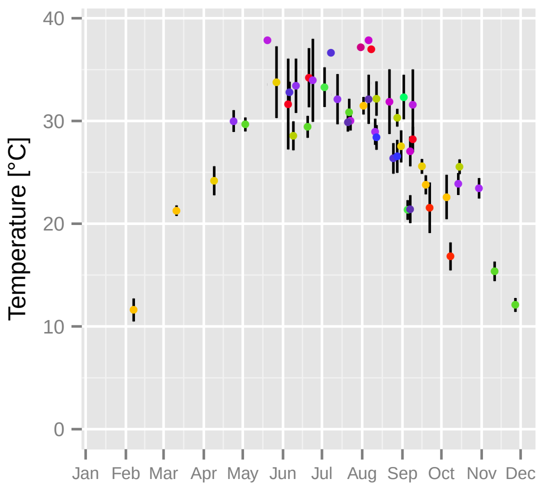

(c) $\overline{T}$ in Reicher peatland

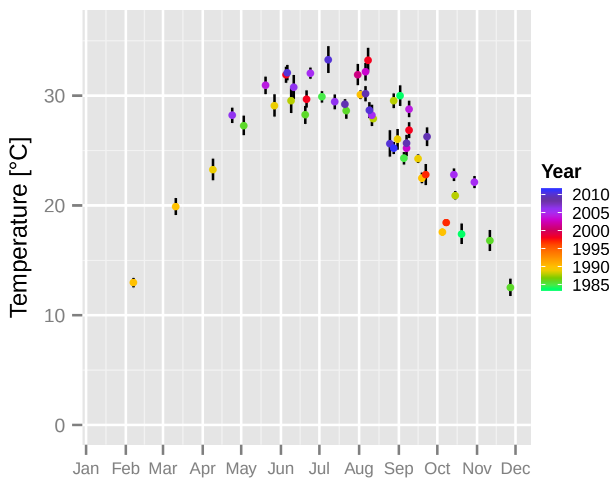

(d) $\overline{T}$ in Goettlishofen peatland

Figure B.1: Additional plots representing the yearly cycle of at-sensor mean temperatures and standard deviation on small peatland areas.

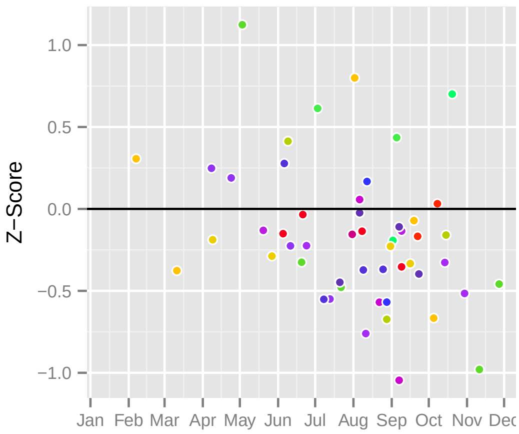

(a) Arriesrieder

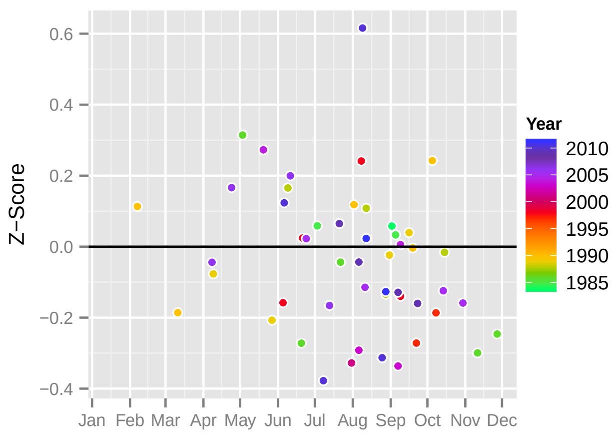

(b) Fetzach-Taufach

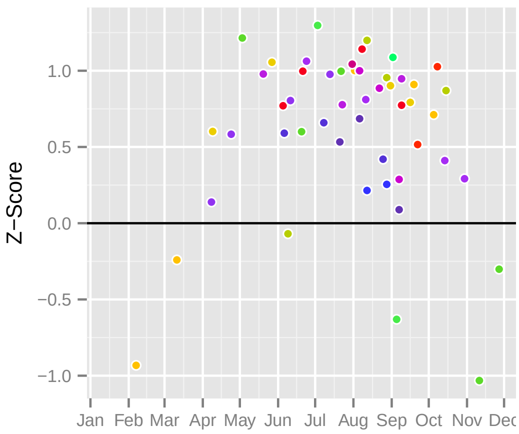

(c) Reicher

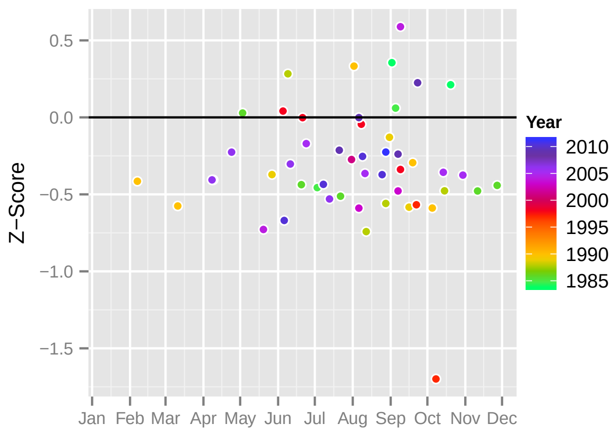

(d) SW of Goettlishofen

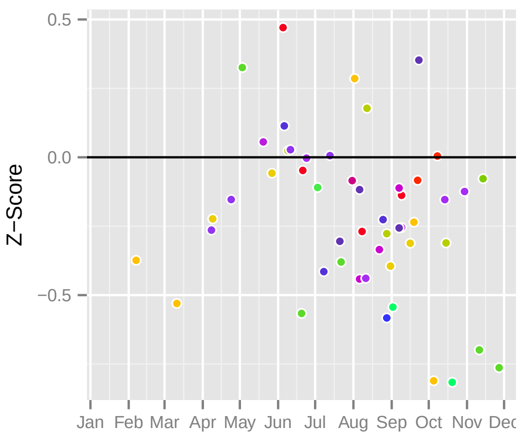

(e) Isnyer

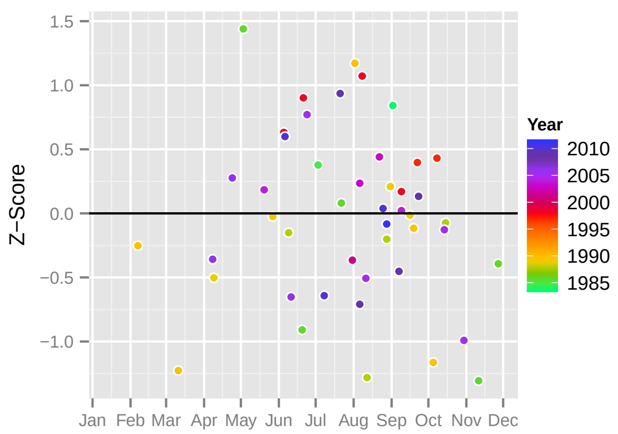

(f) bei Rengers

Figure B.2: Additional plots representing yearly cycle of z-score values (Peatland vs. Peatland & Surrounding) on small peatland areas.

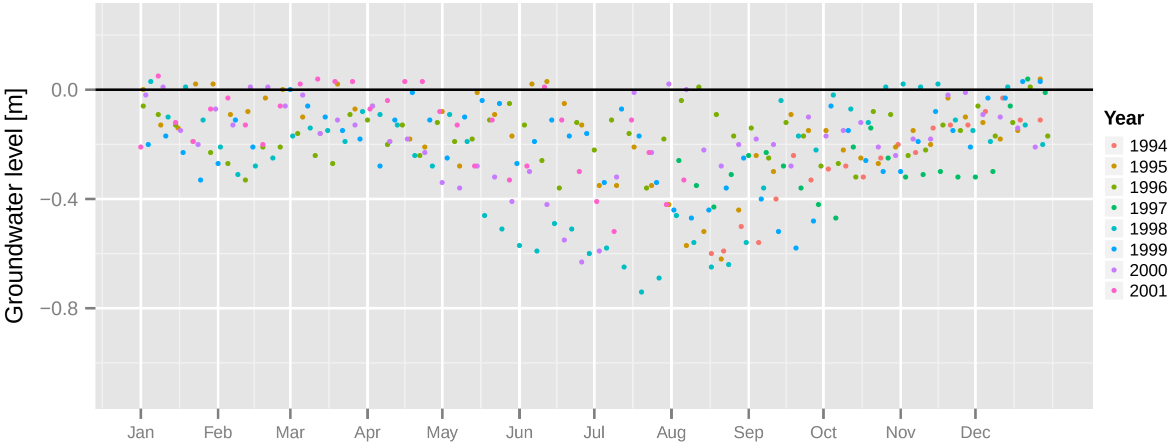

(a) Groundwater station station 2056/570-0

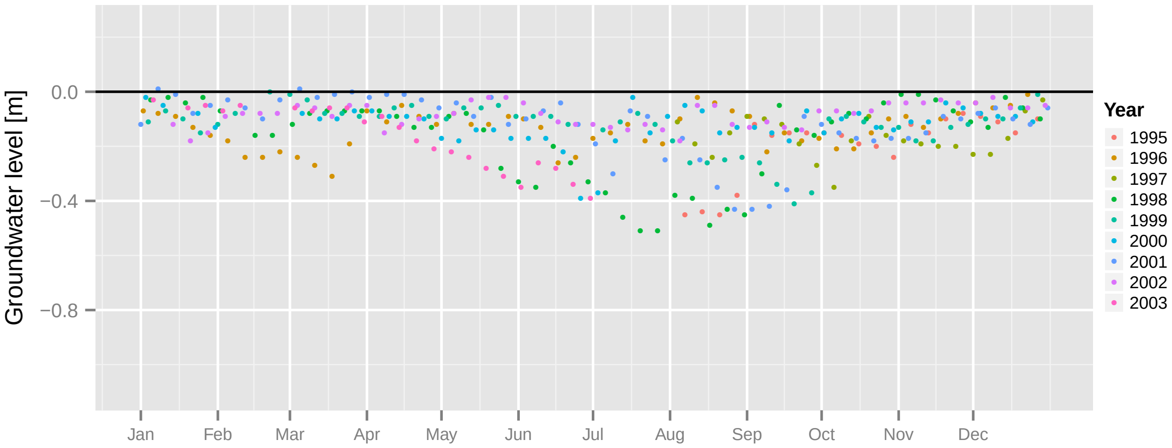

(b) Groundwater station station 2064/570-5

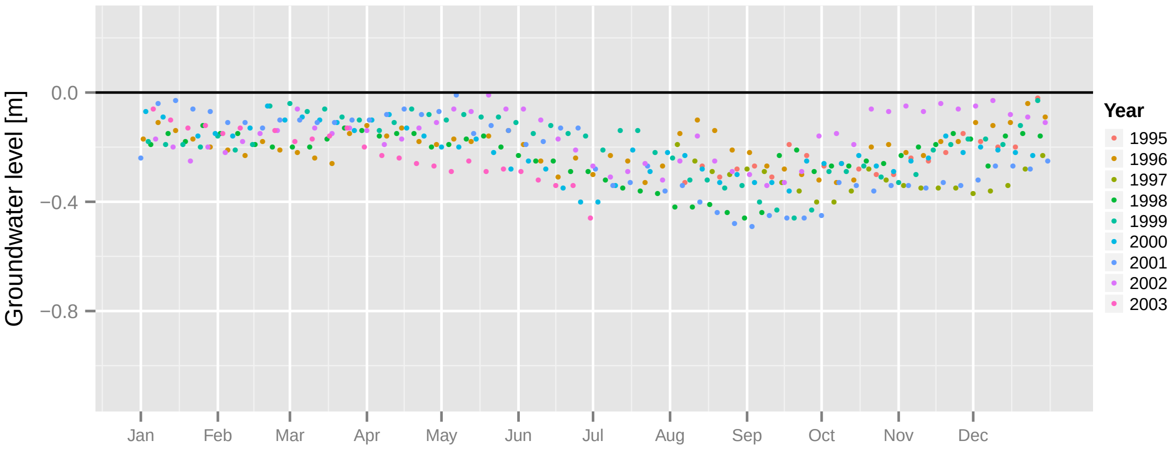

(c) Groundwater station station 8514/571-1

Figure B.3: Additional plots representing the groundwater level on other groundwater station in the Pfrunger-Ried.

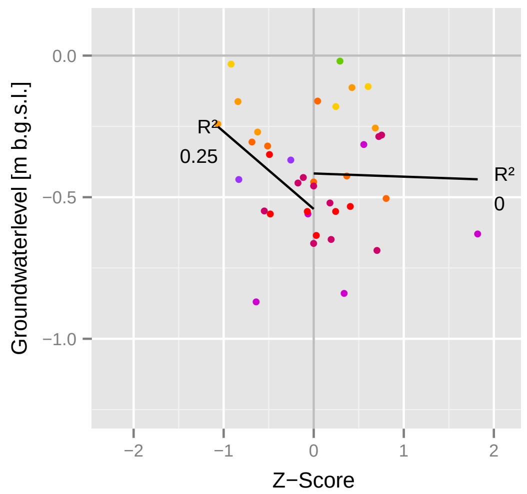

(a) GW2025pr vs. GW2025pr & EastCZ

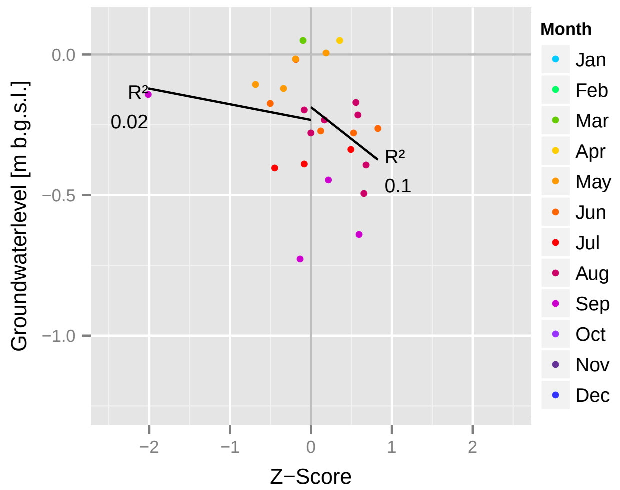

(b) GW2013pr vs. GW2013pr & WestCZ

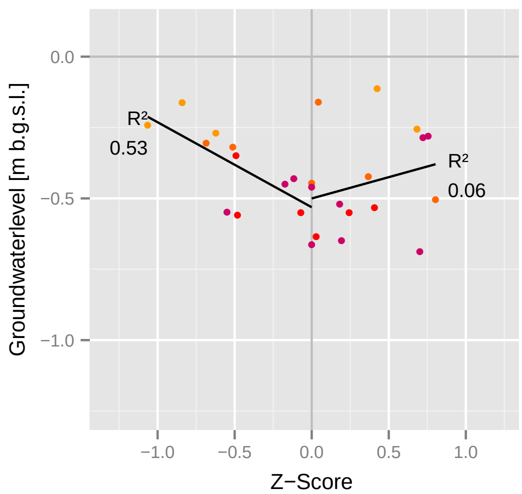

(c) GW2025pr vs. GW2025pr & EastCZ, excluding transition months

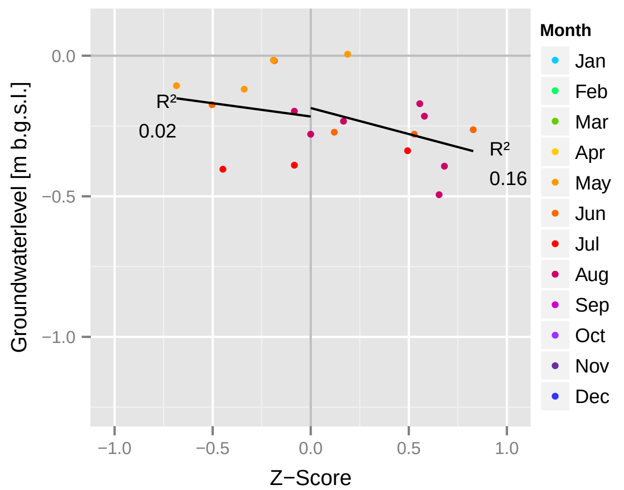

(d) GW2013pr vs. GW2013pr & WestCZ, excluding transition months

Figure B.4: Additional plots representing the relationship between z-score to interpolated groundwater level.

Affidavit

I declare that I wrote this thesis independently and on my own. I clearly marked any ideas borrowed from other sources as not my own and documented their sources. The thesis does not contain any work that I have handed in or have had graded earlier on.

I am aware that any failure to do so constitutes plagiarism. Plagiarism is the presentation of another person's thoughts or words as if they were my own, even if I summarize, paraphrase, condense, cut, rearrange, or otherwise alter them. I am aware of the consequences and sanctions plagiarism entails.

Freiburg in Breisgau, December 10, 2015